PDMS-based optofluidic systems

Jordi Vila i Planas

Doctorat en Física

Directors:
Dr. Andreu Llobera i Adan
Dr. Xavier Muñoz i Berbel

Tutor: Dr. Jordi Mompart i Penina

Departament de Física
Universitat Autònoma de Barcelona
Bellaterra, 2014

Als amics i la família.


SOLO LUCHANDO UNIDOS PODEMOS LOGRAR UN CAMBIO TOTAL DE ESTRUCTURAS


ES PRECISO QUE CONSTRUYAMOS UN MUNDO NUEVO, SIN BARRERAS SOCIALES, SIN SECTARISMOS, EN EL QUE TODOS SEAMOS EXACTAMENTE IGUALES, ¿ENTIENDES?
SÍ


¡"SÍ, DOCTOR"!

Agraïments

Durant la carrera, de tant en tant, et preguntes que hi fas allà, qui et manava posar-te a fer física i complicar-te la vida, i aleshores fas una assignatura que canvia com veu el món que et rodeja, això és tant mèrit de l'assignatura com del professor. A mi em va passar amb una assignatura que donava en Jordi Mompart i no puc estar d'agrair-li que apart d'això també em dirigís cap al CNM al grup de l'Andreu Llobera per començar la tesis i acceptes ser el meu tutor.

Una vegada ja al CNM, l'Andreu es va encarregar d'ensenyar-me un món absolutament desconegut que era la micro fabricació i com funciona la recerca de debò. La seva dedicació no es va acabar aquí, i durant tots els anys següents ha estat a la meva disposició per què seguis formant-me i aprenent, això ho va fer a base d'hores i dedicació, per la qual cosa li estic molt agraït.

Quan ja portava un parell d'anys al CNM va venir de postdoc en Xavi. La veritat és que a tot el grup li va anar d'allò més bé. Personalment en Xavi m'ha ajudat molt, especialment a veure les coses des d'un altre punt de vista (menys físic) i buscar autèntiques aplicacions per als meus xips. A part d'això també m'ha ajudat molt en l'escriptura i vull agrair-li el seu esforç i, sobretot, paciència.

My biggest thanks to Prof. Helen Andersson Svahn for giving me the opportunity to stay at her group at Albanova and make me feel like one more. I can not forget Hakan, I want to thank him for his patience and dedication, but specially for the beers, pingpong and football games. I would like to thank all the people I met on Stockholm: Staffan, Prem, Harisha, Emily, Lovisa, Joans, Aman and Tom. Specially, *crazy bitch* Ali, for the really nice time spend in Stockholm, Barcelona, Stockholm again and I expect Iran soon.

No em puc oblidar d'agrair la paciència que en Joan i la Sandra han tingut durant la infinitat, i no es una figura literària, d'hores que m'han

hagut de suportar a mi i els meus dubtes i ximpleries. En Joan m'ha aguantat al màster, la biblioteca, el despatx, el laboratori, hores de dinar, congressos i alguna que altre festa. La Sandra (trueskin o la rubia) encara s'ha sacrificat més i a aquesta llista i hi hem d'afegir la llicenciatura i la sala blanca, tot un rècord! Moltes gràcies! Per cert, després toca astrofísica?

No vull deixar-me d'agrair a la resta del grup d'òptica (si el considerem com a tal), en Bergoi, l'Ester, l'Alfredo, en Pere, en Tobi, en Victor, en Jorge, en Pedro, en César i en Carlos sense els quals hagués estat impossible fer aquesta feina. A tot el grup de GTQ (present i passat) i per extensió a tot el CNM. Vull destacar el seu esforç a la meva salut mental a n'Alvaro i n'Andrés i el "flow" que tots dos m'han transmès. També vull agrair la feina i suport rebut de tots els col·laboradors, co-autors i col·legues que han fet possible aquesta tesis, molt especialment a en *Richardas*, sobretot per les hores despotricant i per el sopar que espero que em paguis en breu ;).

Al llarg d'una tesis, per sort, es té una vida apart, i sense ella acabaríem tots més bojos.

Primer agrair a l'assemblea de tercer cicle, Ritxo, Elisa, Marta, Paula, Gael, Ricard, Martí, Flor... per compartir la lluita per unes condicions de feina dignes i unes millors opcions per fer ciència. Seguint en la lluita no puc estar-me de donar les gràcies a la gent de 9 barris el seu indefugible esperit de lluita i les seves ganes de passar-ho bé, que tot i haver-los deixat penjats/des aquests últims mesos són uns/es amics/gues collonuts/des!

Gràcies al XV del Vallès/Spartans/Parets, m'ho he passat molt bé coneixent el món del rugbi al vostre costat, patint, suant, lluitant i bevent. ¡SPARTANOS, AU, AU, AU! En especial agrair a la Mireia i en Pau per suportar les meves crisis i a la Marina per les bones i males estones que hem compartit.

També vull tenir unes paraules per els amics de la Garriga, en altres paraules, *les polles*, que tot i que no ens veiem gaire s'han portat sempre com mai. Sou una gent increïble i per sobre de tot, bellíssimes persones.

Moltes gràcies a la Elena i la Marta per oferir-me casa seva en un moment important i per fer-me sentir magníficament bé! Elena estic molt content d'haver-te conegut i haver tingut la possibilitat de viure amb tu. Tot i que no ens coneixíem gaire em vas convidar a casa teva, que ara és la nostre, i sempre m'has tractat fantàsticament bé. He sigut un afortunat! A tu Marta que t'haig de dir carinyu (o amor, com prefereixis), ets la meva

millor amiga des de fa un munt d'anys (diria que 14), no recordo ni una discussió amb tu (vols veure algo que sí que recordaràs?), sempre em fas riure i mires pels meus interessos, sempre que t'he necessitat hi has sigut, moltes gràcies. Moltes gràcies també a l'Albert, Lobo, Crosta,..., per els farts de riure que ens hem fet plegats, pels seus dissenys (en especial la samarreta de Menorca que encara espero) i evidentment per la portada ;)

Aquests últims anys han sigut especialment durs degut, entre altres, a que en Milhaus ens va deixar, ara vull tenir un rècord per ell, et trobo molt a faltar. Com no pot ser d'una altre manera agrair als meus amics del LOKAL, que sou la meva segona família. A en Sancez i la Fatima per les hores perdudes a casa seva, a en Melen i la AAA per estar sonats i fer-me riure sempre, a en Jaume per les increïbles calçotades i festes d'aniversari, a en Vicenç per tots els moments viscuts i per l'oportunitat de marxar de casa, a la Diana i en Martí per ensenyar-me el camí i fer-me veure que és possible acabar una tesis, a en Cuervo per estar allà sempre que l'he necessitat, a la Xatina per aguantar en Cuervo a diari (que té merit) i a mi de tant en tant, a la Sophie per les correccions tant a l'anglès com en les maneres, a en Tadeo, Pobre!, pel que ric amb ell i d'ell sempre que ens veiem o parlem, a la Tinto per tenir la porta de casa sempre oberta a *gorrons* i a en Bistek, Homilido!!, que és la cola que ho aguanta tot junt, encara que ja se que no t'agrada veure't així.

Per últim, a la meva família, a tota ella, cosins i cosines, tiets i tietes, el meu fillol, iaias i iaius, que ja no hi són. Molt especialment als meus germans, l'Helena, en Ferran i l'Anna, amb els que m'ho passo molt bé. Tots sou molt diferents, tots bastant cabronets i a tots us estimo molt! A la Montse i al Papa pel suport incondicional, tot i que se que he tingut les meves relliscades i les meves temporadetes difícils de tractar sempre heu estat allà. A la meva Mare per desviure's per nosaltres, estar sempre al peu del canó i fer l'impossible per què avui sigui on sóc. Moltes gràcies, us estimo molt.

The research leading to these results has received funding from the European Research Council under the European Community's Seventh Framework Programme (FP7/2007-2013)/ERC grant agreement no. 209243.

Contents

Objectives and overview

The idea of a total chemical analysis system (TAS) [Wid83] describes a system capable of carry out sampling, sample transport, any necessary chemical reaction and detection in an automatic way. Due to the reduction in cost and size of integrated electronic circuits as well as the improvement of microfabrication technologies, the micro total analysis system (µ-TAS) [MGW90], also known as Lab on a chip (LOC) [HMF+92], emerged in early 90s. Lab on a Chip was originally conceived as a micrometer-scale analysis system with all the required steps for a complete chemical analysis. Nevertheless, micrometric scale also has drawbacks that have to be solved, *e.g.*, within laminar flow, mixing is limited to diffusion mechanism, with mixing time increasing exponentially with distance. Hence, micrometric scales [KVBA98] and imaginative mixing solutions [GJM+99, LSL+12, FSGHL05, BP08] are essential to obtain reasonable mixing times. Besides this setback, LOC systems have certain unique features such as, sample volume reduction, laminar flow working regime and much larger surface/volume ratio than macroscopic scale.

Due to their unique features LOC is a promising system in fields like clinical diagnosis [NHM+14], pharmaceutical industry [NGL+12], environmental [JZL+11] and biological analysis [YCCF10]. Several interrogation mechanisms have been integrated in LOC systems for sample analysis and among them, the most used are electrochemical and optical.

Electrochemical interrogation is compatible with microfabrication technologies but generally requires electroactive samples and is difusion-limited. On the other hand, light may provide bulk or surface analysis, it is non-invasive and is immune to electromagnetic interferences. Furthermore, light offers different parameters *e.g.*, refractive index, wavelength, polarization, etc, that could be analysed depending on the final application and also allows multiplexing capabilities *e.g.*, analyse multiple wavelengths simultaneously. As a result, optical interrogation mechanisms are

widely used in (bio)chemical analysis techniques such as, enzyme-linked immunosorbent assay (ELISA) [YB60], based on absorbance, or polymerase chain reaction (PCR) [MEA+87], based on fluorescence detection.

Besides these advantages, integration of optical elements within a photonic lab on a chip (Ph-LOC) is not straightforward due to the required high quality surface which, often requires hybrid or non-standard fabrication technologies, increasing complexity and cost of the final Ph-LOC.

Gai *et al.* [GLY11] divide Ph-LOC in two main groups: (*i*) free-space (off-chip) interrogation mechanism, in which the optical elements are external *e.g.,* microscopes, CCD cameras, etc. and (*ii*) optofluidic (inside-chip) interrogation mechanism, where the optical elements are integrated on the Ph-LOC.

Free-space Ph-LOC still require bench-top equipments to perform some of the required steps of a complete analysis, limiting some of the main advantages of LOC, *e.g.*, disposable and highly integrated systems. On the other hand, optofluidic systems do not require the use of bench-top equipments, with reduction of size and cost. Hence, optofluidic systems are a good candidate for a highly integrated, disposable, low-cost, portable and flexible LOC.

The main objective of this thesis is the integration, monolithically and though modules, of simple and low-cost optical and fluidic elements for production of highly-integrated, disposable, and flexible optofluidic systems. In order to do so, a basic set of elements, *e.g.*, microchannels, lenses and optical filters, are designed and simulated. Afterwards, we develop the required technologies for optofluidic elements fabrication. Optofluidic elements are individually characterized and then integrated in different optofluidic systems, demonstrating their usefulness in (bio)chemical applications.

In order to tackle this main objective, the concrete objectives are defined as follows:

1. Development and optimization of soft-lithography based [XW98] microfabrication techniques to manufacture different optofluidic elements and systems. Microfabrication techniques should provide smooth surfaces to guarantee optimal optical performance as well as low-cost to ensure disposable final elements, as outlined in Chapter 3.

2. Design, optimization, fabrication and characterization of a set of

basic optofluidic elements such as lenses, mirrors, beam splitters, filters and emitters, that will be either monolithically integrated in an optofluidic system, or heterogeneously in a modular system. Each of these elements have to be fabricated using the same technology in order to ensure integrability in more complex systems without either increasing fabrication requirements complexity or requiring major modifications, as detailed in Chapter 4.

3. Next objective, detailed in Chapter 5, is the integration of the previously developed elements in a jigsaw shaped modular optofluidic system that allows an easy and fast way to assemble optofluidic systems on demand. This modular configuration aims to provide extra flexibility to LOC in order to allow in-field system reconfiguration for *in situ* measurements. The modules are tested individually and assembled together in a modular system.

4. Chapter 6 objective consists of the design, fabrication and characterization of a monolithically integrated optofluidic system capable of generating monodisperse microdroplets [TMQ02] and its optical detection and screening. Such a system uses the previously designed optical elements as well as a droplet generation element developed by Professor Andersson-Svahn. This system will reduce the volume and cost of the previous readout equipment, *i.e.*, inverted microscope, photo multiplier tube (PMT) and laser source. Moreover, this optofluidic system has been the first to detect droplet inner medium in real time.

5. Finally, the goal of Chapter 7 is the design, fabrication and characterization of a fluidically controlled optical router (FCOR) to overtake the state of the art in integrated routers for LOC applications. In order to do so, the concept of phaseguides [VMA$^+$06] is used to provide a dual element, *i.e.*, an element with a fluidic and optical functionality, which is a passive valve that also acts as a mirror. This configuration allows the redirection of light beams to different optical outputs without need of any movable parts. FCOR is used in a biological application for simultaneous glucose and lactate detection using previously reported optofluidic systems [LDWB07] in order to ensure its applicability and usefulness in more comple optofluidic systems.

1 | Introduction

This chapter is a review of the lab on a chip concept through main breakthrough on the field, detailing the main features of lab on a chip systems and the challenges yet to be solved.

1.1 Lab on a chip

Micro Total Analysis System (µ-TAS) or Lab on a chip (LOC) concept was coined by Manz et al.[MGW90] as a micrometer-scale system capable to perform "sampling, transport, any necessary chemical reactions and detection" in an automatic way and using only a fraction of the samples and reagents volumes needed to do the same process in the macrometric scale. Even though Manz was who proposed the concept, the first reported lab on a chip was published by Terry *et al.* [TJA+79]. This first LOC was a gas chromatographic air analyser.

The miniaturized gas chromatography had three basic roles, a sample

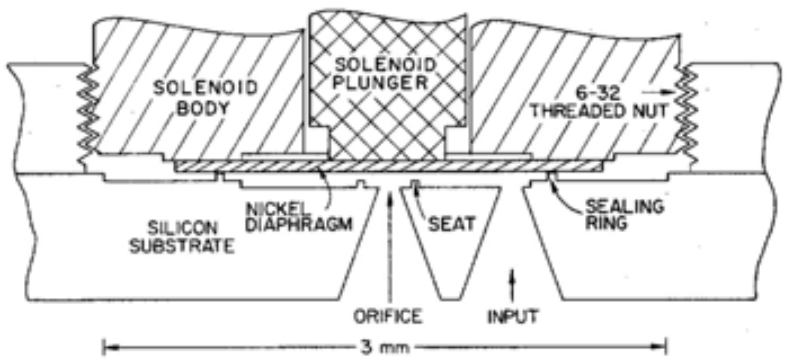

Figure 1.1: Cross section of miniature valve extracted from [TJA+79].

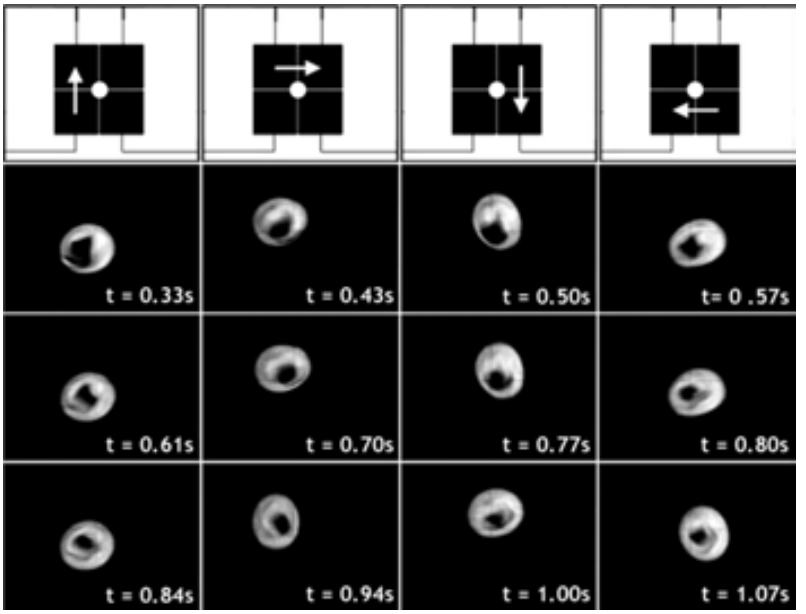

Figure 1.2: Reported mixing process in a 2x2 array mixer at 16 Hz [PPF03].

injection system, *i.e.*, a valve based on a solenoid-actuated diaphragm, detailed in Figure 1.1, a separator column and finally, a thermal conductivity detector. That LOC was based on micromachining techniques inherited from integrated circuits (ICs) industry and, as such, was based on silicon. Silicon and glass were the preferred materials in the early stages of LOC systems due to the widespread equipments of ICs fabrication and use of electrophoretic phenomena, where glass was the preferred material. These technologies and materials facilitated the digital microfluidics or electro wetting on dielectrics (EWOD) [Col90]. EWOD working principle is based on the possibility to change the wetability of a surface applying electric fields. With this technique droplets with characteristic size of less than 1 mm are formed, moved and actuated. EWOD are programmable devices, and then a basic chip design could be optimized and used in many different applications. For instance, mixing could be improved by simply spinning the droplet around a point or a circuit [PPF03], as it can be seen in Figure 1.2.

Nonetheless, EWOD devices have severe drawbacks such as are not disposable due to their fabrication cost, risk of (bio)chemical contamina-

tion, take few seconds to mix a single droplet in a serial process and the droplet analysis is not integrated on the chip. When silicon and glass are used in flow microfluidics another difficulties arise. Silicon and glass have complex bonding protocols for creating microchannels and generally require expensive fabrication methods.

The solution appears on mid 90s when polymers started being used as constituent material, and from that moment on polymers became the preferred fabrication material for LOC systems. There are a myriad of different polymers that encompass a wide range of prices and physicochemical properties providing great flexibility to design new LOC systems. LOC systems exploit this flexibility to improve existing performance at the macroscale [PB08] but, the most promising applications are the ones that are only possible within microfluidic scale, few examples are detailed below.

1. Chemical Synthesis:

   Chemical synthesis in industrial environments is well studied. However, fast and exothermic reactions are usually slowed down to prevent non desired side reactions. Use of microfluidics opens the novel process window [Hes09]. Using flow chemistry synthesis there is no need to slow down these exothermic reactions, increasing therefore the productivity. Furthermore, flow chemistry synthesis aided with high temperature and pressure [HHL05] or explosive regime [KWBC09], allow new chemical reaction pathways, *e.g.*, solvent-free synthesis of ionic liquids [RHL$^+$07], difficult to obtain in macroscopic environments.

2. Diagnostic tools for developing world:

   Size and cost reduction could also change diagnosis tools, with an important impact in developing world. LOC systems for this application should focus on three main features: (*i*) simple to operate systems, (*ii*) disposable and (*iii*) low-cost mass production. Two examples are:

   ELISA, Chin *et al.* [CLC$^+$11] reported a LOC system capable of and ELISA-like assay for simultaneous detection of HIV and syphilis using few µL of unprocessed blood without any external pumping system. As detection method they used a Light

emitting-diode (LED) and a photodetector incorporated into an easy-to-use compact device [LCM+09]. An illustration of the different characterization steps and biochemical reactions in the detection regions can be seen in Figure 1.3. The cost of the chip material is $0.10 and the detection device is $0.50 for the LED and $6.00 for the photodetector, which are used multiple times.

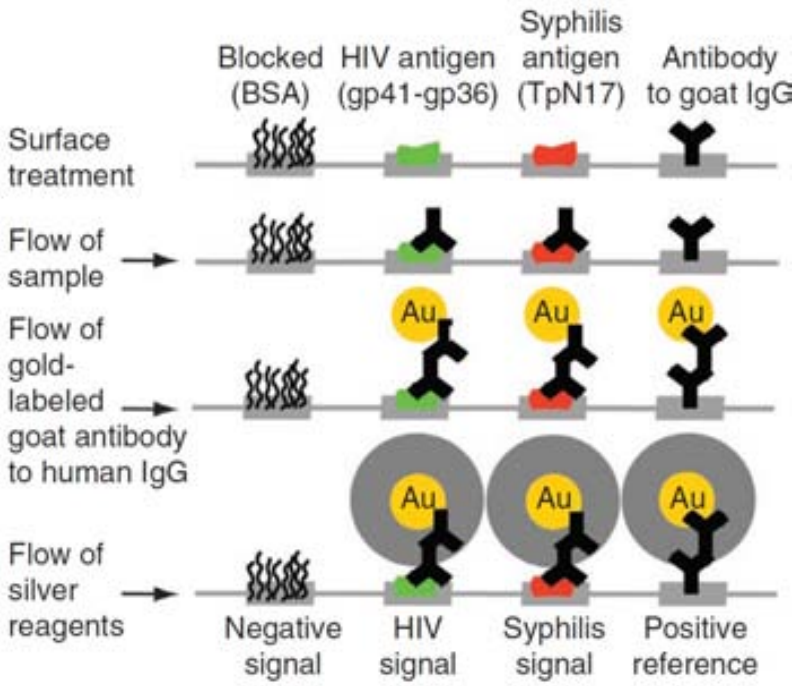

Figure 1.3: Illustration of biochemical reactions in detection zones at different immunoassay steps. The reduction of silver ions on gold nanoparticle-conjugated antibodies yields signals that can be read with low cost optics or examined by eye. [PPF03].

Paper-based LOC, Another promising example of an easy-to-use, low cost µTAS is the microfluidic paper-based analytical devices (µPADs) [MPC+08]. These devices use paper as substrate and drive microfluidics *via* capillarity forces and hydrophobic patterned regions, avoiding the need of external microfluidic pumps. Moreover, paper can be easily destroyed, *e.g.*, burned, drastically reducing contamination risk. µPADs

are becoming more sophisticated [OLF+10] and allow 2D [FLKY10] and 3D [MPW08] networks. Using µPAD with 2D networks a low cost, easy-to-use, multistep assay for malaria antigen detection was recently reported.

3. Biomedical applications: Recent advances in microfluidics and LOC systems are used in drug discovery and organ-on-a-chip technologies.

   Drug discovery, Screening of chemical libraries for drug discovery typically consist in the identification of promising compounds. Then, these compounds are more carefully studied in a dose-response analysis with few points, usually 10. Using picolitre, high-throughput,automatic methods, *i.e.*, monodisperse microdroplets, for screening of chemical libraries a 1000 times increase of screening points, 10000 per compound, is achieved with an automatically generated gradient concentration. Moreover, this new drug screening technique reduces the screening time per compound to 157 s and reagents consumption to 17.5 µl[MEM+12], 18 times smaller than the macroscopic analogous.

   Organ on a Chip another problem for biomedical and pharmaceutical industry is the *in vivo* testing of new drugs. Increasing the hit rate of new drugs before moving to *in vivo* analysis will reduce cost and time of drug discovery. In order to increase the hit rate the so called organ-on-a-chip are starting to be developed. Several approximations are already published for different organs [HMM+10, TKL+12, JS10]. Using these chips the animal testing phase may be reduced. Moreover, organ-on-a-chip with the functionalities of a kidney may reduce the dialysis equipments volume, becoming even portable devices [SJA+11, KM12].

These examples show the possibilities of LOC systems and technologies. However, most of LOC systems are still published in engineering journals, as can be seen in Figure 1.4. This phenomenon may be due to the difficult of creating a LOC system from scratch. LOC complexity is sufficient to deter most of biomedical researchers, and hence, the developers of microfluidic systems are engineers with shallow knowledge

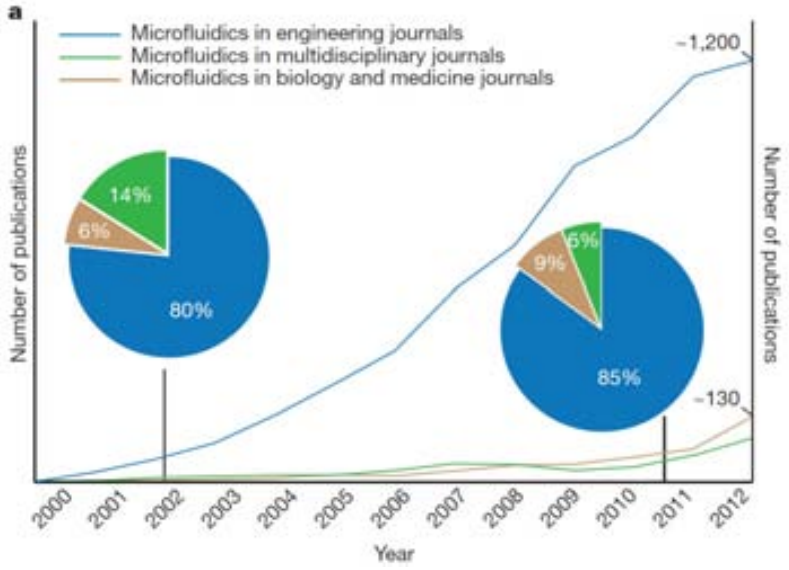

Figure 1.4: Microfluidic publications in engineering, multidisciplinary and biomedical journals.

on biomedical needs. Collaborations between these two groups should increase, but meanwhile some approaches to create LOC systems on demand are being developed.

Smartphones, Since smartphones ubiquity an interesting new approach has appeared. Using smartphones as readout reduces, if not eliminates, the need of bench-top equipments. Several LOC system for smartphones readout have already been reported. Develop a software to use the smartphone as a colorimetric sensor for already reported LOC is common [YAL13, PLMY13, HC14]. However, other groups develop a completely new LOC and use the smartphone to process data and comunicate to the chip *via* bluetooth [JWC+14], as it can be seen in Figure 1.5. This idea may be used to facilitate and increase implanted sensors, for example for glucose screening in diabetic patients.

Modular systems, in a modular system engineers design several modules with basic functionalities, *e.g.*, microfluidic mixers, droplet generators, microbioreactors, etc., and then the biomedical researchers plug the modules that they need to create personalized LOC systems

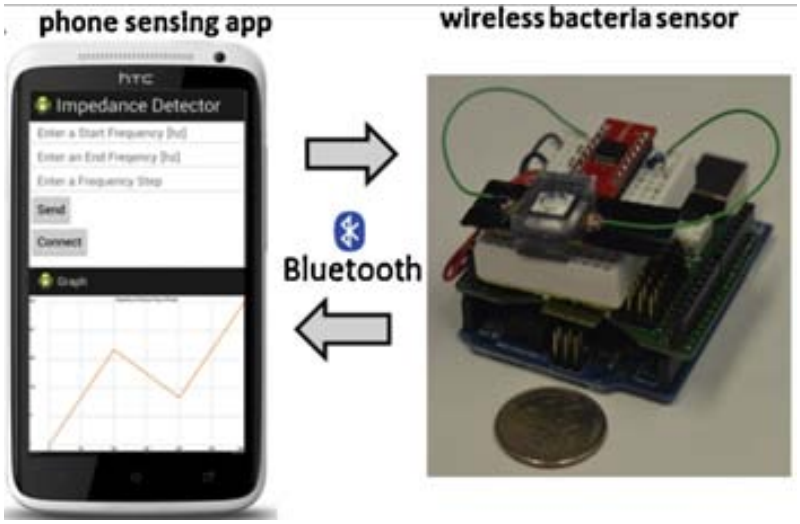

Figure 1.5: Amperometric sensor controlled by an smartphone, image from [JWC+14].

[IAMC02]. However, readout systems may be difficult to implement in such configuration.

1.2 Materials

Development in microfluidics and LOC systems can hardly be understood without a parallel improvement in fabrication technologies and building materials. IC and Micro Electro Mechanical Systems (MEMS) fabrication technologies are mainly based on silicon and glass technologies and not surprisingly, these two materials were the first ones used for implementing microfluidics channels [TJA+79]. Nonetheless, being limited to only these two technologies was a serious limitation for further development because of fabrication and material prices. Rapidly new materials and technologies arose, *e.g.*, polydimethylsiloxane (PDMS).

Nowadays, polymer materials and technologies are the most widely used in LOC systems, as can be seen in Figure 1.6 where use of PDMS as constituent material rapidly overcomes glass. Becker *et al.* [BG00] summarize the main features of polymers as follows: (*i*) low cost material, which is a key issue for many applications such as point of care (POC), biological or (bio)chemical analysis, where a disposable chip reduces con-

tamination risk; (*ii*) wide range of materials with different chemical and physical properties; (*iii*)several fabrication technologies for many different geometries, aspect ratios[1] and purposes, for example, mass production or rapid prototyping.

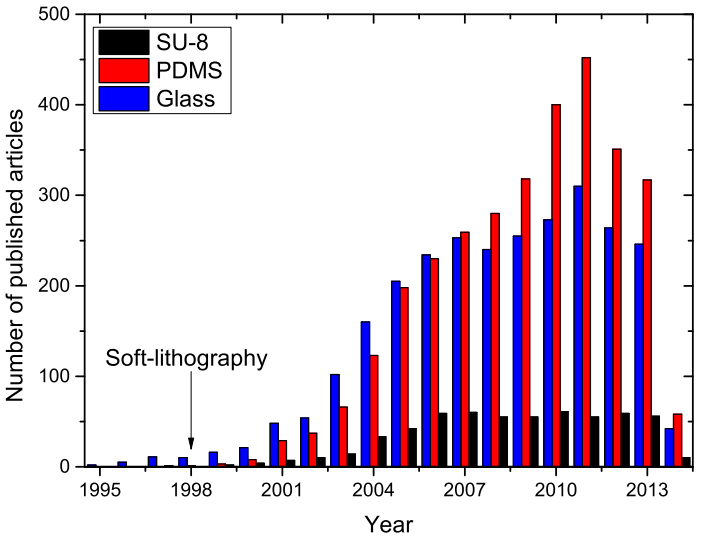

Figure 1.6: Total number of published articles on the topic of microfluidic build of SU-8, PDMS or Glass.

Nonetheless, each polymer is designed against an specific technology considering its most significant properties, namely:

Glass transition temperature (τ_g) It is determined by the molecular behaviour of the polymer chain. Below τ_g polymer behaves as a solid, amorphous glass, while over τ_g materials becomes soft and flexible.

Heat distortion temperature (HDT) Is an empirical parameter and describes the maximum temperature for structural use of the material.

[1]Aspect ratio is the ratio between height and width of the structure.

Decomposition temperature (τ_d) At this temperature the polymeric chains are broken and the polymer decomposes, changing then the nature of the polymer itself.

As a function of τ_g, τ_d and mechanical behaviour, polymers can be separated in three groups:

Thermosets, often called resins, start the cross-linking, also known as curing, when they are heated or exposed to light. Once cured, the thermosets are hard and rigid and can not be reshaped. In fact, when a thermoset is heated up again it decompose or burn instead of melting due to proximity between τ_g and τ_d. A typical example is SU-8 photoresist.

SU-8 is a negative epoxy-photoresist and as such, SU-8's long molecular chains cross-link causing the solidification of the material when it is exposed to UV light (λ_{max} = 365 nm). SU-8 was first developed as protection mask for IC industries but due to its high aspect ratio, once cured SU-8 acquires a high physical and chemical stability achieving aspect ratios up to 20 [LCZ+04]. Nowadays is mainly used in MEMS.

Thermoplastics materials present large temperature difference between τ_g and τ_d, and can be reshaped simply heating them up again. Hot embossing and injection moulding fabrication techniques use thermoplastics and will be explained later. Typical examples of thermoplastics are Poly(methyl methacrylate) (PMMA), Polycarbonate (PC), Polypropylene (PP), Polystyrene (PS), Polyethylene terephthalate (PE), Polyether ether ketone (PEEK), Polyimide (PI), Cyclic Olefin Polymer (COP) and Cyclic Olefin Copolymer (COC).

Elastomers are polymers with an elastic elongation of at least 200%. Their molecular chains do not show chemical but physical interactions. For this reason elastomers are mixed with a curing agent that creates 3D chemical bonds. Polydimethylsiloxane (PDMS) is one of the most used elastomers in academia and rapid prototyping processes.

In table 1.1 the most used polymers with their main physical properties are detailed. As it can be seen, polymers offer a great range of τ_g,

from -213 to 410°C, and HDT, from 70 to 400°C. Nonetheless, it is difficult to obtain polymers with RI lower than 1.4. In fact, the theoretical lower refractive index (RI) limit of a polymer is 1.29 [GZ91], only achieved using "construction plans" for low index polymers. Then, is difficult to work with polymers with a RI lower than water, avoiding use of water or culture medium as waveguide.

Table 1.1: Most used polymers with their main physical properties

Name	Density (g/cm^3)	τ_g (°C)	HDT (°C)	RI
PMMA	1.19	110	90	1.492
PC	1.19 - 1.24	148	125	1.58 - 1.6
PP	0.9	0 - 10	100 - 110	1.49
PS	0.9 - 1.24	100	70	1.59
PE (LD/HD)	0.91 LD - 0.967 HD	110 - 140	80 - 100	1.51 LD
COC	1.02	78	170	1.53
COP	1.01	138	140	1.525
PEEK	1.3	143	250	-
PDMS	1.03	-120	200	1.42
SU-8	1.19	210	-	1.58
PI	1.42	360 - 410	400	1.7

1.3 Photolithography

Photolithography is the basic process of IC fabrication industry and it is based on two main steps. Firstly, a photoresist is spinned over the wafer. Then, it is exposed to light under a Cr/glass mask that blocks the light under Cr regions. With negative photoresists, ultraviolet (UV) exposure cross-link the resist and harden it while in positive one the UV light degrades the resist and soften the material. Soft regions are eliminated simply developing the photoresist with specific chemical reagent. At this point the photolithographic process is ended. After that, the desired process over the wafer, *e.g.*, etching, implantation, metallization, etc. is applied. The regions of the wafer without photoresist are exposed to the process and then modified, while the shielded regions remain unaltered. Repeating these basic steps the substrate is modified in complex multilayer chip.

However, photolithography is a wavelength-dependent process, hampering resolutions below diffraction limit, and it has limited tolerance to nonplanar topography. Even though there are ways to overcome these drawbacks, *e.g.*, phase-shifting masks [LVS82], X-ray [AM89], Electron-beam [Hei73], Ion-beam [BVW81] and Scanning probe [MS96] lithographies among others, these alternatives are expensive, do not allow 3D structures and some of them are serial process. Holographic lithography [BD90] and stereolithography [IH93] offer alternatives to create 3D structures but technological requirements are substantially stronger than standard photolithography.

1.4 Non-UV Fabrication Technologies

Several fabrication techniques are available to shape polymers and an overview of them *i.e.*, hot embossing, injection moulding, laser micromachining and soft-lithography [XW98], is detailed below. In order to provide a clear view of differences between the fabrication techniques, the main properties are compared in table 1.2. As it can be seen, contact methods are the ones with best resolution and also these that provide parallel process. On the other hand, the need of a master limits the possible geometries.

Table 1.2: Polymer microfabrication technologies

Technology	Master		Resolution	Production
	Durability	Price		
Hot embossing	+++	€€€	$\sim$ 10 nm	Parallel process
Injection Moulding	+++	€€€	$\sim$ 10 nm	Parallel process
Laser Micromachining	Maskless		$\sim$ 100 nm	Serial process
Soft-lithography	++	€	$\sim$ 10 nm	Parallel process

Hot embossing and injection moulding are the most used fabrication techniques for mass production. Both of them are restricted to thermoplastic materials and their working principle is based on heating the thermoplastic over its τ_g and reshape it by applying pressure. Hot embossing generally uses and hydraulic press with a couple of heaters in each side to increase the temperature of the thermoplastic. An schematic example can be seen in Figure 1.7. Contrary, injection moulding usually use ther-

moplastic granules transported through a heater until the material melts and is injected into the mould cavity.

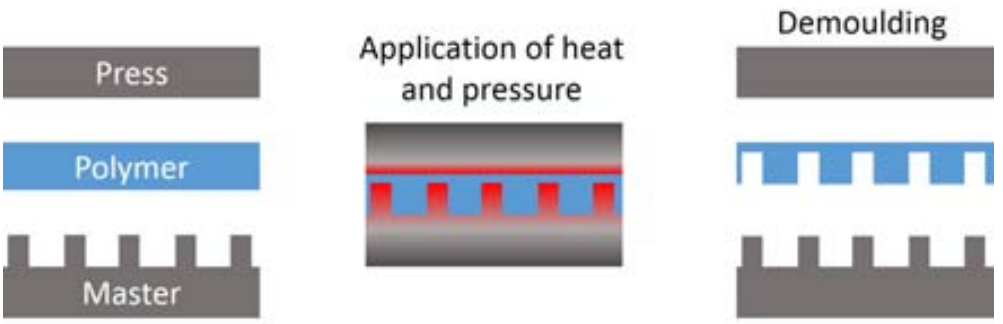

Figure 1.7: Schematic representation of a hot embossing process

Hence, masters should withstand high pressures and temperatures over many repetitions. The master cannot has undercuts and also, an antiadherent layer over it is desirable in order to facilitate the posterior replica demoulding. Masters used in hot embossing and injection moulding typically are fabricated *via* lithography, electroplating and moulding process (LIGA), usually with X-ray lithography, in order to obtain a final metallic master. These masters are expensive but allow a parallel process reducing the overall cost of the final devices when used in mass production. In other words, these fabrication techniques can achieve good production costs for mass production, but are extremely expensive for rapid prototyping. However, is good to keep in mind the fabrication limitations of mass production technologies, *i.e.*, no flanges, to ease the step when moving from prototypes to larger production quantities.

Laser micromachining is a maskless technology and can pattern most of polymers, glass or silicon in 3D structures. Moreover, this fabrication technique could be used to micromachine either the final device (in a serial process) or a master for a posterior, parallel process. However, it is a serial process with typical scan speed below 1 mm/s[SWT+06] and the fabrication of a single device could take from minutes to days, depending on the total dimensions as well as the resolution. Additionally, laser micromachining usually increase surface roughness, complicating the integration of optical structures on the final device, and can even change surface chemistry and surface charge [JRGL01, PTC+02].

Soft-lithography, which is the most published fabrication technique

for LOC systems, needs a master but, contrary to previously detailed methods, the master is not exposed to high pressures or temperatures, simplifying the production and reducing the costs. Moreover, the master can be build using photolithography, in a very short period ($\sim$ 1 day) and with both, low roughness and high aspect ratios. Furthermore, the master withstand several replica process (depending on master and replica materials) and the replicas can be done in less than 20 min. The replica is usually made with elastomeric materials and three dimensional structures can be achieved defining several layers [CHC+10].

1.4.1 Soft-lithography

Fabrication of polymer-based LOC systems started with SU-8. In 1995 Lee et al. [LLR+95] reported the first exhaustive study of SU-8 properties to use it as constituent material for MEMS due to its high aspect ratios (> 20) [LCZ+04].

While the microfabrication of ICs is based on standard photolithography and several photoresist are used, in fabrication of polymer LOC systems SU-8 is practically the only photoresist used. This circumstance is due to SU-8 properties: photosensitivity, biocompatibility [NMB+13], transparency in the UV-NIR range [PB09] and mechanical properties [LDF+97].

On 1998, Xia et al. [XW98] changed the fabrication technology reporting a series of fabrication techniques, *i.e.*, microcontact printing (µCP) [KW93], replica moulding [XKZ+96], microtransfer moulding (µTM) [ZX96], micromoulding in capillaries (MIMIC)[KXW95], solvent-assisted micromoulding (SAMIM) [KXZW97], phase-shift photolithography [RPJW97] and cast moulding [TMB+96], with common features: Inexpensive, no need of photosensible materials and allow replication size much smaller than optical diffraction limit. Rapidly this strategy, called soft-lithography, became the predominant in fabrication of LOC systems.

Soft-lithography techniques are optimized to use elastomeric materials instead of thermoplastics avoiding heat and pressure treatment and then reducing the master requirements. From all polymers, PDMS arises as the most used one principally for its physico-chemical properties and low-cost. PDMS consist of a base elastomer and a curing agent that has to be mixed to obtain the final polymer. It is transparent in the whole visible spectrum [CNKH08], it is permeable to gases [LES96, DM98, WLX+06],

hydrophobic and biocompatible [LSF04, NTC+09], and thus, is a perfect candidate for LOC devices and specially for biological applications *e.g.*, cell cultures. Since then, LOC systems and microfluidic platforms have become an important research topic with several specialized journals edited, *e.g.*, *Lab on a Chip*.

1.5 Detection mechanisms

From the beginning of LOC systems, miniaturization of detection mechanisms are one of the main stumbling blocks to solve. Although analyte transportation and handling are miniaturized with great efficiency, it is not the case for the vast majority of detection mechanisms. Among chemical sensors, the International Union of Pure and Applied Chemistry (IUPAC) differentiate 7 kinds depending on the operation principle of the transducer [HGI91]: Optical, electrochemical, electrical, mass sensitive, thermometric and others.

Over these transduction mechanisms two of them, electrochemical and optical, are the most used in LOC applications.

Electrochemical detection is defined by the IUPAC as [MW06]:

"A method in which either current or potential is measured during an electrochemical reaction. The gas or liquid containing the trace impurity to be analysed is sent through an electrochemical cell containing a liquid or solid electrolyte and in which an electrochemical reaction specific to the impurity takes place".

Electrochemical detection could be divided in three main branches,

Potentiometry A detection method in which the potential of a cell is related to the concentration (activity) of a reactant which is a component of the cell fluid.

Amperometry A detection method in which the current is related to the concentration of the species generating the current.

Coulometry A detection method in which the current is directly proportional to the flow rate of the substance involved in the electrochemical reaction, and the amount of charge which flows is proportional to the amount of substances taking part in the reaction.

There is a group of features common on the three main branches. Among them, some are very interesting for LOC *e.g.*, electrochemical detection is highly integrable, has fast response times and high sensitivity, but some of the features are drawbacks to avoid *e.g.*, electrochemical detection depends on the electrode area, the sample generally needs to be electrochemically active, requires electrodes (usually metallics) and is limited to interface detection. These restrains limits electrochemical detection applicability in LOC.

On the other hand, optical detection offers faster response, is non-invasive, may detect either in surface or in bulk depending on the method and does not require electroactive analytes. Moreover, optical sensors can use several optical properties as tranduction mechanism in chemical sensors [HGI91]:

absorbance, measured in a transparent medium (material that allows light to pass though without being scattered), caused by the absorptivity of the analyte itself or by a reaction with some suitable indicator.

reflectance is measured in non-transparent media, usually using an immobilized indicator.

luminescence, based on the measurement of the intensity of light emitted by a chemical reaction in the receptor system.

fluorescence, measured as the emission effect caused by irradiation. Also, selective quenching of fluorescence may be the basis of such devices.

refractive index, measured as the result of a change in solution composition. This may also include the surface plasmon resonance effect.

optothermal effect, based on a measurement of the thermal effect caused by light absorption.

light scattering, based on effects caused by particles of definite size present in the sample.

In (bio)chemical applications at the macroscale, the most used methods are fluorescence, specially used in biology, and absorbance mostly used in chemical analysis.

However, albeit many Ph-LOCs have been reported, usually bulky optical equipments, such as microscopes, are used. While it is true that some macroscopic optical components such as lenses [QHW+10] or filters [BA11] have been miniaturized without any design changes, the technologies used to build and integrate these reduced optical elements in LOC are expensive and time consuming due to the non-automatized, precise alignment work needed, increasing the final cost of the chip and hence limiting its use as disposable system for *in situ* (bio)chemical analysis.

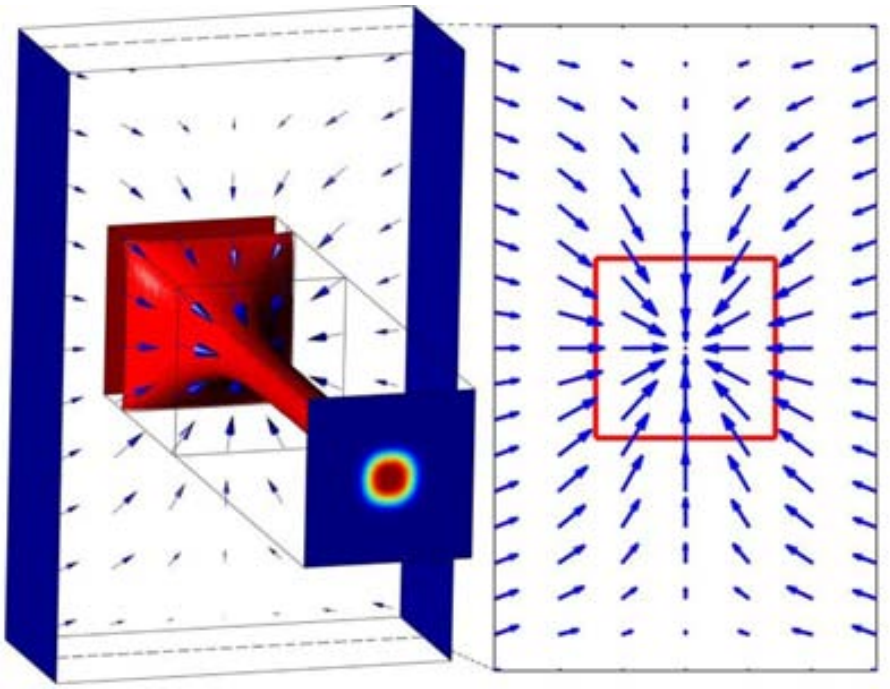

Figure 1.8: schematic representation of an L^2 waveguide using 3-dimensional hydrodynamic flow focusing [TB12].

In order to maximize the integration and miniaturization of optical components, a complete redesign of the optical elements is often desirable. Optofluidic systems integrates these modified optical elements and often changes the fluidic parts of LOCs to play an optical role within the device. For instance;

- Liquid-core liquid-cladding (L^2) waveguides, where the hydrodinamic focusing of two liquids with different refractive index is used

to produce the waveguide [TB12]. In Figure 1.8 a 3D flow focusing of a high refractive index liquid is used to create an L^2 waveguide.

- Tunable lasers, where the elastic properties of PDMS are exploited to change the size of the laser cavity increasing or decreasing the pressure [SP10].
- Optical filters, where anti-resonant reflecting optical waveguide (ARROW) is used to demultiplex excitation and emission wavelengths [MPC+11].
- Tunable lenses, that uses several different mechanism [DABJ06, LL07, Ngu10] to control shape of the lenses.
- Fabry-Perot interferometer, based on the change of the polymer size due to sample absorption [SGMS+13].
- Mach-Zehnder interferometer, where ARROW configurations are exploited [THS+10].
- Optical switches, where L^2 waveguide thickness is modified to steer the light to a concrete output optical channel [SLL09].
- Optical routers, where air bubbles are thermically created to act as air mirrors have been reported using fluids to play an active role on the optical performance [Fou00].

However, most of the optofluidic devices do not integrate a complete set of optical elements *i.e.* waveguides, lenses, filters, light sources, etc., due to the specific and non-standard technologies used in the fabrication of each one of the single optical elements, impeding the integration of several of them in a single LOC.

Therefore, the challenge to build a complete, low-cost, disposable, highly-integrated and highly-sensitive optofluidic device for (bio)chemical analysis still remains and will be addresses in this Thesis.

2 | Fundamentals

In this chapter, an explanation of the theoretical background about optics, fluidic and mathematical analysis relevant for this thesis is detailed.

2.1 Optics

In this section, physical laws that rules the light behaviour used in this thesis are detailed. Firstly, Snell's law, which relates light behaviour when changes its propagation medium and how this conduct can be exploited to create lenses using the Lensmaker's equation. Secondly, Lambert-Beer's law, which relates light absorbance in a medium with the optical path and concentration and an application of this demeanour to create optical absorbance filters.

2.1.1 Snell's Law

Law of refraction or Snell's law has its name after who proposed it, Willerbord Snel van Royen in 1621. It is used for almost any optical design and is the base of ray tracing simulations software. It is noteworthy mentioning that Snell's law can only be applied in isotropic materials, such as glass, water or air. In the present thesis Snell's law is used to design air mirrors, waveguides and lenses.

Snell's law can be expressed as:

$$n_1 \sin \beta_1 = n_2 \sin \beta_2 \tag{2.1}$$

where β_1 is the angle between the incident light beam and the interface surface normal, β_2 is the angle between the refracted light beam and the interface surface normal, n_1 is the RI of the medium 1 and n_2 is the RI of medium 2. In Figure 2.1a an incident light beam propagates

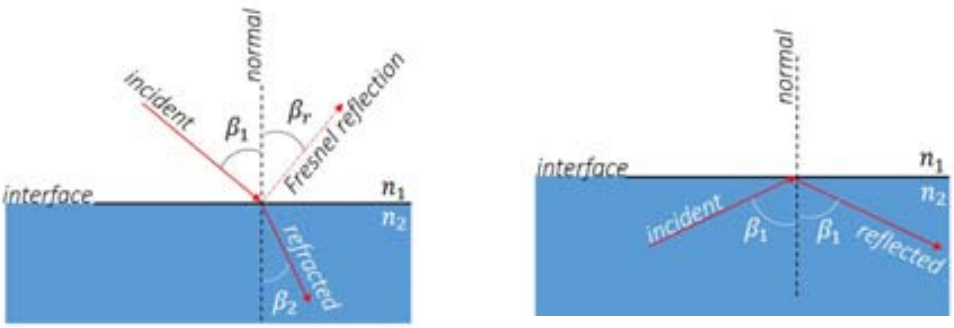

Figure 2.1: Schematic representation of (a) refracted and (b) reflected light beams ($n_1 < n_2$).

into a low RI material, reaches the interface of a second material with higher RI. Then a fraction of the incident light is transmitted. This fraction is determined by Fresnel coefficients, which predicts the fraction of the incident power that is refracted, from the interface, given by the transmittance, T, and, without absorbance, the fraction that is reflected, defined as $1 - T$. Fresnel coefficients are polarization dependent. As a numerical example, when non-polarized incident light moves between an air/glass interface the typical ratio of transmitted light is $T = 0.96$.

When light propagates from a medium with higher RI, n_2, to a medium with lower RI, n_1, represented in Figure 2.1b, there is an angle, called critical angle ($\beta_c = \arcsin \frac{n_2}{n_1}$), at which the light is no longer refracted. For incident angles bigger than critical angle the light undergoes total internal reflection (TIR) condition and the interface behaves as an specular mirror (Figure 2.1b). TIR situation is widely used in this thesis and TIR conditions will be exploited in many different systems.

Sandwiching a high RI between two low RI materials a waveguide, being the most well known the optical fibre. They only propagate light that reach the fibre within a certain range of angles that ensure TIR condition in the core-cladding interface, forming the acceptance cone. In Figure 2.2 an schematic representation of an optical fibre with the maximum acceptance angle, $\beta_{\max}$, is detailed.

Acceptance cone of a fibre depends on the refractive index contrast between fibre core and cladding and it is characterized by the numerical aperture, NA. Numerical aperture is a dimensionless parameter defined

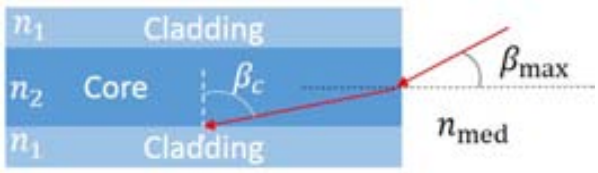

Figure 2.2: Schematic representation of an optical fibre acceptance cone.

as,

$$NA = n_{\text{med}} \sin \beta_{\max} = \sqrt{n_2^2 - n_1^2}, \tag{2.2}$$

where n_{med} is the refractive index where the fibre is immersed in, typically air, $\beta_{\max}$ is the maximum angle of the acceptance cone, n_2 is the RI of the optical fibre core and n_1 is the RI of the optical fibre cladding. When optical fibres are immersed in air, $n_{\text{med}} = 1$, NA have a clear geometrical interpretation, $NA = \sin \beta_{\max}$, and for typical acceptance cone, where $NA < 0.5$, $NA \approx \beta_{\max}$.

2.1.2 Lensmaker's equation

Before any other consideration, a detailed description of lens geometry is needed. In order to illustrate the lenses geometry, a schematic representation of a biconvex lens with the main parameters of the system is detailed in Figure 2.3. The object at the left-hand side produce and amplified image at the right-hand side. The main parameters to be considered are: The curvature radius of the lenses, R_1 and R_2, the lens thickness, d, the lens refractive index, n_l, the focal length, f, the first focal point, F_0, the second focal point, F_i, the first principal point, H_1, the second principal point, H_2, and the distance between the object and the lens interface, s_0, and between the lens interface and the image, s_i.

In the particular case of a lens immersed in air the equation to determine the focal length of a lens can be written as,

$$\frac{1}{s_0} + \frac{1}{s_i} = \frac{1}{f}. \tag{2.3}$$

The focal length can also be rewritten [Hec01] as,

$$\frac{1}{f} = (n_l - 1) \left[\frac{1}{R_1} - \frac{1}{R_2} + \frac{(n_l - 1)d}{n_l R_1 R_2} \right]. \tag{2.4}$$

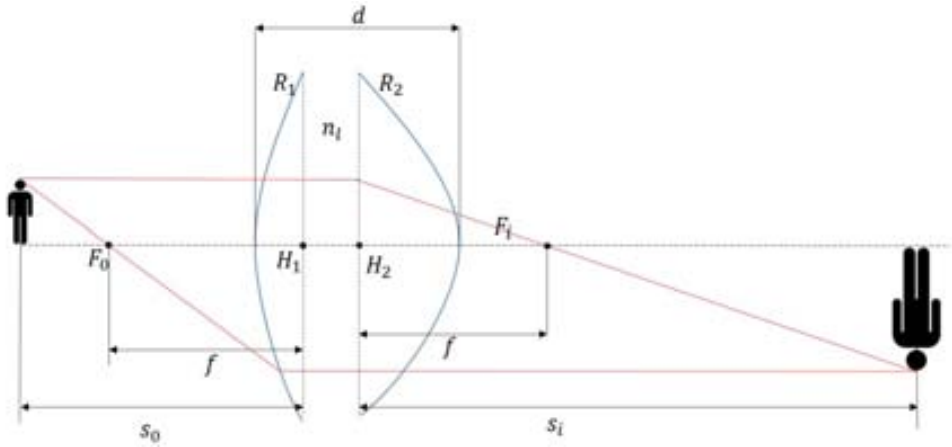

Figure 2.3: Schematic representation of lens parameters.

With equations 2.1 and 2.4, the tools to determine a complex systems with several interfaces are ready. This equations are used in ray tracing software to simulate complex optical systems behaviour.

2.1.3 Lambert-Beer's Law

Lambert-Beer's law relates light absorbance with the analyte concentration and the interrogation length. It is specially relevant in both, detection mechanisms and interrogation region.

When light propagates through any material four different physical mechanisms may be responsible of a measured decrease in light intensity; (*i*) reflection, (*ii*) interference, (*iii*) scattering and (*iv*) absorption. In order to focus on absorption itself some assumptions have to be made. Assuming normal incident light towards an isotropic and homogeneous sample, with no particles on it, reflection and scattering have a negligible role. Furthermore, interference for standard non-coherent light sources is only obtained with very precise equipments or very small system dimensions, typically of the light wavelength order. In this case the interference contribution may be neglected. Hence, assuming this, intensity variations are only due to absorption.

Absorbance is mathematically defined as:

$$A = \log \frac{I_0}{I_T} \tag{2.5}$$

where I_T is the transmitted light intensity and I_0 is the incident light intensity. Contrary, transmittance is the light that reaches the second point respect to the light at the first point, mathematically:

$$T = \frac{I_T}{I_0} \rightarrow A = -\log T \tag{2.6}$$

Lambert-Beer's law states that absorbance can be expressed as:

$$A = \varepsilon C \ell \tag{2.7}$$

where C is the sample concentration, ℓ is the distance the light travels through the material, *i.e.*, the path length, and ε is the molar absorptivity. The SI units for ε are m^2/mol and is an intrinsic property of the material experimentally determined.

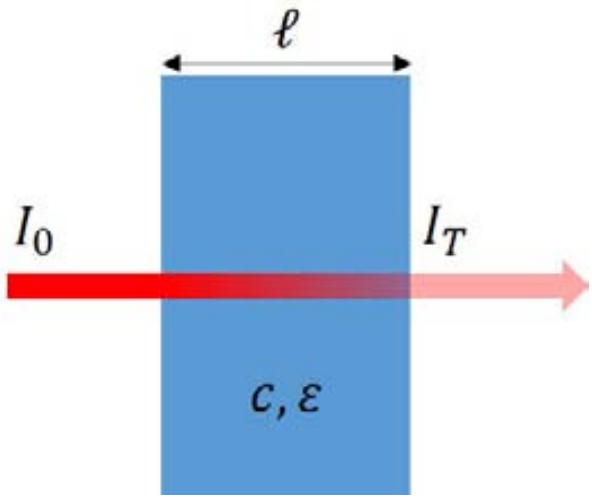

Figure 2.4: Schematic representation of the Lambert-Beer's law parameters.

It is important to emphasise that, for a given substance, absorbance only depends on the path length and the substance concentration (Figure 2.4). Thus, for a given LOC design (fixed ℓ), absorbance will only depend on the sample concentration.

2.1.4 Optical Filters

Using the Lamber-Beer's law several absorbance filters are developed along the thesis. An absorbance-based optical filter is usually a trans-

parent material, typically glass, doped with coloured compounds that absorb certain wavelengths while transmitting others.

Blocked wavelengths are placed on the stopband of the filter, T_s, while transmitted ones are on the passband, T_p. Depending on whether stopband absorbs short, long or central wavelengths, the filters can be classified as, longpass, shortpass and bandpass, respectively. In Figure 2.5 a transmittance graphic of these filters is detailed. In this theoretical representation, the longpass band filter absorbs, almost perfectly, wavelengths under 500 nm while transmits 99% of the light at wavelengths over 600 nm. The shortpassband absorbs wavelengths over 600 nm and transmits under 500, and the passband transmits between 500 and 600 nm and absorbs the rest of the spectrum. In bandpass filters, bandwidth is a relevant characteristic, and is defined as the range of frequencies or wavelengths at which the intensity value is less than 3 dB below the maximum.

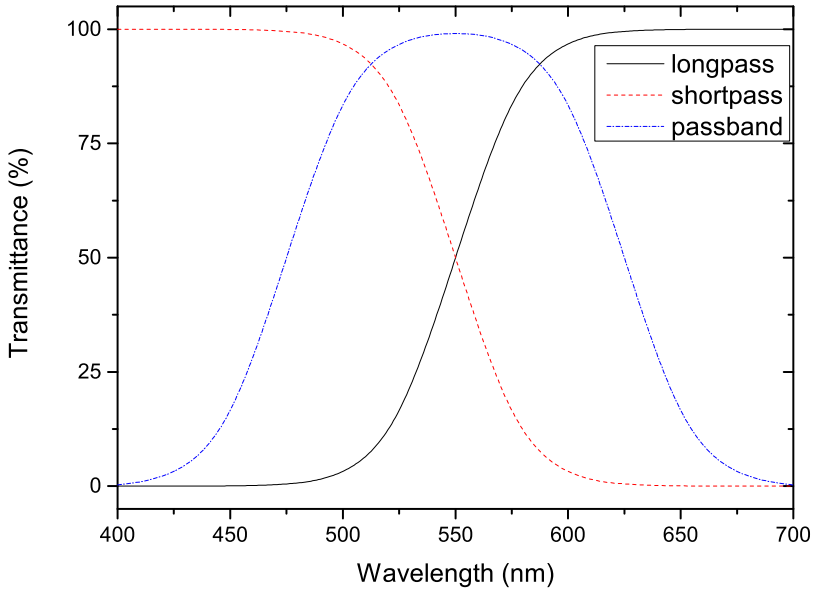

Figure 2.5: Transmittance as a function of the wavelength for theoretical longpass, shortpass and passband filters in the visible region.

2.2 Microfluidic

In this section an overview of the main characteristics of liquids constrained to micrometric scale, also known as microfluidics, will be detailed as well as two different techniques for liquid control, microdroplets and phaseguides.

Navier-Stokes equation describe the motion of a Newtonian fluid in the absence of free surfaces as follows[Tab05]:

$$\frac{D\boldsymbol{u}}{Dt} = -\frac{1}{\rho}\nabla p + v\Delta\boldsymbol{u} + \frac{1}{\rho}\boldsymbol{F}, \tag{2.8}$$

where bold letters represent vectors, $\boldsymbol{u}$ is the fluid velocity, v is the kinematic viscosity, ρ is the density, p is the pressure and $\boldsymbol{F}$ is the external force per unit volume. In order to solve this equation it is useful to introduce the Reynolds number, defined as:

$$\mathrm{Re} = \frac{ul}{v}, \tag{2.9}$$

where l is the typical channel width. At micrometric scale the typical flow velocity do not exceed $\sim$cm/s and their dimensions are on the order of tens of micrometers. At this scale the Reynolds number is very small ($\mathrm{Re} \ll 1$). There are some exceptions of microfluidic channels with bigger Reynolds number [WYZ14] and are not considered in this thesis.

Assuming incompressible fluids, Navier-Stokes equation (eq. 2.8) at low Reynolds number can be simplified as the Stokes equation:

$$-\frac{1}{\rho}\nabla p + v\Delta\boldsymbol{u} + \frac{1}{\rho}\boldsymbol{F} = 0. \tag{2.10}$$

The flows governed by the Stokes equation have two important properties [Tab05]:

Reversibility, changing the time direction does not affect the solutions or, in other words, the flow will behave identically forwards and backwards.

Uniqueness, the Stokes equation solution is unique. Hence, there can not exist bifurcations or turbulences. Consequently, the mixing process at laminar flow is a diffusion process.

It is important to remember that these properties only apply in the absence of free surfaces. Hence, working with free surface, one can avoid these restrictions. In the present thesis two different microfluidics tools, phaseguides and monodisperse microdroplets, are used to avoid these restrictions.

2.2.1 Phaseguide

At the edge of the propagating liquid (free surface) a meniscus is observed. There are two different kind of meniscus, convex and concave, depending on the liquid and the material of the walls (Figure 2.6a).

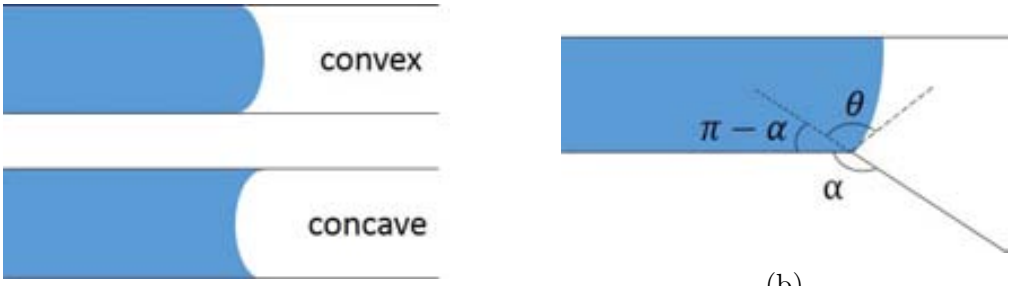

(a) (b)

Figure 2.6: Top view of fifferent meniscus shapes with (a) typical shapes, concave and convex, and (b) shape produced due to pinning on a convex edge.

However, when the geometry of the channel changes, the meniscus shape may vary. This phenomenon occurs when an edge on the channel appears, see Figure 2.6b. The meniscus behaviour is radically different when the edge shape is concave or convex [GW05]. In the convex case the meniscus stops at the edge and more pressure has to be applied to enable movement. This is called meniscus pinning effect. In a concave edge the liquid tends to flow along the edge.

Using this behaviour, passive microfluidics structures, called phaseguides, have been developed. Phaseguides are physico-chemical pressure barriers that increase the fluidic resistance in a delimited region of the chip, creating a passive valve. Vulto *et al.* [VMA+06] are the first to create this pressure barriers. They pattern 20 µm-thick strips of a dry film resist, Ordyl SY330, on the top [VMA+06] or bottom [VPM+11] of the

microfluidic channel. Chibbaro *et al.* [CCD+09] demonstrate, using computer simulations, that vertical edges produced by the phaseguides play the same role than convex edges in a channel. Accordingly to these simulations, when meniscus pinning effect is produced, the meniscus shape changes. In Figure 2.7a two situations can be seen. In dark black the meniscus moves over the phase guide leftwards with two liquid contact angles, θ_1 and θ_2, with the channel top and the phaseguide respectively and a liquid-air area A_{la1}. Once the meniscus reaches the phaseguide edge, it is pinned and starts to change its shape and contact angles, represented as the gray area, while the upper region still propagates, modifying contacts angles and liquid-air area A_{la2}.

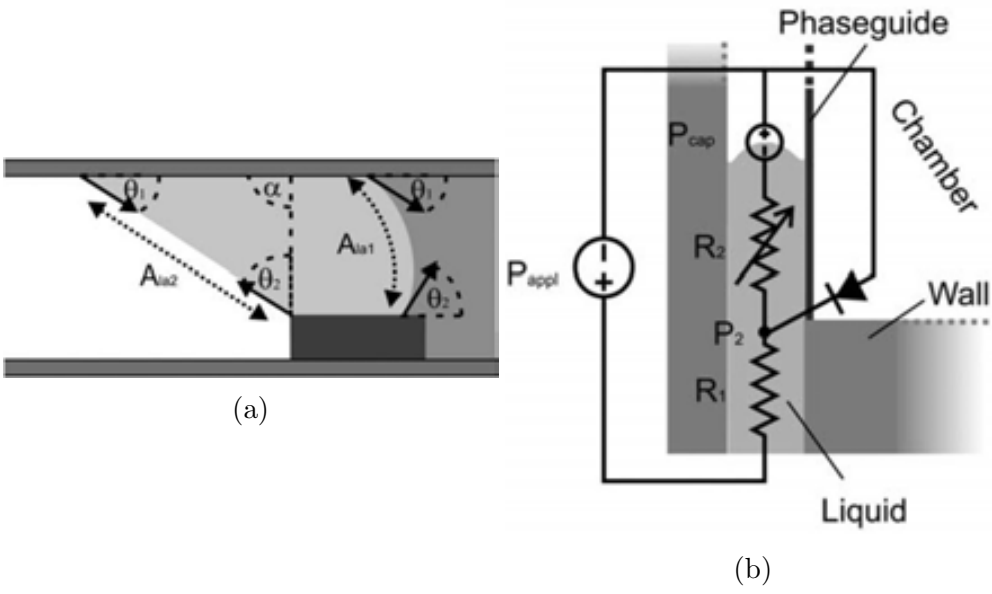

Figure 2.7: Schematic representation of, (a) a cross-section view of the phaseguide where the liquid flows perpendicular to the paper surface and, (b) top view of the pahseguide with the electronic circuit analogy, the fluid is moving upwards. Images reproduced from [VPM+11] with permission from the Royal Society of Chemistry.

Phaseguides generate a channel where the liquid flows. However, the channel is open and when a certain pressure threshold is achieved, the liquid overflows the phaseguides filling the next channel. In order to get a quantitative approximation, the analogy of an electric circuit can be used (Figure 2.7b). In this case the system is described by the following

equation:

$$P_2 = \frac{R_2}{R_1 + R_2} (P_{ap} + P_{ca}) - P_{ca} \tag{2.11}$$

where P_2 is the pressure at the expected overflow position, R_2 is the fluidic resistance from that point until the liquid-air meniscus, R_1 is the total fluidic resistance at P_2, P_{ap} is the applied pressure and P_{ca} is the capillary pressure of the air-liquid meniscus. Breaking pressure can not be theoretically determined but overflow will occur at the wall-phaseguide interface when P_2 is bigger than the experimental breaking pressure. Hence, overflow becomes more probable as liquid moves forwards along the channel. Accordingly to [GSSW03, KBMTD07, CCD+09, VPM+11] the spontaneous overflow occurs when:

$$\theta_1 + \theta_2 > \pi - \alpha \tag{2.12}$$

where θ_1 and θ_2 are the contact angles with the top and the phaseguide respectively, α is the angle between the vertical side of the phaseguide and the horizontal top surface. For rectangular phaseguides, where $\alpha = \pi/2$,

$$\theta_1 + \theta_2 > \pi/2 \tag{2.13}$$

Figure 2.8: A diagonal phaseguide to produce controlled overflow in an specific region.

Using equation 2.12 and designing the phaseguide to form certain angles with the channel walls (Figure 2.8) it is possible to precisely control the point along the phaseguide where the overflow will occur.

2.2.2 Monodisperse Microdroplets

Compartmentalization, extremely low chemical reagents consumption and high-throughput analysis make monodisperse microdroplets an excellent strategy for LOC.

Monodisperse microdroplets are emulsions with constant droplet size ($< 1\%$ size variation). Typical droplet diameter is $\sim$50 µm, obtaining volumes of $\sim$ 65 pl. Moreover, droplet generation rates of few kHz are easily achieved. This high speed generation rates of picoliter compartments allow high-throughput analysis, providing excellent statistical results. Compartmentalization and high-throughput provide a unique platform for (bio)chemical analysis. For instance, Hofmann *et al.* [HHJ$^+$12] use osmosis-driven change in droplet size as a quantitative and label-free marker for reactions inside droplets. Furthermore, droplets have been widely used for single-cell analysis [JA12, DUB$^+$12, SKWvdB13].

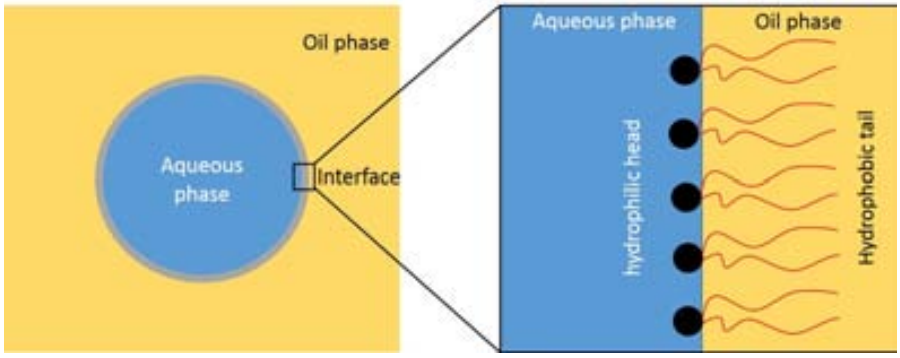

Figure 2.9: Schematic representation of a water droplet in oil phase with surfactant.

In this thesis microdoplets are formed as water-in-oil emulsions but most of the theory can also be applied for oil-in-water emulsions. The physical droplet formation mechanism is based on at least two streams, aqueous and oil, merging in a junction. By surface tension, the interface tends to minimize, adopting an spherical shape, whereas viscous stress drags the interfacing region away generating the droplets jet.

Water-in-oil emulsions are metastable and droplets tends to coalesce with a characteristic lifetime [TCS$^+$10]. Lifetime is determined by the external conditions *e.g.*, temperature, humidity or volume of the sample, and the stabilizing properties of the used surfactant, ranging from

sub-milliseconds to years. Surfactant are typically molecules with an hydrophilic head and a hydrophobic tail which creates a stabilizing layer on the water-oil interface (Figure 2.9). Choosing the surfactant characteristics one may change the droplets properties. For instance, long fluorocarbon tails such as perfluorinated polyethers (PFPE) provide longer lifetimes [ZTI04], whereas short fluorocarbon tails such as polyethylene glycol (PEG) are biocompatible [CTLB$^+$08]. Therefore, using an specific combination of surfactants the droplet properties can be precisely tuned.

3 | Materials and Methods

In this chapter, an exhaustive description of chemical reagents, simulations, fabrication techniques, equipments and set ups used during the thesis are detailed.

3.1 Chemical Reagents

In this section a list of the chemical reagents used along the thesis can be found.

a) LOC fabrication,

- SU-8 2005, MicroChem Corp., (USA)
- SU-8 2025, MicroChem Corp., (USA)
- SU-8 2050, MicroChem Corp., (USA)
- Poly(dimethylsiloxane) (PDMS), sylgard 184 silicone elastomer kit, Dow Corning, (USA)

b) Doping materials,

- Pelikan red 1 4K351 221, Pelikan S.A., (Spain)
- Pelikan blue 1 4K351 213 Pelikan S.A., (Spain)
- Pelikan green 1 4K351 239 Pelikan S.A., (Spain)
- Toluene, Sigma-Aldrich Química S.A. (Spain)
- quinoline yellow 234133, Sigma-Aldrich Química S.A. (Spain)
- phenol red 32661, Sigma-Aldrich Química S.A. (Spain)
- crystal violet C6158, Sigma-Aldrich Química S.A. (Spain)

- Atto 390, Atto-Tec GmbH (Germany)
- Dimethyl sulfoxide (DMSO) D9170-1VL, Sigma-Aldrich Química S.A. (Spain)
- phenyltrimethoxysilane (PhTMOS), Sigma-Aldrich Química S.A. (Spain)
- Hydrochloric acid 258148, Sigma-Aldrich Química S.A. (Spain)
- Sodium chloride S1679, Sigma-Aldrich Química S.A. (Spain)
- Potassium chloride 746436, Sigma-Aldrich Química S.A. (Spain)
- Calcium chloride 499609, Sigma-Aldrich Química S.A. (Spain)
- Potassium dihydrogen phosphate, Panreac (Spain)
- Disodium hydrogen phosphate, Panreac (Spain)

c) Droplet generation,

- 3M^{TM} Fluorinert^{TM} Electronic Liquid FC-40 (FC-40)
- 3M^{TM} Novec^{TM} 7500 Engineered Fluid (HFE-7500)
- Fluorescein 46955, Sigma-Aldrich Química S.A. (Spain)
- Bromothymol blue 114413, Sigma-Aldrich Química S.A. (Spain)
- Aquapel, Pittsburgh Glass works (USA)

d) Biological applications,

- d-Glucose G0350500, Sigma-Aldrich Química S.A. (Spain)
- L-(+)-Lactic Acid, Sigma-Aldrich Química S.A. (Spain)
- 2,2'azino-bis (3-ethylbenzthiazoline-6-sulfonic acid) (ABTS), Sigma-Aldrich Química S.A. (Spain).
- lactate oxidase (LOX), E 1.13.12.4, Sigma-Aldrich Química S.A. (Spain)
- glucose oxidase (GOX), E.1.1.3.4, Sigma-Aldrich Química S.A. (Spain)
- horseradish peroxidase (HRP), E 1.11.1.7, Sigma-Aldrich Química S.A. (Spain)

– Rat serum samples, Obese Zucker rats and their littermate controls, lean Zucker rats (Charles River Laboratories, Barcelona, Spain) are fed standard diet and water adlibitum. At 28 weeks old, animals are kept during 12 h fasting and are anesthetized with chloral hydrate 12% intraperitoneally. Blood samples are collected by intracardiac puncture for biochemical assays in serum. The protocol for animal handling and experimentation agreed with the European Union European Community guidelines for the ethical treatment of animals (EEEC Directive of 1986; 86/609/EEC) and is approved by the Ethical Committee for Animal Research of the University of Seville.

  Rat serum samples are obtained from blood by centrifugation for 20 min at 4,000 rpm and room temperature.

3.2 Optical Simulations

Different software simulation tools have been used during the thesis. All of them are based on ray tracing.

Auto CAD The master layout is realized using computer-aided design (CAD) software. The design is limited to closed polylines with less than 200 points in order to allow file format conversion to gds file extension. File conversion is need to create the Cr/glass Mask used to define the master through a UV-photolithographic process.

Oslo Edu is a relatively simple free ray tracing software that is specially useful for lenses design. However, Oslo Edu has a maximum limit of 10 interfaces and do not allow to simulate 3-D structures. Oslo Edu has been used for cylindrical lenses simulations.

Trace Pro/Zemax are much more robust software that has no interfaces limit, allow fluorescence analysis and 3D structures imported directly from a CAD software. These softwares are used for optically complex structures, such integrated emitters and the fluidically controlled router.

Simulation and design are iterative processes where, after simulation results, the LOC is redesigned and simulated again until we obtain the desired behaviour.

3.3 Fabrication

In order to built an optofluidic system several fabrication processes are required. Soft-lithography is divided in two main steps. Master fabrication and replication. Master fabrication is usually defined using an standard UV-photolithography with SU-8 as photoresist, without neglecting other techniques or materials. Once the master is defined the replication can be easily done in an inexpensive parallel process. Among the different replication techniques that soft-lithography offers, we use two of them, replica moulding [XKZ+96] and MIMIC [KXW95]. In this section they both are explained in detail, as well as the experimental parameters used to fabricate them.

3.3.1 Master fabrication

All the masters needed for this thesis have been done using the same process, UV-photolithography, with only minor changes to obtain different number of layers and thicknesses. In Figure 3.1 an step by step master fabrication scheme can be observed. The main processes for every layer are spinning, soft-bake, exposure and post exposure bake (PEB). These are repeated for every master layer.

Master fabrication starts with a silicon or glass wafer dehydrated during 10 min at 200°C in an oven. First layer is called seed layer. In order to create the seed layer the wafer is placed in a spinner and a drop of SU-8 2005 (MicroChem, Newton, MA) is poured on the centre of the wafer. After that, the spinner accelerates up to 400 rpm during 15 s in order to planarize this first layer. Immediately afterwards, the spinner rises its speed up to 3000 rpm during 30 s to achieve a final SU-8 thickness of 5 µm. Once the photoresist is uniformly distributed, a soft-bake is applied to harden the SU-8 and evaporate its solvents. Soft-bake consists of a thermal bath during 13 min with temperature rising from 65°C to 95°C. Afterwards, a flood exposure, *i.e.*, a non-patterned exposure of the whole wafer to a UV light ($\lambda = 315$nm), with an insulation dose of 55 mJ/cm^2 is performed to activate SU-8 cross-linking. Finally, a post exposure bake (PEB) from 65°C to 95°C during 10 min is made. PEB step catalytically performs and finishes the photo-reaction initiated during exposure. Performed near the glass transition point of the SU-8 reduces mechanical stress formed during softbake. This step finishes the seed layer, repre-

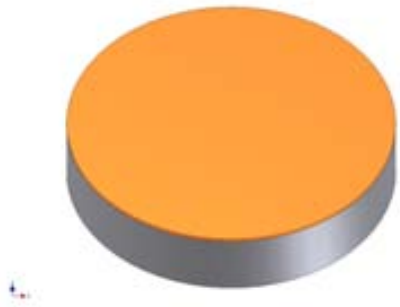

(a) Finished seed layer.

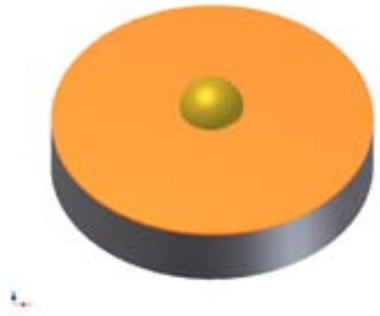

(b) SU-8 drop over the seed layer.

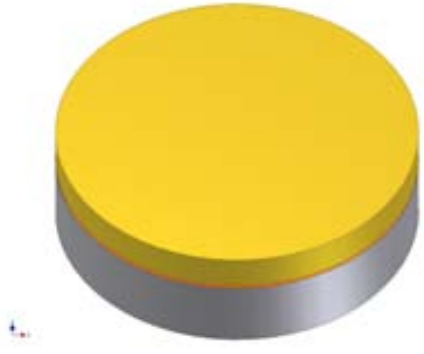

(c) SU-8 layer ready to define the photolithographic structures.

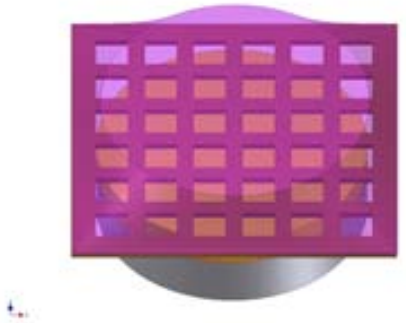

(d) Mask over the wafer.

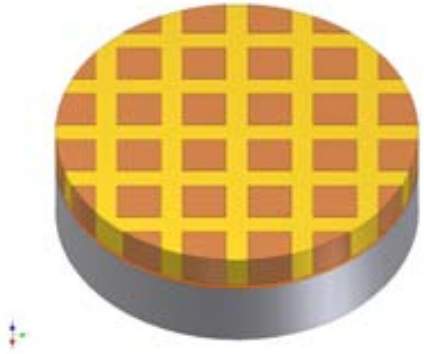

(e) SU-8 once the exposition is over.

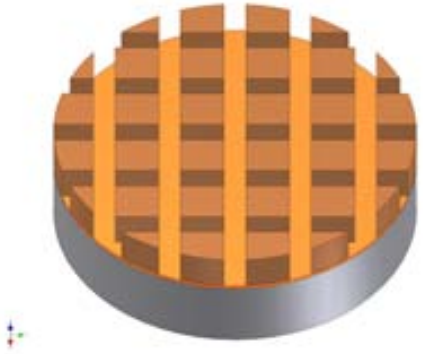

(f) Final master structure.

Figure 3.1: Schmatic view of all the steps need for the SU-8 master definition.

sented in Figure 3.1a. This layer is identical for all the masters presented in this thesis in order to improve adherence of posteriors layers and hence master durability.

Further steps on master fabrication depend on the desired layer thickness and will differ in every particular case. Nonetheless, and in order to provide a clear reading, a detailed example of a 230 µm single level master is here detailed. In this case, SU-8 2050 photoresist[1] is chosen. Then, SU-8 is poured over the seed layer (Figure 3.1b) and spinned 15 s at 400 rpm to plannarize the photoresist. Immediately afterwards, the spinner velocity[1] (ω) changes to 700 rpm, to obtain the exact layer thickness, see Figure 3.1c. Then, a soft-bake is realized in a hot plate, with temperature rising from 65° to 95°C during the time[1] (t=3h) needed to evaporate the solvents. At this point, the wafer is carefully aligned against a Cr/glass mask that blocks the light in a certain pattern and the SU-8 layer is exposed to UV light dose[1] (E=350mJ/cm^2) to define the pattern, as it can be seen in Figure 3.1d. Once the layer is exposed, the wafer is placed on the hot plate for the PEB (10 min from 65 to 95°C). PEB ends the layer fabrication. In order to build additional layers the same procedure can be repeated, *i.e.*, SU-8 photoresist, spinning, planarization, soft-bake, exposure, PEB, changing the specified parameters.

Finally, the wafer is developed dipping it in developer (mr-dev600). Requested time[1] depends on total SU-8 thickness. Last step is a hard bake, *i.e.*, a bake at 120°C within a nitrogen environment for 3 h. Hard bakes reduces the stress or cracks that could appear on the structure and finalizes the master fabrication.

3.3.2 Replica moulding

Replica moulding is based in 5 steps: (*i*) Mixing of pre-polymer and curing agent, (*ii*) Pouring the mixture over the master, (*iii*) curing the mixture, (*iv*) peeling off the cured polymer and (*v*) bonding the polymer to a substrate. Here we detail the parameters that has been used in our chips, which may differ from other authors.

PDMS consists on a base elastomer and a curing agent that is mixed in a 10:1 volume ratio, following supplier's recommendation, to obtain the final polymer. The mixing process generates bubbles. In optofluidic systems bubbles are specially critical because, besides structural problems,

[1]These parameters will be detailed on the fabrication of every particular master.

(a) Master ready for the replica process.

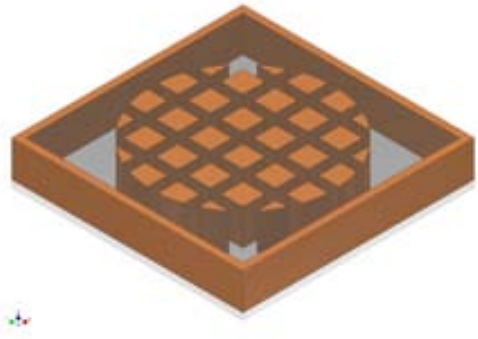

(b) PDMS poured over the master.

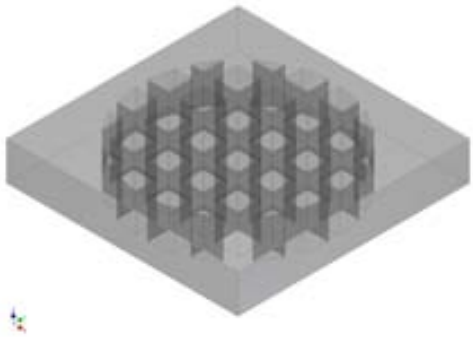

(c) PDMS replica cured and peeled off from the master frame.

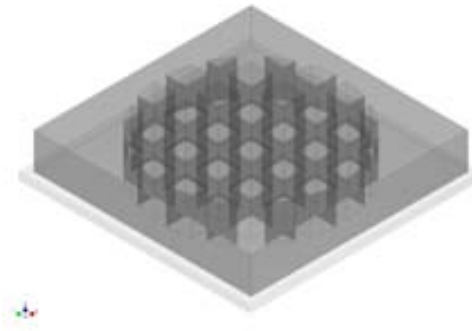

(d) Final chip once the PDMS is bonded to the glass substrate.

Figure 3.2: Schmatic view of all the steps needed from master replication to final chip definition.

they are scattering centres that can change the optical path in a dramatic way. Therefore, avoiding bubbles, *i.e.*, degassing, is extremely important. Degassing is performed by introducing the PDMS in a vacuum chamber just after mixing.

After the polymer is degassed, it is gently poured over the SU-8 master (Figure 3.2a) to fill the structure (Figure 3.2b). Once the structure is completely filled, another degasification is required to ensure that no bubbles are trapped in the structure. Afterwards, the polymer is cured placing the wafer on a hot plate or an oven at 80°C for 20 min. Finally, one proceeds to peel off the PDMS replica from the master (Figure 3.2c) and bond it into a glass substrate (Figure 3.2d). For bonding, PDMS

surface is activated with O_2 plasma [CW91]. Reactive oxygen radicals attack the methyl groups ($Si-CH_3$) and substitute them by silanol groups ($Si-OH$), as it can be seen in Figure 3.3. Two activated surfaces can be pressed together with temperature (80°C) and left until covalent bonding spontaneously occurs (typically 15min). The condensation reaction between silanol groups ensure permanent bonding.

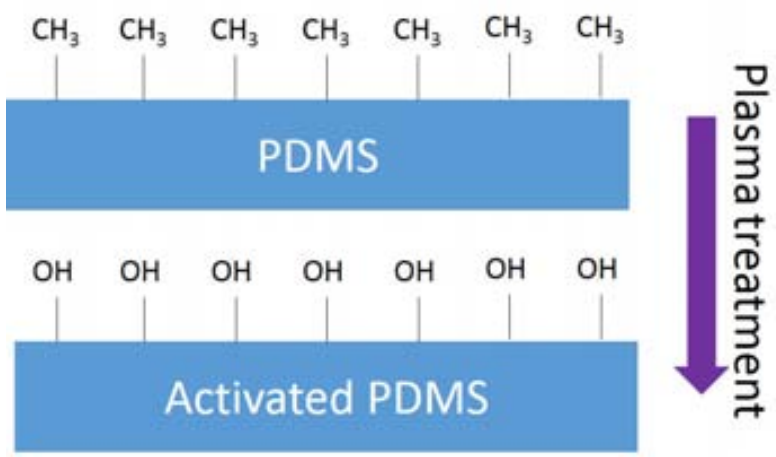

Figure 3.3: Oxygen plasma PDMS activation.

Some chips are finished at this point. Nonetheless, more complex optofluidic systems, *e.g.*, integrated filters and emitters (see chapters 4 and 5), require more fabrication steps, which are detailed below.

3.3.3 Micromoulding in capillaries (MIMIC)

The original MIMIC process follows the first step. Just after peeling off the PDMS, it is placed over the substrate. Mechanical properties of PDMS ensures non-permanent bonding. The microfluidic channels can then be filled with another polymer (filler) and cured. Finally the PDMS is removed. This simple process allows working with several types of polymers, generally non-photocurables, without increasing fabrication complexity.

This process is only valid for using PDMS as scaffold. If the combination of PDMS and the filler wants to be used, MIMIC requires some modifications, for example, to develop absorbance based filters and liquid or solid state integrated emitters, a permanent bonding of the replica is

mandatory to limit leaking. In Figure 3.4 a schematic view of the process is detailed. Once the PDMS is bonded to the substrate (Figure 3.4a), the fluidics reservoirs are opened (Figure 3.4b) and the filter is injected (Figure 3.4c). Finally, the filler may be either photo or thermally cured (Figure 3.4d).

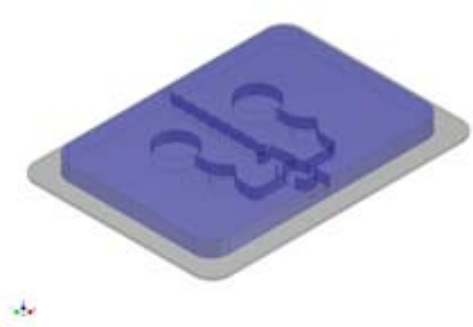

(a) PDMS replica bonded to a glass substrate.

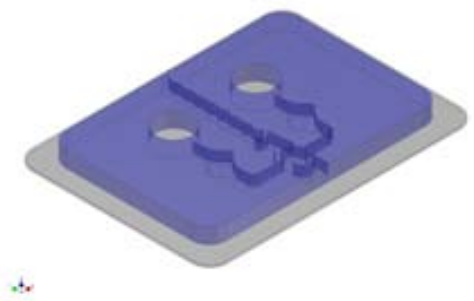

(b) Opening of the fluidic ports.

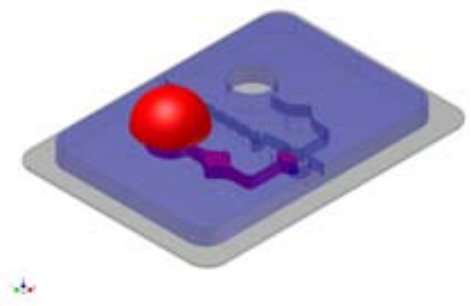

(c) A drop of filler is placed in one of the fluidic ports and fills the cavity.

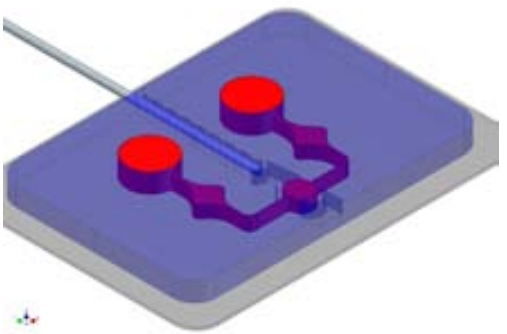

(d) The filler is cured and the optical fibre fixed in place.

Figure 3.4: Schmatic view of the extra steps needed when a MIMIC process is required.

These technological changes allow implementing: (*i*) solid and liquid state filters and emitters and (*ii*) reconfigurable optical elements, *i.e.*, the microfluidic ports can be emptied and filled again with another material. The fabrication protocol of the different fillers used in MIMIC fabrication technique is here detailed.

Filters, are divided in two groups:

(i) PDMS doped with comercial ink (Pelikan red: 1 4K351 221, Pelikan blue: 1 4K351 213 or Pelikan green: 1 4K351 239) at four different dye concentrations: volumes of 0.1 mL, 0.25 mL, 0.5 mL and 1 mL ink are added to 5 mL of the PDMS base elastomer: concentrations are 0.02, 0.05, 0.1 and 0.2 (v:v), respectively. The ink-doped base elastomer is manually mixed until homogeneous colouring is observed and a homogeneous dispersion is achieved.

To fabricate the different filters, 1 mL of the ink-doped base elastomer is mixed with 0.1 mL of the hardener (10 : 1 ratio) and sufficiently homogenized before degassing in a vacuum chamber.

(ii)Doped Sol-gel. The pre-polymerization solution (sol) is prepared by mixing phenyltrimethoxysilane (PhTMOS) monomer with dye aqueous solutions at pH 3 (adjusted with diluted HCl). Three different dyes at single concentration of 200 µM are used: quinoline yellow (QY), phenol red (PR) and crystal violet (CV). The dyes have stopbands centred at $\lambda_{QY} = 420$ nm, $\lambda_{PR} = 515$ nm and $\lambda_{CV} = 600$ nm, covering the whole visible spectrum. Except QY, these dyes are pH sensitive, showing different colours for the acidic and the basic forms. PR colour changes from yellow ($\lambda = 450$ nm) to red ($\lambda = 560$ nm) (pH, 6.8-8.0), as can be seen in Figure 3.5 and CV from yellow ($\lambda = 420$ nm) to blue ($\lambda = 600$ nm) (pH 0.0-1.8). These colour changes can substantially modify the filters performance and the pH should be carefully controlled to avoid unexpected shift on the spectral response. The mixture is gently stirred using a magnet until a homogeneous solution is achieved. At this point the resulting sol solution is ready for filling the test microstructure.

Emitters modules are filled with H_2O: dimethyl sulfoxide (DMSO) 5:1 (v/v) solution containing 500µM Atto 390 (Atto-Tec GmbH, Siegen, Germany) fluorophore, with a controlled pH 3 (adjusted with diluted HCl). Atto has its absorbance peak at 390 nm and its emission peak at 479 nm.

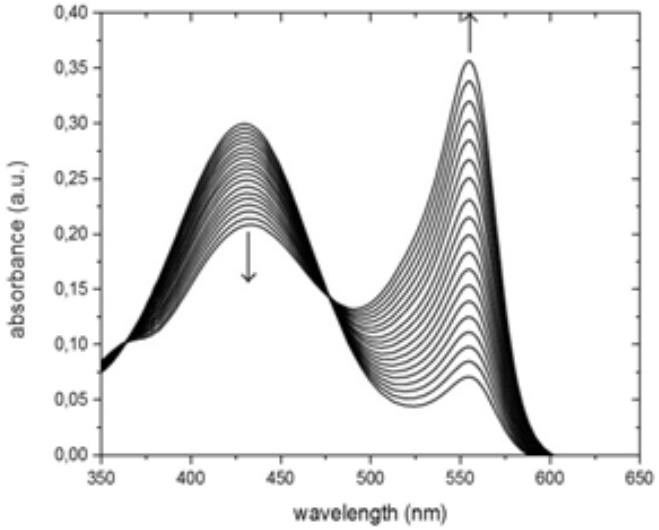

Figure 3.5: Image of absorbance wavelength shift in phenol red with pH variations. Arrows indicates an increase of pH.

3.4 Equipment

Two main types of equipment can be clearly differentiated, fluidics and optics.

Regarding fluidic equipment, a neMESYS cetoni GmbH low pressure (3 bar) microfluidic pump (Figure 3.6) and Hamilton syringes (1mL Model 1001 TLL SYR and 100 µL Model 1710 TLLX SYR) are used to pump the liquids through Poly Ether Ether Ketone (PEEK) tubing.

Optically, three main groups of equipment are used: (*i*) light sources, (*ii*) optical fibres and (*iii*) readout equipment.

3.4.1 Light sources

Different light sources are available on the laboratory for characterization purposes.

Ocean Optics white light source HL-2000 (Figure3.7a) has an emission range from 360 to 2400 nm (Figure 3.7b) with a total output power of 5 W manually controlled. HL-2000 is mainly used in spectral response

Figure 3.6: Image of 5 independent low pressure microfluidic pumps, neMESYS Cetoni GmbH.

characterization, notwithstanding its use in other kind of measurements.

(a) Picture of the Ocean Optics HL-2000 light source.

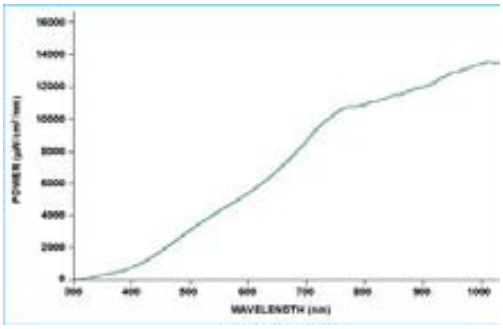

(b) Ocean Optics HL-2000 light source emission spectrum.

Figure 3.7: Ocean Optics HL-2000 light source.

Three different laser light sources are used in intensity measurements, *i.e.* absorbance, scattering and fluorescence measurements. Theis specifications are:

1. Thorlabs S1FC635 is a 2.5 mW laser source with an emission peak centered at $\lambda = 635$ nm.

2. Qioptiq Nano 250-532-100 is a 100 mW laser source with an emission peak centered at $\lambda = 532$ nm.

3. Qioptiq Nano 250-405-80 is a 80 mW laser source with an emission peak centered at $\lambda = 405$ nm.

3.4.2 Optical fibres

Optical fibres are used to connectorize the light source and the readout with the LOC. Three different optical fibres are used, whose properties are detailed in table 3.1. All of them are step-index fibres and have a NA= 0.22.

Table 3.1: Fibres used on the thesis.

Fibre	Core diameter	Cladding diameter
FG050LGA	50 µm	125 µm
FG105LCA	105 µm	125 µm
FG200UEA	200 µm	220 µm

These optical fibres have FC or SMA connectors depending on the light source and readout equipment.

3.4.3 Readout equipments

The readout equipments are:

1. Powermeter Newport 1930-C, has an intensity detection range from nW to W. It has been used for all the intensity-based measurements.

2. Microspectrophotometer Ocean Optics QE65Pro, with a wavelength measurement range of 200-1100 nm, an optical resolution of $\sim 0.14-7.7$ nm of full width at half maximum (FWHM), a dynamic range of 20 dB and a maximum time resolution of 8 ms.

3. Microspectrophotometer Ocean Optics USB2000+ with a wavelength range of 200-1100 nm, an optical resolution of ~ 2 nm of FWHM, a dynamic range of 20 dB and a maximum time resolution of 1 ms.

3.5 Set ups

Previously reported equipments are used to build up several set ups. Five different set ups for the fluidic and optical characterization of the chips are here presented.

Fluidic set up consist in a PEEK tubing connected with a high precision Hamilton syringe, syringe volume may vary depending on the desired flux or pressure. The syringes are fixed in position over the neMESYS pumps, which is controlled with a commercial software (neMESYS user interface software, Cetoni GmbH).

Intensity characterization determines the output power (W) at a specific wavelength. The set up consists on a light source (usually monochromatic) connected to an optical fibre to guide the light towards the LOC input. Then light propagates inside the LOC and reaches the output, where another fibre is placed to guide the light into the powermeter. A picture can be seen in Figure 3.8.

Spectral response characterization provide an intensity measurement, in arbitrary units, of single wavelengths with a resolution fixed by the microspectrophotometer along the whole visible spectrum. The set up is practically the same than for intensity measurements, but this time the light source is a white light source, to provide a wide spectrum and the readout can be either Ocean Optics QE65Pro or Ocean Optics USB2000+ microspectrophotometers depending on desired time and wavelength resolution. The spectral response set up can be seen in Figure 3.9.

Modal profile characterization provide information on whether the light guidance is mono or multi modal and which modes are propagating. The set up consist of a monochromatic light source coupled to an optical fibre. The optical fibre guides the light to the LOC input. The readout consist on a microscope objective in close proximity to the chip output to expand and collimate the light beam. The light is steered to a CCD camera placed at certain distance (tends of centimetres) where an image is recorded. A picture of the set up can be seen in Figure 3.10.

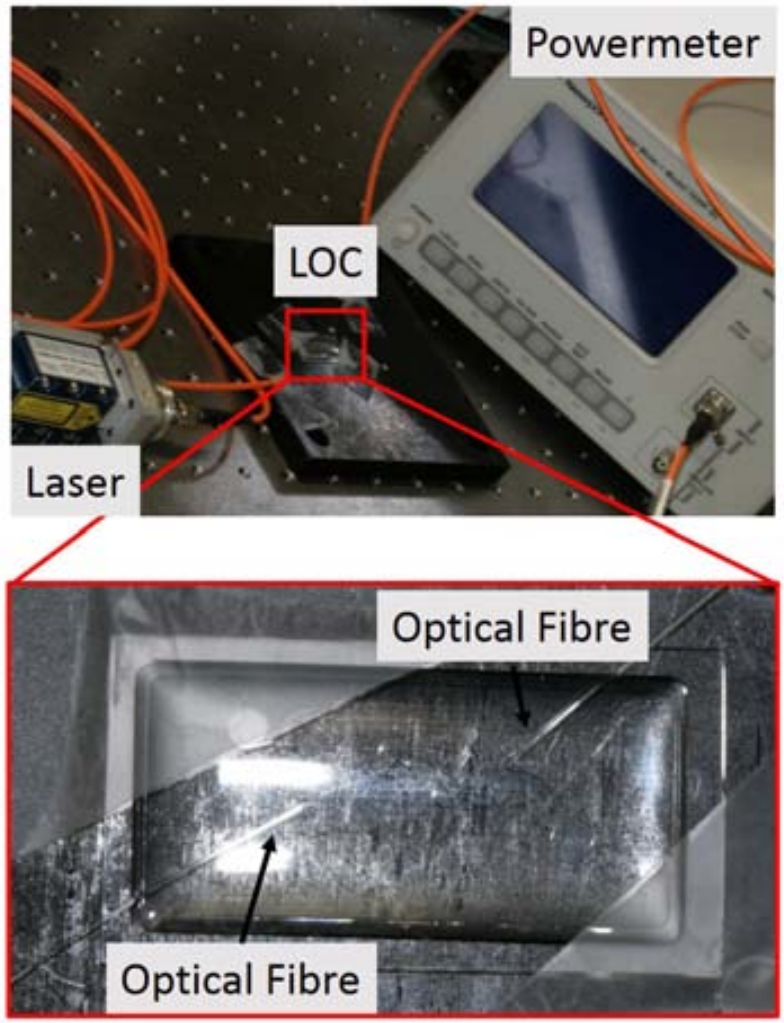

Figure 3.8: Set up for intensity measure, in W, at a single wavelength.

Emission mapping The emission performance of given active system as a function of the excitation spot position is measured using the following set up. It consists on an FG050LGA optical fibre to steer the light from the excitation laser light source to the emitter. It is important to choose the fibre with the smallest core diameter available in order to keep excitation spot as small as possible and hence, increase the mapping spatial resolution. Nevertheless, the smaller the core the fewer the light intensity coupled to the optical fibre.

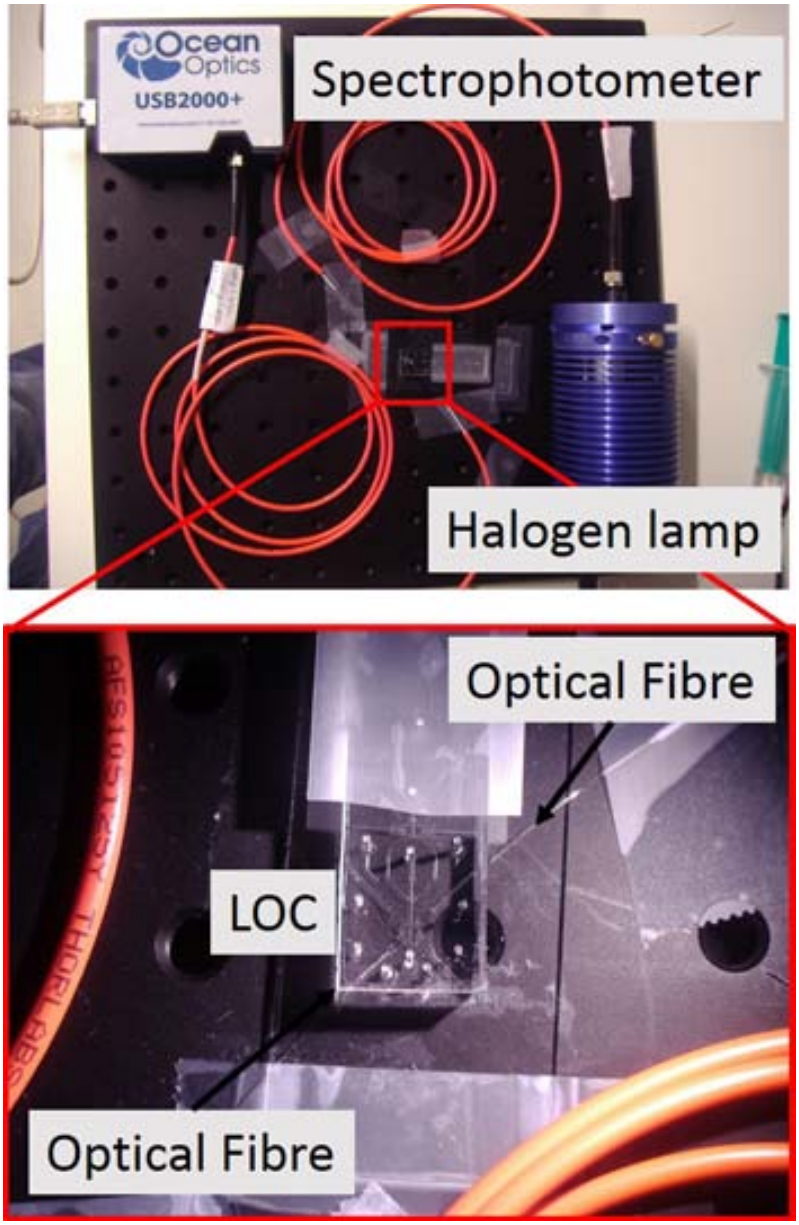

Figure 3.9: Spectral response set up.

Hence, the agreement done has been to select 50 µm core optical fibre as a compromise between resolution and coupled power. The optical fibre is positioned perpendicularly to the plane of the emitter at the smallest distance possible, without touching the emitter

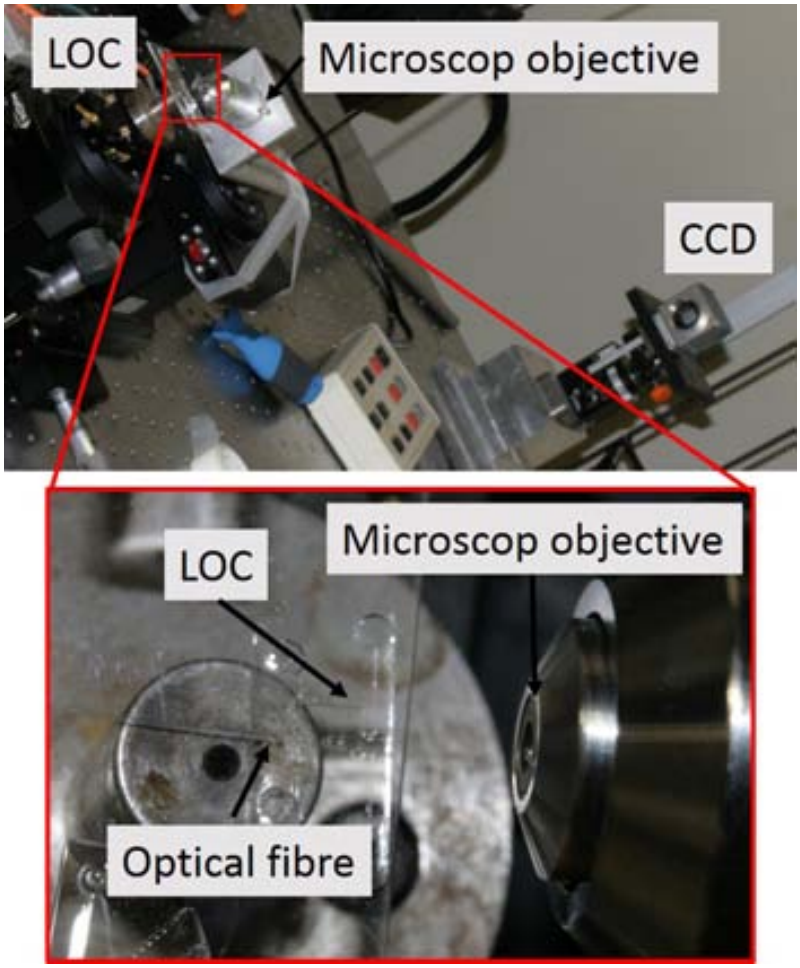

Figure 3.10: Modal profile set up.

itself.

The readout system has an optical module connected through a FG200UEA optical fiber to a microspectrophotometer. The mapping has been performed using a XYZ linear stage (Micos VT80, Eschenbach, Germany), as shown in Figure 3.11, which allowed the precise ($\sim$ 40x40 µm) mapping of the device.

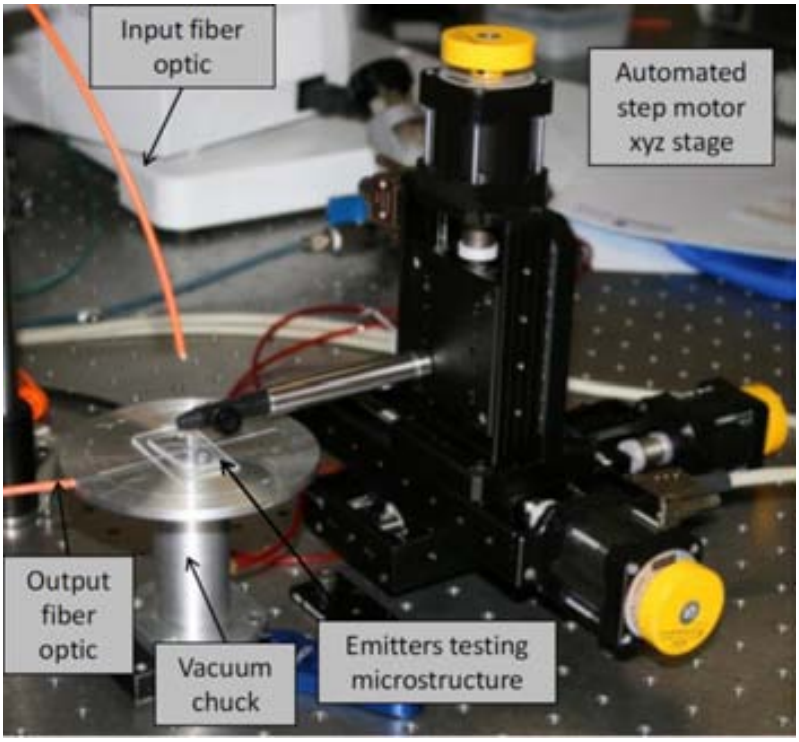

Figure 3.11: Emitter mapping set up

4 | Optical elements

In this chapter a set of highly integrable, low cost, optical elements are designed and optimized in order to be integrated in more complex optofluidic systems. Part of this work is already publised in [VPDBL12] and [LDJ+10].

Among Ph-LOC detection methods, the need of lenses, filters, light sources and detectors is ubiquitous as basic optical components to manipulate light. However, the components for optical detection in Ph-LOC are rarely miniaturized, and when they are indeed miniaturized the components are sophisticated and expensive [HSH+13, CWK+13, SRKB+11].

Considering that microfluidic systems are basically intended to conduct handy, cheap, user-friendly, and *in situ* analysis, it is obvious that a reduction of cost and size of the optical elements for Ph-LOC is mandatory. Moreover, this will allow more complex systems with better performance. In order to tackle this challenge, many researchers have made efforts to miniaturize waveguides [VMWW05, CQSW13], filters [DAS07, YKDD12], lenses [LAJ12, HW12, ZJ13], emitters [SP10, FZYZ12, TMK+13] and detectors [Wal11] so that they are tiny and simple enough to be integrated on a system. Each of these optical elements is made using different technologies and materials, complicating the creation of a single optofluidic LOC. Approximations to include some of these optical elements have been reported [BJB+06] but the cost and fabrication complexity of the Ph-LOC increases.

Developed optical elements are divided in two main categories, passsive and active elements. Passive elements are those which do not require external energy sources to work.

4.1 Passive elements

4.1.1 Lenses and alignment elements

First, micro-lenses can be tracked down until 17 th century, when Anton van Leeuwenhoek built glass lenses that were about 700 µm in diameter [Zuy81]. Using ICs technologies and materials, *e.g.*, silicon, Fresnel's zone plates were fabricated and used as thermal detectors [SYHM88] and X-ray lenses [WBD$^+$93, BMG94]. In early 90s, manufacturing of polymeric micro-lenses started to spread using a technique consistent on melting small cylinders of thermoplastics [SNA$^+$90]. This technique allowed precise control of the radius of curvature [PM94] in a parallel process, reducing fabrication cost and time. Micro-lenses produced with such technique have been used, for example, in 3D imaging of micro-objects [JJ04]. However, these lenses are difficult to integrate in Ph-LOC and require non-standard fabrication techniques, increasing dramatically the fabrication complexity, cost and time of the final device.

Camou *et al.*[CFF03] proposed integrated cylindrical lenses to collimate the optical beam. These lenses are limited to collimate in a line, not in a point, due to their cylyndrical shape. Nonetheless, the lenses are made only of PDMS and air, and are monolithically defined with the rest of the system. In Figure 4.1 a SEM image of the SU-8 master to replicate the lens is shown. Achieved integration level using these lenses is outstanding and make them perfect candidates for disposable optofluidic systems, reducing fabrication requirements, time and cost.

Camou's lenses were designed to collimate the light coming from an optical fibre with an specific NA placed at a very precise point, hence, optical fibre position is crucial to ensure good collimation performance. In order to fix the optical fibre position within the system, self-alignment structures were developed [LWB04]. These structures consist of: (i) a rectangular channel of the same width than the optical fibre cladding diameter, (ii) an stopper, at the end of the channel, that fixes the distance between the optical fibre and the integrated lens at its optimal position. Using the same notation than in the lensmaker's equation, detailed in section 2.1.2, Llobera *et al.* design is schematically represented in Figure 4.2a. The optical fibre is inserted along the self-alignment channel until it reaches the stopper, which is only a constrain on the self-alignment channel. This geometry fixes the optical fibre in the focal point of the

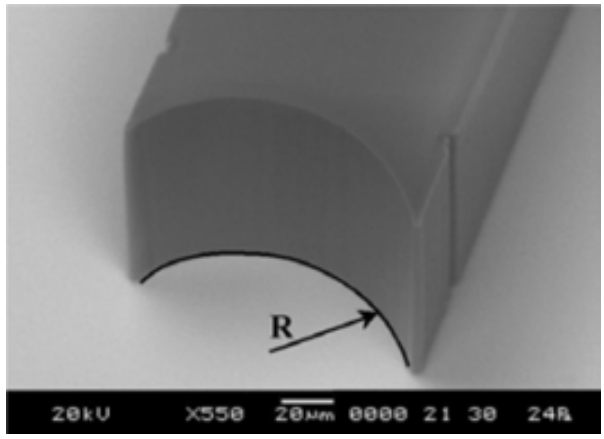

Figure 4.1: SEM image of Camou's SU-8 master [CFF03].

collimating biconvex lens.

Mirrors are also ubiquitous in optical systems to steer the light and to increase the optical path without increasing the device dimensions [LDWB07]. Hence, an easy, cheap, fast and reliable way to integrate them in optofluidic systems is required. With the experience of PDMS/air lenses Llobera *et al.* [LWB05] proposed air mirrors based on Total Internal Reflection (see sec. 2.1.1) to achieve a high degree of monolithical integration. In the precise case of PDMS and air the critical angle is $\beta_c = 44.77°$. Therefore, light reflection without losses should be obtained if the incidence angles are higher than β_c.

Optimization

The first problem detected is the high resistance that PDMS generates over the fibre, resulting in occasional fibre break. In order to fix this problem, a new alignment system has been designed. As can be seen in Figure 4.2b the second generation of self-alignment channel is no longer straight, now it is a wider channel with a set of periodic narrowing zones or constrains. This change offers a drastic resistance decrease, since now only a few points clamp the fibre, and provide certain flexibility in the fibre diameter. Due to PDMS elasticity this structure could be valid for different optical fibre diameters, being the smallest fibre that one with cladding diameter equal to the separation between constrains.

The second problem to be solved is the stopper inefficiency. First

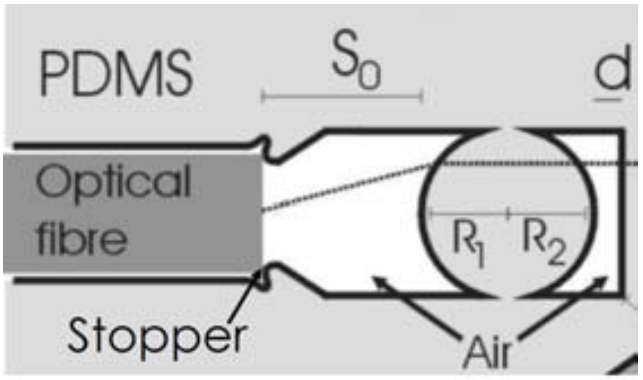

(a)

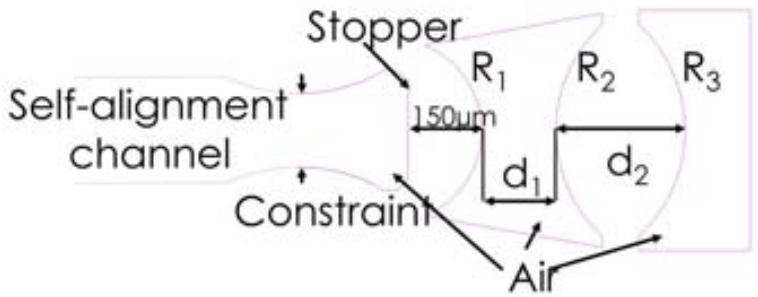

(b)

Figure 4.2: Schemtaitc top view of (a) 1st generation and (b) 2nd generation lenses and self-alignment structures.

generation of stoppers do not generate enough resistance to ensure the positioning of the optical fibre at the focal point. Occasionally, the fibre does not reach the desired position or passes over the focal point. This observed behaviour demands to visually check fibre positioning and reposition the fibre when needed. In order to avoid this problem, the stopper has been replaced by a PDMS wall, as it can be seen in Figure 4.2b. This PDMS wall fixes the optical fibre position at the focal line. In order to ensure a strong enough bonding between PDMS stopper and glass substrate, the thickness of the wall is fixed to 150 µm for all the designed lenses. Second generation stopper also offers an extra PDMS/air interface that can be used to implement a new lens, providing more design flexibility.

This second generation of lenses, with 3 PDMS/air interfaces are simu-

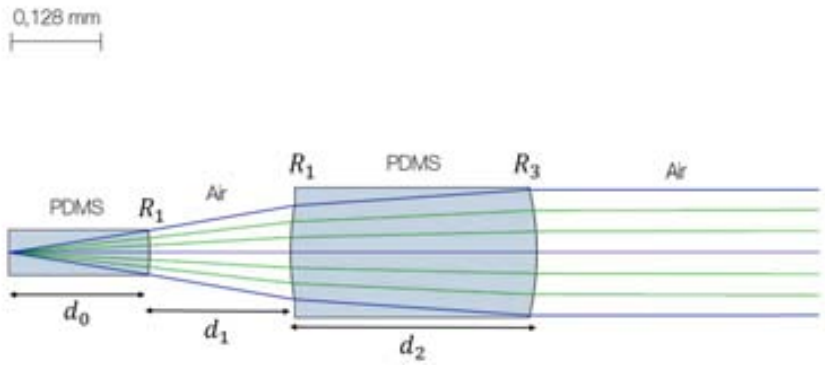

Figure 4.3: Ray tracing simulations run in OSLO Edu©, where dimensions are in mm.

lated using Oslo edu© ray tracing simulation software with $n_{PDMS} = 1.42$, $n_{air} = 1$ and numerical aperture of $NA = 0.22$. A simulated scheme of light propagation is plotted in Figure 4.3. d_0 is fixed in all simulations to 150 µm.

Three different sets of collimation lenses for the three different optical fibres are simulated. The lenses radius and distances are detailed in table 4.1 using the same notation as in Figure 4.3.

Table 4.1: Collimation lenses parameters for different optical fibres core diameter with constant $N.A. = 0.22$.

Core diameter(µm)	R_1 (µm)	d_1 (µm)	R_2 (µm)	d_2 (µm)	R_3 (µm)
50	250	230	390	330	390
105	400	150	450	250	390
200	700	200	750	330	760

S. W. Lee et al. [Lee07] reported a PDMS temperature dependent shrinking process when cured. In order to check these results the PDMS lenses where cured at 80°C during 20 min and then measured using an scanning electron microscope (SEM). The results are shown in Figure 4.4, and no appreciable PDMS shrinking is observed. Hence, the curing conditions, *i.e.*,20 min @ 80°C, will be kept constant for all the devices.

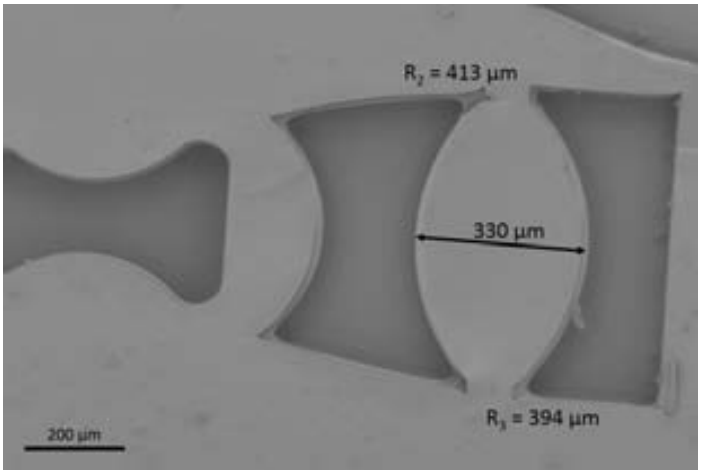

Figure 4.4: SEM image of the PDMS collimation lenses for a 50 µm-core optical fibre with the measured radius and distances.

4.1.2 Beam splitter

Using previously designed optical elements, more complex optical structures can be built. Since early 1970's [Mil69] many kind of BS have been studied and reported, taking advantage of many different optical properties and considering the final application.Heaton and co. [HJW+92] presented one of first integrated beam splitters called Multimode Interference (MMI) splitters. This kind of beam splitters consist of a wide region, as can be seen in Figure 4.5a, that generates an interference pattern resulting in a beam division. Beam division are used in arrayed waveguide gratings (AWG) for (de)multiplexing in telecomunications. These systems are capable of (de)multiplexing up to NxM channels, with N,M= 128 [Sey12]. MMI beam splitters are still used and improved [THRF10], *e.g.*, number of channels. However, MMI beam splitters require very precise fabrication techniques and are strongly wavelength-dependent. This is a drawback in LOC due to the different working wavelengths used in these applications, focusing towards the "white light spectroscopy" concept.

Another different approach for integrated optics applications with promising results are photonic crystals [YGL91]. Photonic crystals are crystalline structures with defects implemented *ad hoc*, as can be seen in Figure 4.5b, to create band gaps at certain wavelengths or propagation directions. Photonic crystals have shown excellent optical properties and a myriad of applications in LOC systems [CC06, HH11], however the wave-

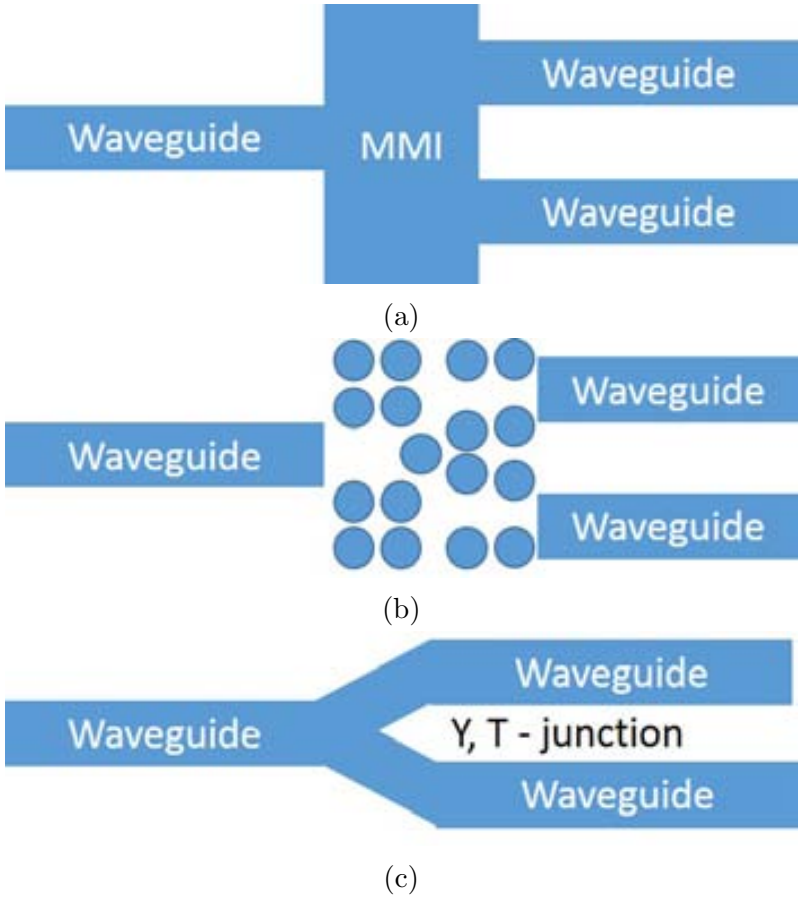

Figure 4.5: Schematic representation of different kinds of beam splitters, (a) MMI, (b) photonic crystal and (c) Y or T-junction.

length dependence, design and fabrication requirements are even stronger than in previous cases, hampering their application in real systems.

Y or T-junction beam splitters have simpler design requirements and their wavelength dependence only depends on the light confinement in the waveguide. Nevertheless, the shape of the junction and concretely the edge, clearly seen in Figure 4.5c, requires high-resolution fabrication techniques. These geometries can be used with different confinement mechanism, *e.g.*, TIR or ARROW waveguides. These structures are also difficult to align with input and output optical fibres.

Combination of two junctions form a Mach-Zehnder interferometer, which can be obtained either with Y-junction [BTZS08] or T-branch [THS+10],

shown in Figure 4.6. However, in this configuration they have used ARROW confinement, requiring multilayer fabrication steps at the clean room [BDB+06]. Polymer-based ARROW structures are extremelly challenging to be built [THZ+12].

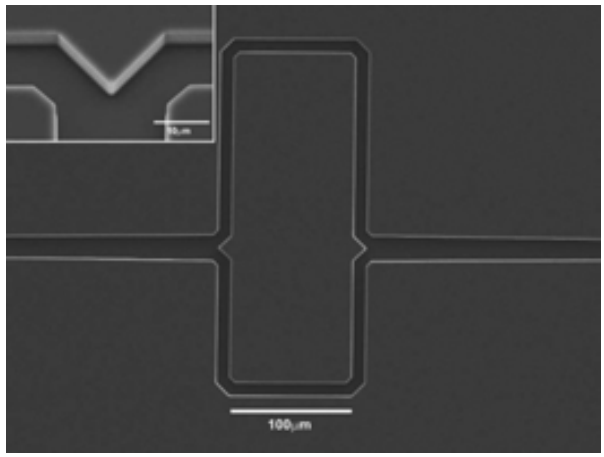

Figure 4.6: Integrated Mach-Zehnder interferometer [THS+10] that uses two T-junction beam splitters.

In order to solve these drawbacks, a highly integrable, low-cost, continuous spectrum response and low fabrication requirements beam splitter is here reported [VPDBL12].

Design

Using previously designed collimation lenses, self-alignment structures and air mirrors, an integrated BS is designed. The BS working principle is based in specular reflection. The BS consist of a sharp pyramid with tilted air mirrors at 45°. Therefore, this structure turns the light 90°. Due to the working principle of the beam splitter an incident collimated beam is key to achieve a good intensity rate distribution between all the channels. Hence, the previously described collimation lenses and self-alignment structures are implemented here.

Once the beam collimation is ensured, two different configurations are designed, 1x2 and 1x4 beam splitters. Optical fibres with a core diameter of 200 µm are chosen to maximize the beam width.

After the beam division produced by the 45° air mirror, the light is turned 90° with another 45° air mirror to reach the output (Figure 4.7b).

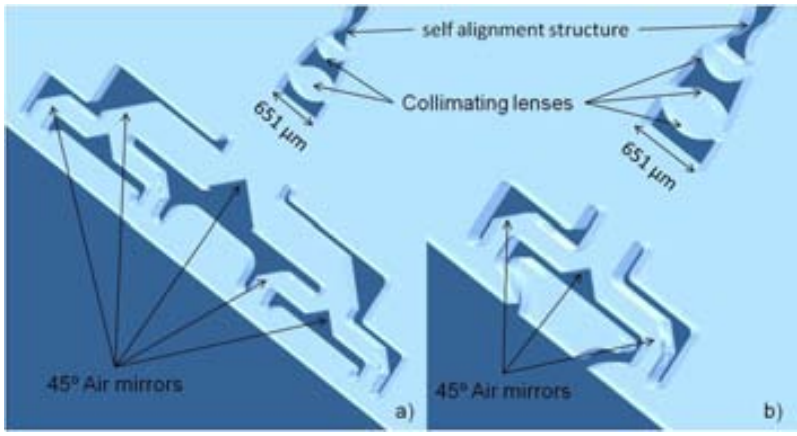

Figure 4.7: Detailed view of both configurations, a) 1x4 and b) 1x2 beam splitters.

At this point, light reaches the output in the 1x2 configuration. In the 1x4 configuration each beam is split again with the 45° air mirror and turned again to finally reach the outputs, as can be seen in Figure 4.7a.

Fabrication

Fabrication procedure is detailed in section 3.3.1. Here only the parameters to obatin the desired thickness are detailed. SU-8 2050 is spinned at $\omega = 700$ rpm, after that the wafer is soft-baked, $t = 3$ h and exposed at $E = 750$ mJ/cm^2, finally the wafer is developed in a chemical bath during $t = 7$ min.

Characterization

Optical characterization has been done using a 635 nm laser with the intensity set up, detailed in section 3.5. Power results are detailed in table 4.2. The total power calculation for each beam splitter configuration is the sum of all the output channels and the channel output is the intensity measured with the powermeter, see section 3.4.3, nm in each channel. From these results, losses associated to a single beam division are 7.8 $\pm$ 1.2 dB, which are two times bigger than other polymer beam splitters [PLK11]. However, these losses do not properly differentiate between propagation, insertion or beam division. The main issue is the deviation in the output power at each channel. Typical deviations of 10%

Table 4.2: Power results for 1x2 and 1x4 beam splitters.

BS	Total power	channel output (µW)			
1x2	9.1 µW	5.4 ± 0.1		3.7 ± 0.1	
1x4	2.9 µW	0.8 ± 0.1	0.5 ± 0.1	0.5 ± 0.1	1.1 ± 0.1

are expected. Nevertheless, our results suggest some kind of alignment problem that may be due to non-perfect collimation lenses, slightly tilted optical fibre faces or beam division asymmetries, all of which may modify the expected output power ratio.

Figure 4.8: Complete picture of intensity profile at 1x4 BS output.

As it can be seen in table 4.2, there is an increase of relative losses with the number of beam divisions, this is in agreement with the increase of the optical path.

Finally, an analysis of the optical output intensity profile is done using the modal profile set up detailed in 3.5. In Figure 4.8, simultaneous experimental intensity profile for 1x4 BS can be seen. The lines that appears between channel outputs probably are the sharp edge of the 45° air mirror. Moreover, as it can be seen in the 3D reconstruction of the intensity profile in Figure 4.9, for a channel of the 1x2 configuration, the system is multimodal due to the dimensions of the waveguide, and has an square profile due to the shape of the waveguide cross section.

The presented BS offers a reduction of fabrication requirements, low-cost and highly integrable solution. Moreover, presented BS validates the lenses, air mirrors and self-alignment systems to be used in more complex structures.

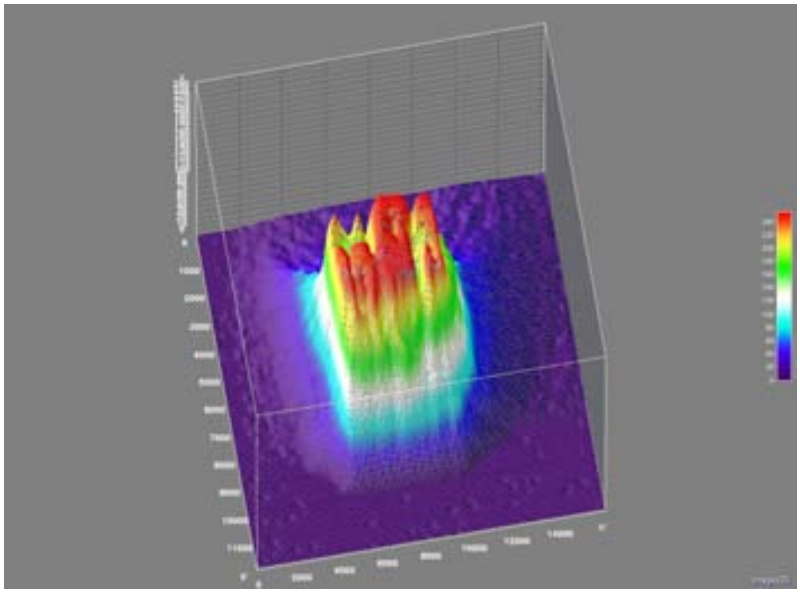

Figure 4.9: 3D reconstruction of intensity profile, using ImageJ software, of single channel in the 1x2 BS output. Dimensions of X and Y axis are pixels while Z axis dimension is an intensity scale normalized to 1.

4.1.3 Integrated Filters

Fluorescence detection is one of the most used techniques in (bio)chemical analysis and in LOC systems[SB09, RDK13, ZHF14]. However, the Stokes shift of fluorescence materials is typically small and the excitation light source intensity is several orders of magnitude higher than the emitter wavelengths. These drawbacks complicate the implementation of fluorescence detection in LOC systems. Several approximations have been done to tackle these issues.

Modern fluorescence materials have been developed. Quantum dots (QD) are semiconductor nanocrystals small enough to have quantum mechanical properties and were first discovered in the early 1980s by Alexei Ekimov in a glass matrix. Nonetheless, a detailed optical study of QD was not done until 1995 [Nor95]. Their quantum mechanical properties make them fluorescent materials with outstanding properties *e.g.*, QD size determines the emission wavelength (larger QD implies red-shifted fluorescence spectrum), are 20 times [WNS09] brighter and present large Stokes shifts in the visible spectrum ($\sim$200 nm).

Three different kinds of optical filters can be found in the literature: (*i*) Interferometric filters, which have sharp pass bands and are reliable optical filters. This kind of interferometric filters are a 1-Dimensional photonic crystals, more recently 2-D [OOI+07] and 3-D[VBSN01] (Figure 4.10) photonic crystals have been used as optical filters due to the possibility to place the stop band of the crystal at almost any energy level. These filters are based in a series of thin layer alternating high/low (HL) refractive index, typical notation indicate the basic structure of layer repeated n times as $(HLH)^n$. Their passband and stopband depend on the incident light angle [Mac10], the fabrication requirements are extremely severe *e.g.*, the thickness and refractive index of all layers must be perfectly controlled. Hence, the implemention in optofluidic systems, although it is possible [BA11], is difficult and present many drawbacks.

Figure 4.10: SEM image (artificial coloring) of a 3D photonic crystal with a band gap around a wavelength of 1.3 µm by Vlasov *et al.*[VBSN01]

Recently, (*ii*) a new technique called light spectral filtering based on spatial adiabatic passage [MELVP+13] has been proved. Their working principle is based in three single-mode waveguides that are coupled along large distances ($\sim$ cm). Filter fabrication does not critically depends on technological variation and theoretically can be made using waveguides of any material, making the filters very robust. However, the dimensions

of the systems and the need of single-mode waveguides on the whole spectrum clearly hamper their applications.

Contrarily, (*iii*) absorbance based filters are only dependent on the filter width and not on the incident angle or the waveguide modes. Moreover, absorbance based filters are made of a single layer and their passband and stop band are only subjected to the used material and Lambert-Beer's law. A more detailed explanation can be found in sections 2.1.4 and 2.1.3. Chabinyc *et al.* [CCM+01] used a colored polycarbonate to filter the light for fluorescence measurements. They worked in an out of plane configuration and their fabrication process is complex and not flexible *e.g.*, detector and input optical fibre are embedded in the structure.

Hofmann *et al.* [HWC+06] used a lysochrome dye (Sudan) to dope PDMS. In this case, diffusion of the dye molecules out the PDMS matrix was observed and non-zero passband transmittance was obtained, resulting on a suboptimal performance of the filters due to this temporal instability.

Richard *et al.* [RRAC09] presented an integrated hybrid absorption and interference filter based on a dye-doped epoxy-based photoresist, obtaining absorption layers with high rejection levels at the stopband with narrow optical path lengths (0.8 - 2 µm). Nevertheless, these filters can only act like high-pass filters (passband at 650 nm) with broad stopband widths ($>$ 250 nm) limiting their applicability in fluorescence detection since most common fluorophores show stokes shift below this value. Moreover, at the optimized maximum dye concentration they did not succeed in developing patterns (e.g. channels), and also the photoresist solvents make this approach not biocompatible. Therefore, a flexible, low cost and integrated optical filter is a desirable tool for more complex optofluidic devices.

Absorbance based integrated optical filter build using MIMIC technologies [LDJ+10] is presented below. Three different dyes have been used to dope the PDMS obtaining optical filters with stop bands covering the whole visible spectrum. Fabrication technology and used materials warrant a flexible, low cost and integrated optical filters.

Design

The filter testing structure is detailed in Figure 4.11. From a microfluidic point of view, the system is a 230 µm thick reservoir with four different widths (100, 250, 500 and 1000 µm). The channel is filled with doped

PDMS to fabricate the optical filter. From an optical point of view, eight alignment systems clamp the input and output optical fibres at the collimation lenses focal plane.

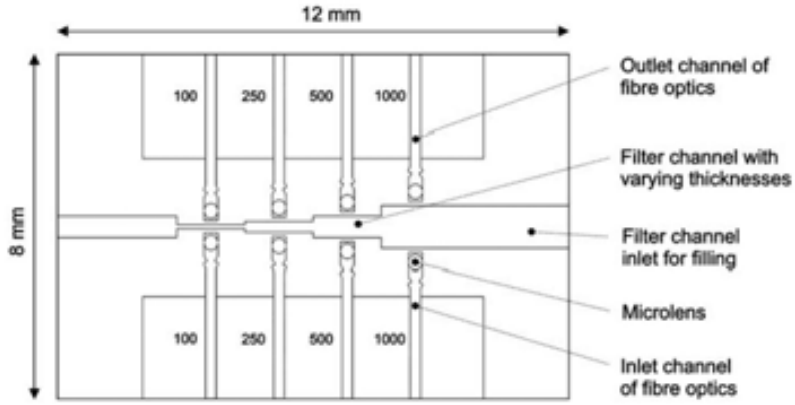

Figure 4.11: CAD image of the absorbance based integrated filters. Filters thickness are 100, 250, 500 and 1000 µm.

Fabrication

For a detailed fabrication process explanation see section 3.3.1. The parameters to obtain the desired master thickness are: SU-8 2050 spinned at $\omega = 700$ rpm and baked during $t = 3$ h. Aftewards the wafer is exposed to UV light, $E = 350$ mJ/cm^2 and developed, $t = 7$min.

Once the master is complete the PDMS replica is cured and bonded to a glass substrate. In doing so, the final system with channels for optical fibres and a filter channel (with in- and outlet) which can be filled with different doped PDMS, detailed in section 3.3.3, via capillary forces is finished.

A drop of the final PDMS/dye solution is placed at the larger opening (1000 µm) of the testing system (see section 3.3.3). After 5 min, the entire filter channel of incrementally decreasing channel width is filled with dyed PDMS. Chips are finally cured at 80°C for 1 h.

Characterization

For the analysis of the 48 different filters varying in colour (3), width (4) and dye concentration (4), the following procedure is carried out: All

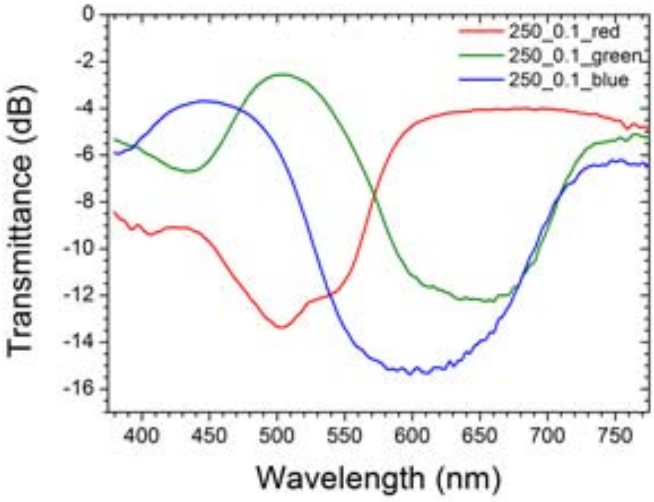

Figure 4.12: Measured transmittance versus light wavelength of PDMS doped with red, green or blue ink at a concentration of 0.1 (v:v) for the 250 µm-thick filters.

filters are scanned using the spectral response set-up, detailed in section 3.5. An integration time of 160 ms is used throughout the filter characterization. A filter channel filled with undoped PDMS is measured and used as reference.

Figure 4.12 illustrates the transmittance of the 250 µm width PDMS filter coloured with red, green and blue dye at a constant concentration of 0.1 (v:v) when illuminated with halogen broadband lamp. As it can be observed, using the three dyes, most of the visible spectra can be accessed.

Transmittances T_s and T_p from Figure 4.12 are summarized in ta-

Table 4.3: Transmittance values of the stopband and passband of the different dyes at a constant concentration of 0.1 (v:v) measured using an halogen light source.

Filter	λ_s [nm]	T_s [dB]	λ_p [nm]	T_p [dB]
Red	505	-13.4	630	-4.0
Green	660	-12.3	502	-2.5
Blue	579	-15.1	442	-3.7

ble 4.3. One can observe that transmittances vary between -15.1 dB and -12.3 dB in the stopband and between -4.0 dB and -2.5 dB in the passband. Non-zero passband decrease the dynamic range of the filters. Used inks do not have a zero pass band due to small particles and aggregations that act as scattering centres. In order to give a more accurate value the relative transmittance, $T_s - T_p$, is defined. Additionally, secondary stopbands, which may be associated to the ink solvent, can be observed for green and red dyes at low wavelengths. The presence of such bands is useful to define passband filters, where a narrow central wavelength is conserved, as opposed to the results presented by Hofmann [HWC+06].

Having shown the basic functionality of the dyed PDMS optical filters, their characteristics have been analysed in more detail for different filter thicknesses and dye concentrations. Figures 4.13, 4.14, 4.15 show the transmittance as a function of the wavelength for the red, green and blue PDMS/dye filter at different widths for constant dye concentration of 0.1 (v:v).

Increase in filter thickness is shown to cause a decrease in T_s as well as T_p, but the position of both bands and the overall shape of the spectra remain unaltered. This behaviour is expected as absorbance filters follow the Lambert-Beer's law. When analyzing the difference in relative transmittance, the maximum appears not at 1000 µm filter thickness, but at 500 µm. This behaviour is more clearly seen in Figure 4.16. This effect is likely due to the fact that, for thickness above 500 µm the dynamic range of the experimental set up is reached and hence, no more reliable results are obtained. This can also be seen in the stopband by the noise in the measurements taken and precludes using the more rigorous Q factor used by Hofmann [HWC+06] for determining the filter quality.

To analyze the dependence of the spectral characteristics of the filters with the filter width as well as dye concentration, the stopband transmittance values versus wavelength are plotted in Figures 4.17, 4.18 and 4.19. Absorbance filters have a linear dependence the concentration of an absorbing dye and path length. Albeit the number of concentrations used is not high enough so as to make a reliable fit, the linear tendency can be observed for all three dyes up to a concentration maximum of 0.1 (v:v). Above this concentration, saturation is reached. An additional drawback of working at the highest concentration tested is inhomogeneous mixing, resulting in agglomerates and incomplete polymerization, making the results inconsistent. Working with smaller filters allows spectral responses

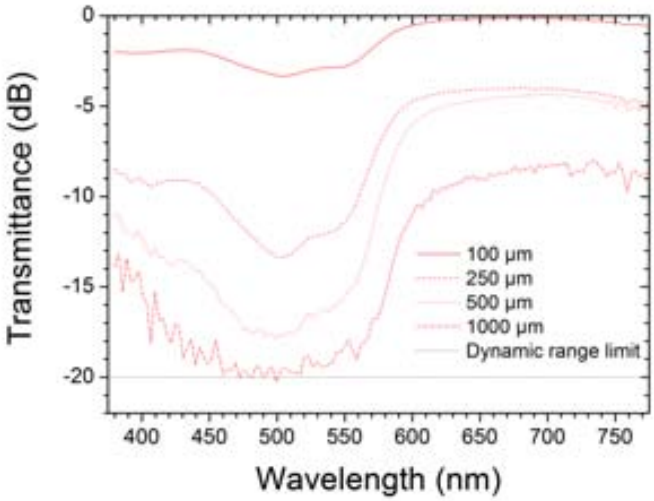

Figure 4.13: Pelikan red PDMS doped transmittance at a constant dye concentration of 0.1 (v:v).

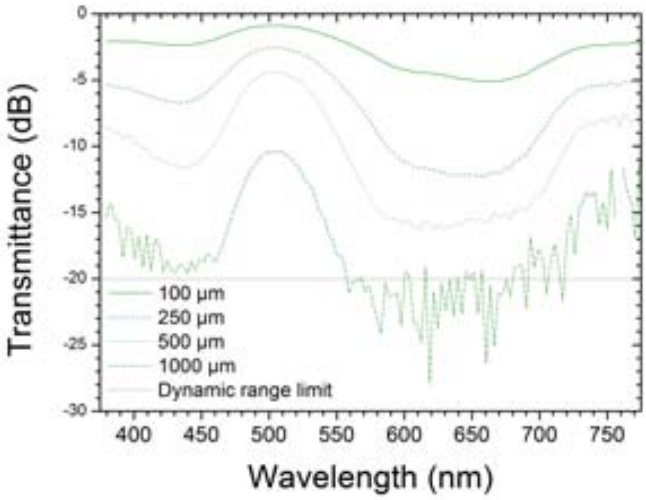

Figure 4.14: Pelikan green PDMS doped transmittance at a constant dye concentration of 0.1 (v:v).

with higher passband transmittance, while retaining a significantly low transmittance value of the stopband. Therefore, working with dye concentrations of maximum 0.1 (v:v) and width close to 250 µm should provide

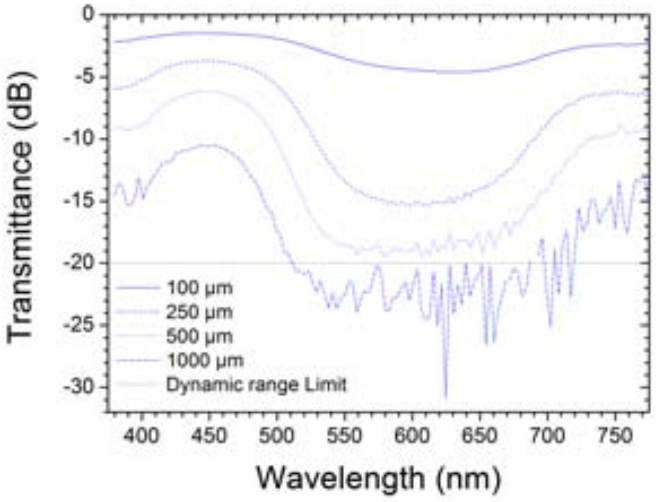

Figure 4.15: Pelikan blue PDMS doped transmittance at a constant dye concentration of 0.1 (v:v).

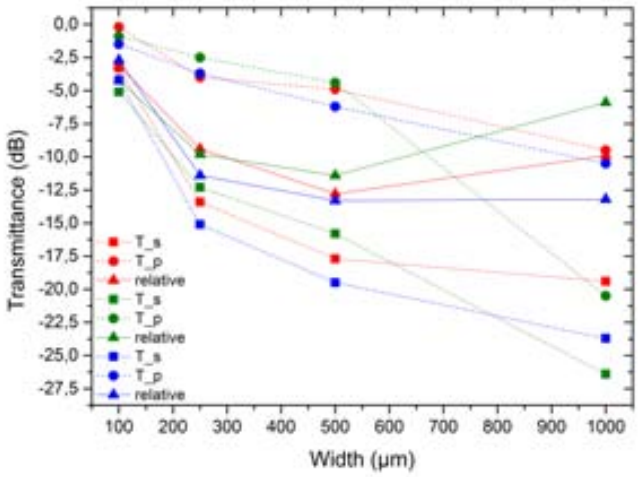

Figure 4.16: PDMS doped T_s, T_p and relative $(T_s - T_p)$ for all the filters. Every dye is represented by its own color.

the optimized filter response characteristics.

Finally, a qualitative study is carried out to determine whether any diffusion of the dye molecules out of the PDMS matrix occurs. As previous

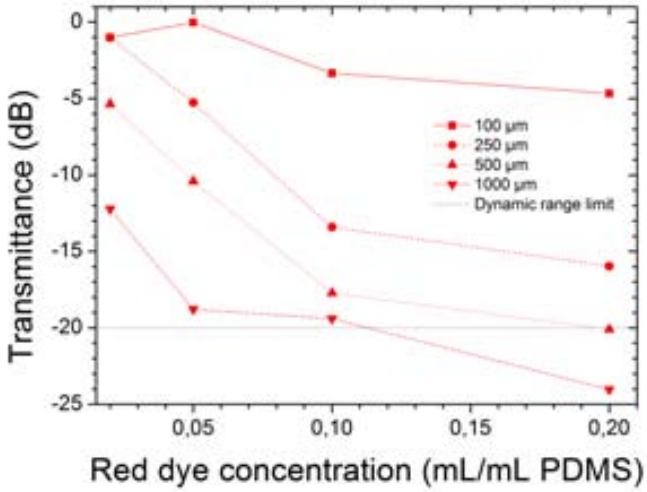

Figure 4.17: Pelikan red. Maximum stopband at $\lambda_s = 505$ nm.

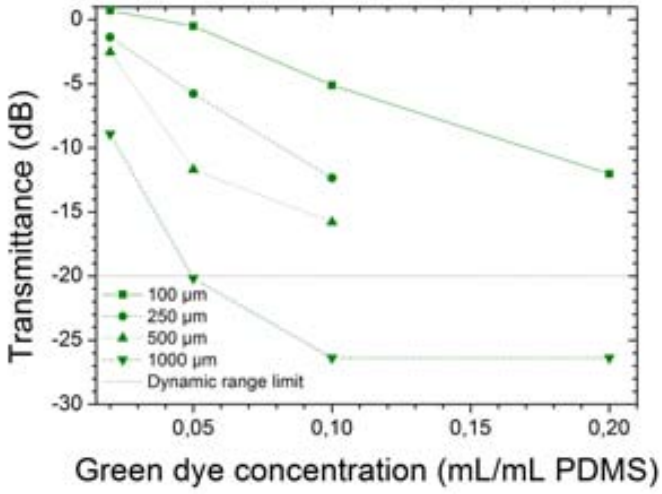

Figure 4.18: Pelikan green. Maximum stopband at $\lambda_s = 660$ nm.

stated, this effect was observed when mixing Sudan II dissolved in toluene with pure PDMS [HWC$^+$06]. Diffusion of solvent reduce the temporal stability of the system.

Two different slabs of coloured PDMS were prepared. The first consisting of 1.2 mg Sudan II per mL PDMS base elastomer in 10 % toluene,

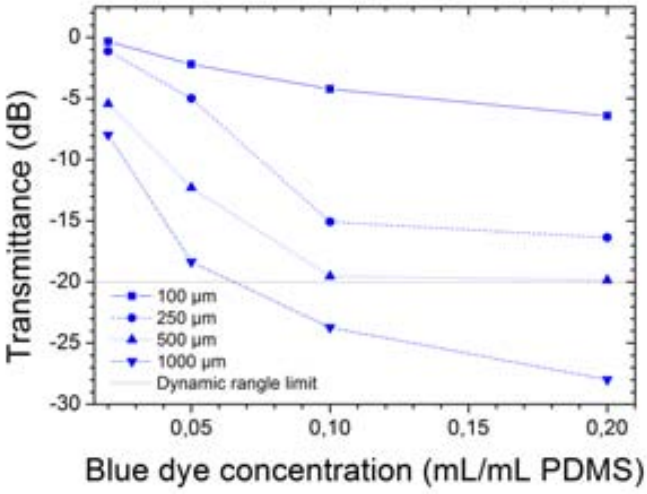

Figure 4.19: Pelikan blue. Maximum stopband at $\lambda_s = 579$ nm.

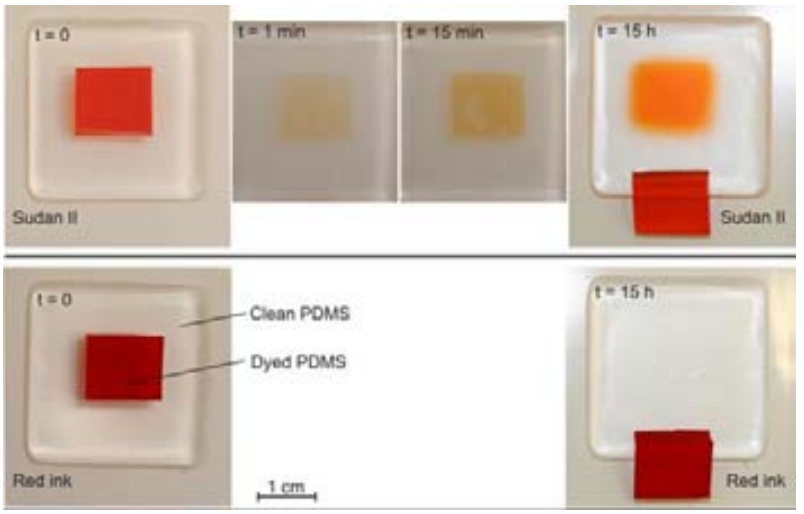

Figure 4.20: Doped PDMS with Sudan II (top) or red ink (0.1 (v:v)) (bottom) temporal stability.

subsequently mixed with curing agent in a ratio of 10:1 (v:v) and cured at 65°C for 4 h. The second was a red ink loaded PDMS slab with a concentration of 0.1 (v:v). Both slabs were reversibly bonded to a pure PDMS slab. Figure 4.20 shows the qualitative comparison of the diffu-

sion of the different dye molecules into a clear PDMS slab. One minute after placing the PDMS slabs in contact, diffusion of Sudan II into the pure PDMS can be observed. However, in the red ink dyed PDMS no observable diffusion occurs, even after 15 h of ageing.

Hence, although the filters proposed in this paper does not reach the -40 dB rejection shown by other authors [HWC+06, JDAS06], the long-term stability of the filtering characteristics of the ink dyed PDMS filters proposed here shows these to be a more reliable configuration as compared to the previously reported PDMS filters based on pigments.

4.2 Active elements

4.2.1 Integrated emitter

Ideal LOC will integrate all the needed parts required for sensing. Particularly, in optofluidics, the optimal configuration have to integrate the light source in the photonic system while holding the cost and alignment requirements at a minimum level. One approach is the implementation of an external device as small and cheap as possible with the required hardware, *e.g.*, photodetector, light emitter and electronic controllers. Then, the system is carefully aligned inside [LCM+09] and the measurement is performed. However, this approach is hardly exportable to different LOC systems, and therefore an external device would be necessary for almost every single application.

On the other hand, integration of light emitters in LOC systems is not trivial, *i.e.*, often need power supplies and IC materials and hybrid technologies increase LOC fabrication cost and time. Recently the organic light emitting diodes are offering an alternative, although used materials, *e.g.*, indium tin oxide (ITO), dramatically increase the cost[KME+13], hampering their use in disposable systems.

Several works show polymer-based monolithic integration of solid-state emitters [YWH+00] as well as liquid-state emitters [BJB+06]. In both cases lasing emission is achieved, even though liquid-state emitters offer few advantages over solid-state in LOC applications such as shape flexibility and more easily integrated in optofluidic systems. However, laser emission is achieved to the detriment of fabrication requirements, increasing then the cost. Furthermore, lasing emission is a key issue for interferometric analysis but not in the much more common fluorescence

or absorbance analysis.

Carregal-Romero *et al.*[CRLC+12] report a disposable solid-state integrated monochromatic emitter based on fluorophore-doped xerogel material with a length of 5 mm. From an optical point of view, this emitter is mainly a doped waveguide fabricated using MIMIC technology. More recently they use the same technology to implement an optofluidic system with integrated solid-state emitters [CRID+12].

Design

In order to built a disposable, integrated, liquid-state emitter the previously reported emitter by Carregal-Romero *et al.* [CRID+12] is used as starting point due to its low-cost, flexibility and monolithical integration. A schematic representation is shown in Figure 4.21a.

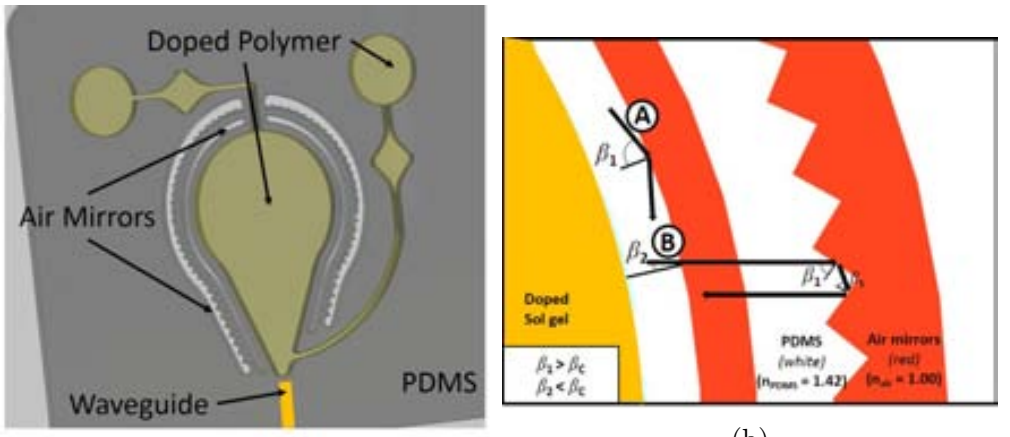

(a) (b)

Figure 4.21: Carregal *et al.* solid-state emitter[CRID+12]. (a) CAD scheme and (b) ray tracing of fluorescence emission for an excitation light on the centre of the emitter.

Air mirrors design to improve system efficiency requires additional justification. The working principle of both air mirrors is schematized in Figure 4.21b. Concretely, the higher refractive index of PDMS should allow the total internal reflection of the light travelling from it to the air mirror with an incidence angle (β_i) higher than the critical angle. This is represented in path A in the figure, where dispersed light beams with high incidence angles are confined in the LOC system by TIR in the inner

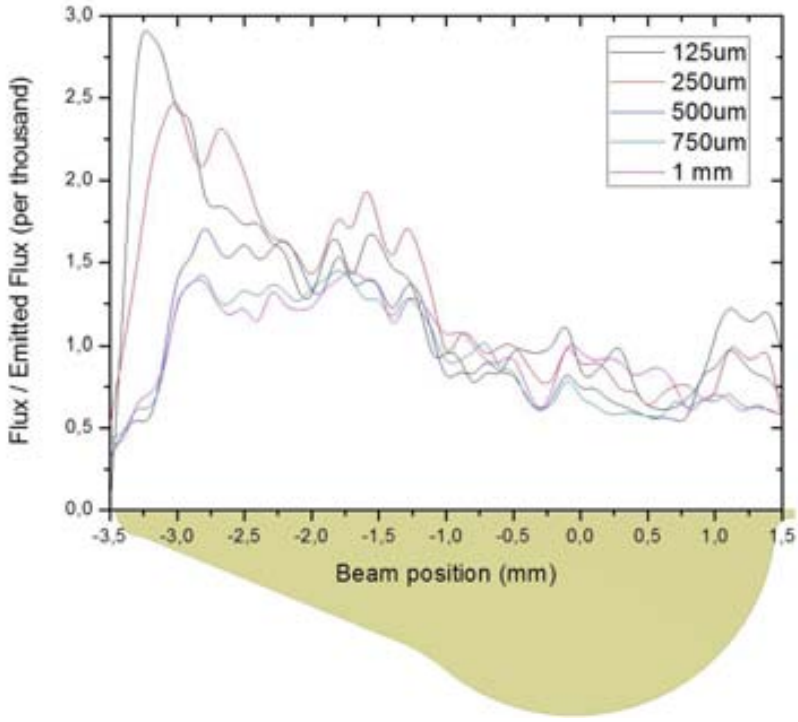

Figure 4.22: Simulated emission along the X axis for different excitation spot sizes.

air mirror. In opposition, dispersed light beams with a smaller incidence angle (path B in the figure) would propagate through the inner flat air mirror until reaching the saw-tooth area in the outer air mirror. There, the same conditions as in A holds, resulting in a double reflection at the PDMS/air interface. As a consequence light beams are redirected inside the chamber.

In order to improve further the optical performance of the reported emitters, an emission mapping is simulated using the commercial available TracePro software, detailed in section 3.2. Two variables have been considered, the excitation light location and the excitation light spot size. The total intensity exciting the emitter has been kept constant. In Figure 4.22 simulated intensities for different spot sizes, *i.e.*, different distances between excitation fibre and light emitter, and different position are plotted. As it can be seen, the maximum of intensity at the readout

is achieved when the excitation light is placed at the end of the emitter with the smallest excitation spot size, *i.e.*, as close to the emitter as possible. These results suggest that most of the emitter's volume does not contribute to the output power. Therefore, the shape and volume of the emitter is reshaped to improve the coupling efficiency as well as reducing the sample volume. Redesigned emitters are cylinders much more compact, with a radius of 500 µm. Air mirror systems is maintained with small changes to adapt it to the new cylindrical shape, as it can be seen in Figure 4.23.

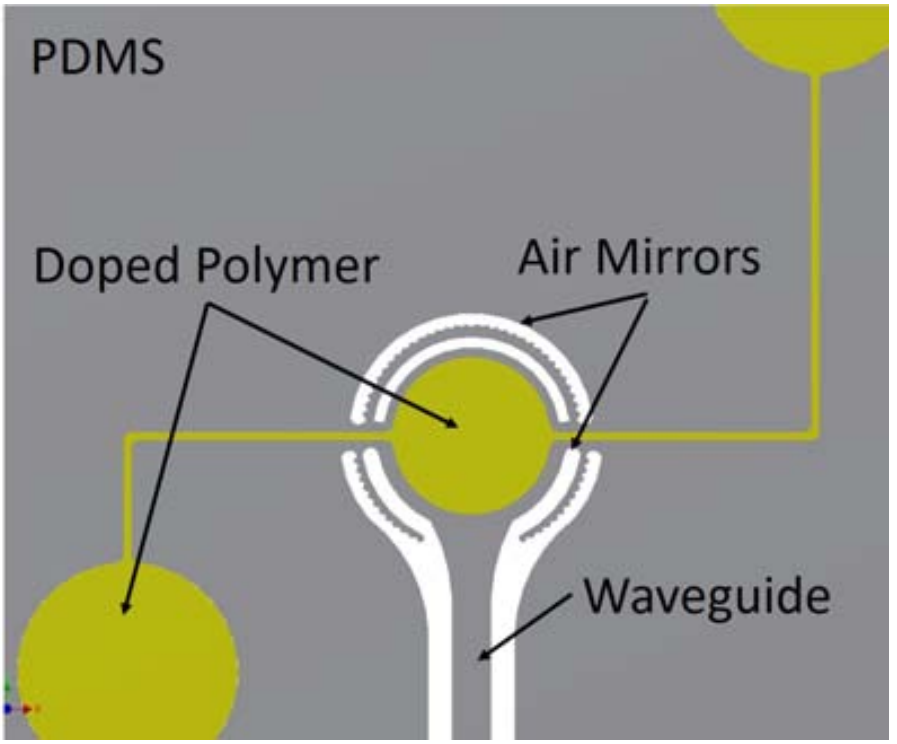

Figure 4.23: CAD scheme of the redesigned integrated emitter.

5 | Modular system

In this chapter several optical elements from Chapter 4 are implemented in a modular system with fluidic counterparts. Once the modules are characterized they are plugged together, forming a LOC system, and tested.

In order to minimize contamination risks LOCs should have a very low fabrication cost to achieve disposable systems. Besides, LOCs are designed for very specific applications and every new application requires a new LOC. Therfore, on the prototyping phase, each chip redesign requires completely new photomasks and masters, increasing the prototyping costs. Moreover, design and prototyping of new LOCs often require state of the art fabrication facilities and materials. These drawbacks are preventing a deep penetration of LOCs in (bio)chemical and medical applications as already exposed in the introduction section.

Serial fabrication process such as, direct laser writing [HJW+10], give us interesting tools for rapid prototyping in a maskless process. However, direct laser writing prototyping hugely increases fabrication time and cost, may modify the surface chemistry and also produces rougher surfaces [PTC+02, JRGL01], critical in most optical elements. Hence, its use in most optofluidic devices is discouraged.

Modular systems offer a promising new landscape on optofluidics to keep the costs low, give enough flexibility to produce new devices, work in different applications and easily replace damaged parts. Besides the prototyping phase, extra flexibility provided by a modular device is specially interesting for *in situ* measurements, where many different LOC systems can be build from few basic pieces, providing a practical solution for unexpected situations. This idea was used for Edmonds *et al.* [ESD05] to introduce the modular architecture on sensor systems. Their concept was applied to sensors networks rather than several parts of the sensor itself. Their work was focused on electronics hardware and the control

software, in a precursor of the so called Internet of things.

In LOC applications, modular systems can be divided in two main groups, microfluidic, i.e., the modular systems only tackles microfluidic elements paying few or no attention to sensing counterparts, and complete, i.e., modular systems with microfluidic and detection elements.

The microfluidic group is the most extensive and several examples can be found in the literature. The first one [GCS98], previous to soft-lithography techniques, was based on silicon, as it can be seen in Figure 5.1. It consisted on two layer bonded together to create the channel. This microfluidic modular system was more focused in the interconnection of the modules than the modules themselves, which is the major concern in microfluidic modular systems. Soon after, a soda-lime glass modular system focused on interconnection of modules was also reported [IAMC02].

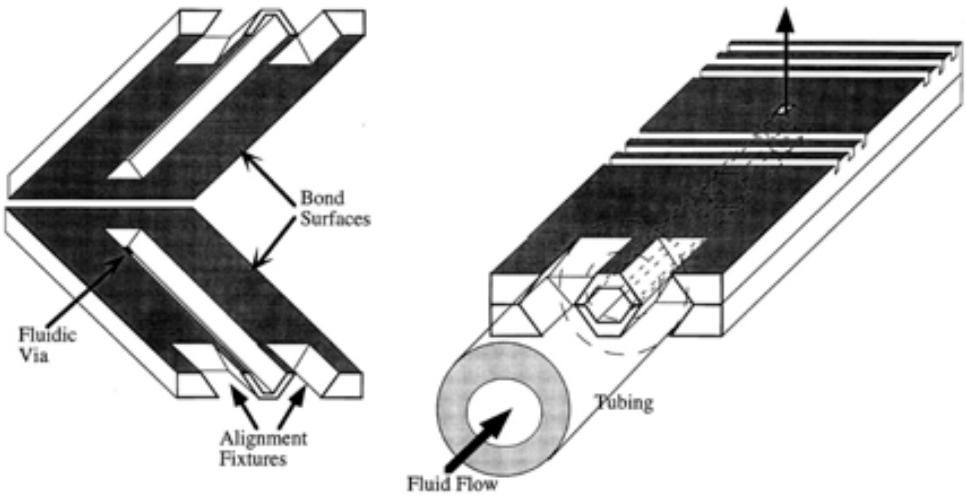

Figure 5.1: Silicon modular microfluidic system [GCS98].

Grodzinski *el al.* [GYLW03] published a microfluidic modular system based on polycarbonate and fabricated using a milling machine and DLW techniques. This paper addressed the microfluidic connections as well as modules design and optimization, *e.g.*, reducing dead volumes, in order to perform cell pre-concentration and genetic sample preparation. Thereafter, several microfluidic modular systems were reported using different materials, mostly thermoplastics [Yue08, LGVK09, TDK+10, CWH+12].

Simultaneously, Rhee *et al.* [RB08] presented a PDMS based modular system. Their system consists of few microfluidic modules done us-

ing replica moulding technique. The modules, illustrated in Figure 5.2, are bonded non-permanently to two different substrates, glass or PDMS-coated glass, achieving inside pressures up to 5 psi.

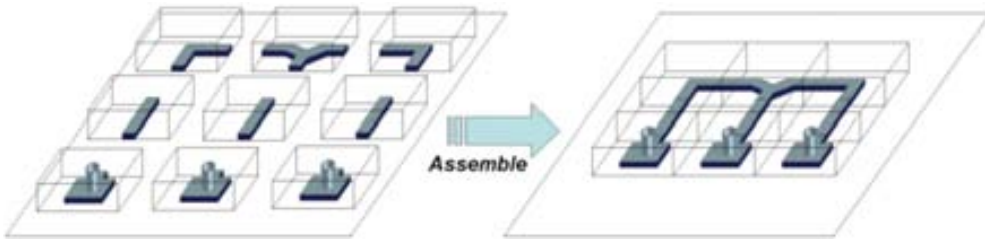

Figure 5.2: PDMS modular LOC system [RB08].

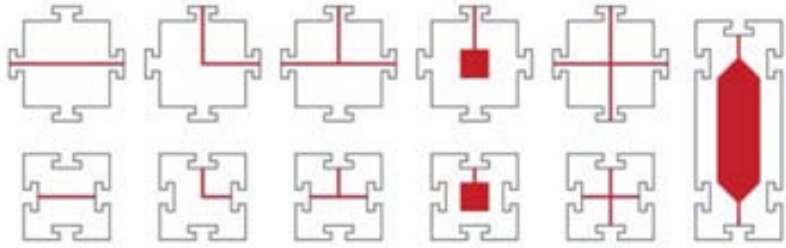

Figure 5.3: Jigsaw shaped modules [LLDM+11].

In order to increase inner pressure they use PDMS curing agent as adhesive, achieving pressures of > 30 psi. Nonetheless, modules do not have any alignment system, limiting channels size. Another PDMS-based modular systems was presented by Langelier *et al.* [LLDM+11]. This system was also based in PDMS microfluidic modules bonded together over a pre-coated substrate. These modules had a jigsaw shape, as is detailed in Figure 5.3, to facilitate alignment and bonding between them. Both system, Rhee's and Langelier's, bonded the modules and hence, there was no possible reconfiguration or replacement of damaged parts.

Few papers claimed for a complete modular system [SK04, GSK+09]. Nevertheless, these LOC systems are not reconfigurable and do not allow LOC systems design on demand. At the best of our knowledge the first complete LOC was published by Shaikh *et al.* [SRG+05]. Their system consisted in three microfluidic layers, (*i*) the passive fluidic chip, (*ii*) the silicon breadbord and (*iii*) the active chip. Changing the passive chip several functions may be realized and multiple chips can be interconnected to a larger system.

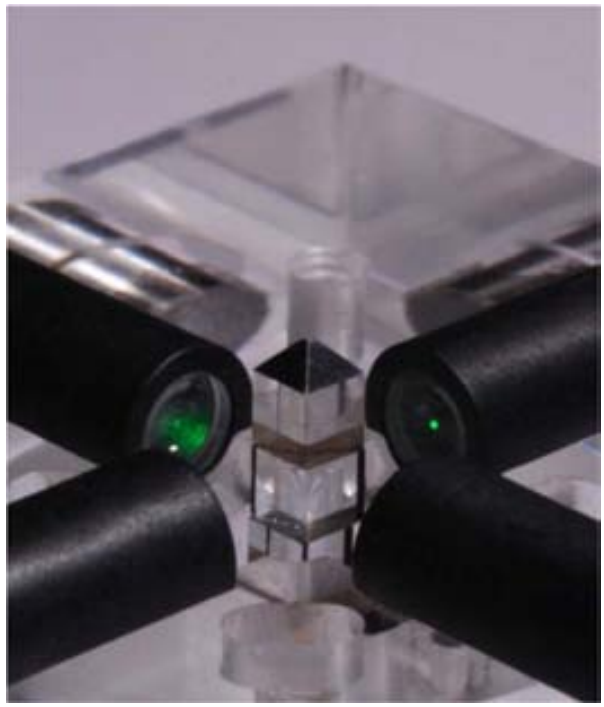

Figure 5.4: Optical module for light redirection [BMV+13].

Finally, a polymer-based modular sensor has been reported [BMV+13]. The reported sensor consists of backplane modules that are magnetically interconnected. "Each backplane module consists of three virtual layers: 1) a microfluidic backplane layer with fluidic channels and microvalves; 2) an optical backplane layer with optical fibers and switches; and 3) an electronic backplane layer with a microcontroller". The presented design is very flexible and allows multiple configurations. Nevertheless, fabrication is a manual process with many steps that will be extremely difficult to automate. In fact, they use 3-mm diameter lenses to focus the light over 3 home-made mirrors with a total volume of 28 mm^3 glued together and mounted over a micromotor, as it can be seen in Figure 5.4. Besides the fabrication complexity and cost miniaturization of the reported sensor seems difficult when not impossible.

Therefore, a complete modular systems focused on LOC has not been presented.

5.1 Modular design

In order to achieve fully reconfigurability modules, they should not be bonded together or to a substrate. The design is based in female/male jigsaw shaped connectors with 4 different configurations, detailed in Figure 5.5. They are designed to ensure optimal results, *i.e.*, no leaking and high optical repeatability.

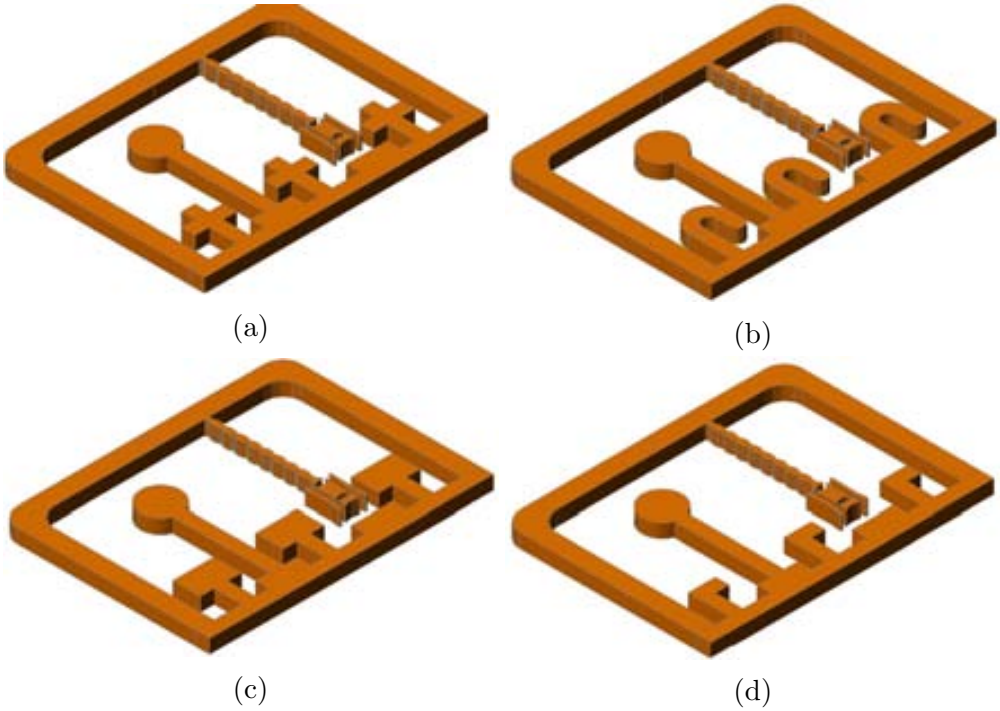

Figure 5.5: CAD schemes of the SU-8 master of the basic jigsaw female connectors. The names of the connectors are (a) cross, (b) hook, (c) rectangle and (d) L connectors.

A set of basic optical and fluidic elements are integrated in different modules. From an optical point of view, waveguides are required to steer the light wherever is needed. The integrated waveguides are PDMS structures surrounded by air mirrors to achieve TIR conditions (Figure 5.6a).

Moreover, an input and output (I/O) optical modules are needed (Figure 5.6b). The I/O module consist of a collimating lens with a self-alignment system for the optical fibres, as it is detailed in section 4.1.1.

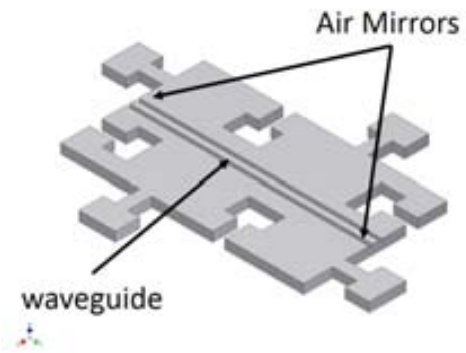

(a) Waveguide module.

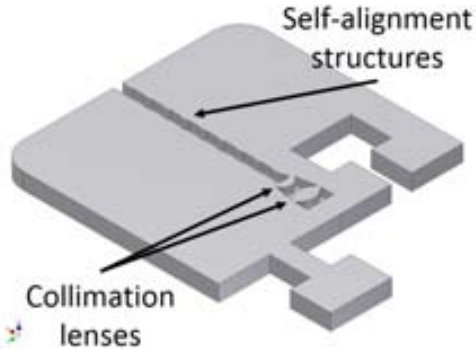

(b) Optical input/output module.

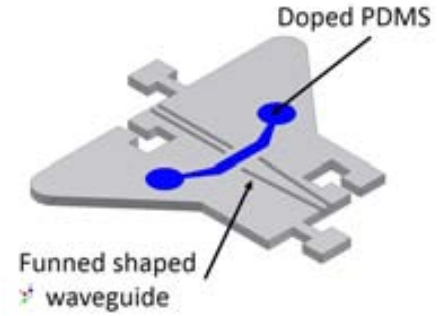

(c) Optical filter module, 500µm-width, called κ filter.

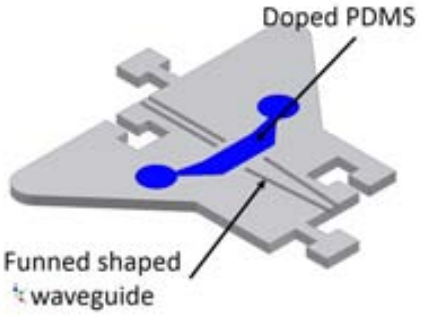

(d) Optical filter module, 1000µm-width, called ξ filter

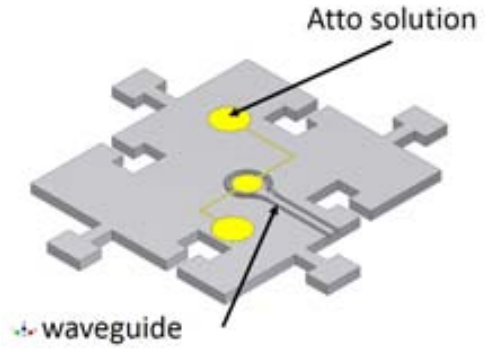

(e) Integrated emitter module.

Figure 5.6: CAD schemes of the basic optical modules.

Two optical filters has been also designed with the only difference of

the filter width, the 500 µm filter is called κ while the 1000 µm filter is called ξ, as it can be seen in Figure 5.6c and 5.6d. These optical filters are not bidirectional due to the relatively large region where the light is freely propagating. Hence, a funnel shaped waveguide is placed after the filter to maximize light recollection. The filters are filled using MIMIC technology (see section 3.3.3) and can be build *in situ* depending on the specific needs. Finally, the integrated emitter designed in section 4.2 is implemented in a module with an integrated waveguide to steer the light towards other modules (Figure5.6e).

From a fluidic point of view, two different modules are designed. Firsly, and I/O fluidical port to connectorize an external syringe with a clamping mechanism to fix the syringe in place (Figure 5.7a). Secondly, an interrogation mechanism based on the previously reported MIR architecture [LWB08]. As it can be seen in Figure 5.7b, waveguides are added to the reported architecture to avoid the use of optical fibres in this module.

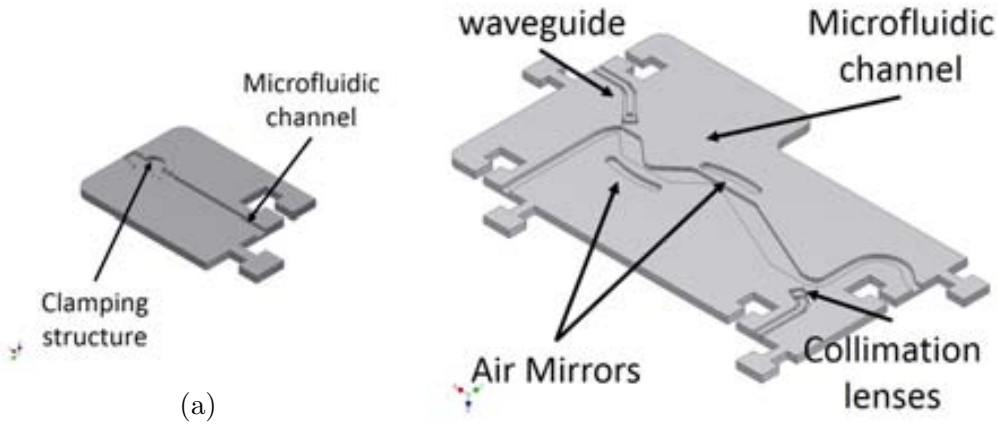

(a) (b)

Figure 5.7: Fluidic modules, (a) the fluidic I/O and (b) the detection chamber.

It has to be noted however, that to assure mechanical stability, easy to fill and leak-free structures, each module consist of two layers, first a substrate consistent only of a flat PDMS piece with the jigsaw shape and then, the optofluidic piece, where besides the jigsaw shape, the optofluidic components are patterned. Afterwards, both pieces, *i.e.*, substrate and

optofluidic pieces, are bonded together as detailed in section 3.3.2.

5.2 Fabrication

Modular fabrication techniques is also based in soft-lithography. However, modules fabrication is slightly different than the rest of the cases studied in this Thesis. Each module is made from two different masters. One master is simply a substrate with the jigsaw connectors and the other has the same contour, including the inner optofluidic parts *i.e.*, lenses, fluidic channels, waveguides, etc.

The substrate master is a single layer master (see section 3.3.1) with total thickness of 250 µm. The exact parameters to fabricate it are: SU-8 2050 spinned at $\omega = 750$ rpm and soft-baked during $t = 3$ h. After that, the wafer is exposed with a dose of $E = 450$ mJ/cm^2 and developed during 9 min.

Contrary, the master with optofluidic components is a two layers master. The first layer defines the optofluidic patterns while the second provides a frame used to planarize the PDMS. The first level is defined using SU-8 2050 spinned at $\omega = 750$ rpm, soft-baked during $t = 3$ h and exposed to a $E = 450$ mJ/cm^2. Then the second layer, of SU-8 2050, is spinned at $\omega = 750$ rpm, soft-baked for $t = 3$ hand exposed to a dose of $E = 450$ mJ/cm^2. Finally, the master is developed in a chemical bath for 15 min.

Once the PDMS replicas are made the fluidic ports are open and then both replicas are bonded together through oxygen plasma surface activation, as detailed in section 3.3.2. In Figure 5.8 the bonding process of the waveguide modules is detailed. In the left hand side the substrate is aligned with the optofluidic counterpart and pressed together. In order to facilitate the alignment a drop of water is place between both replicas.

Filters fabrication require a MIMIC step as detailed in section 3.3.3. The polymer used in this case is doped sol gel obtained following the recipe detailed in section 3.1.

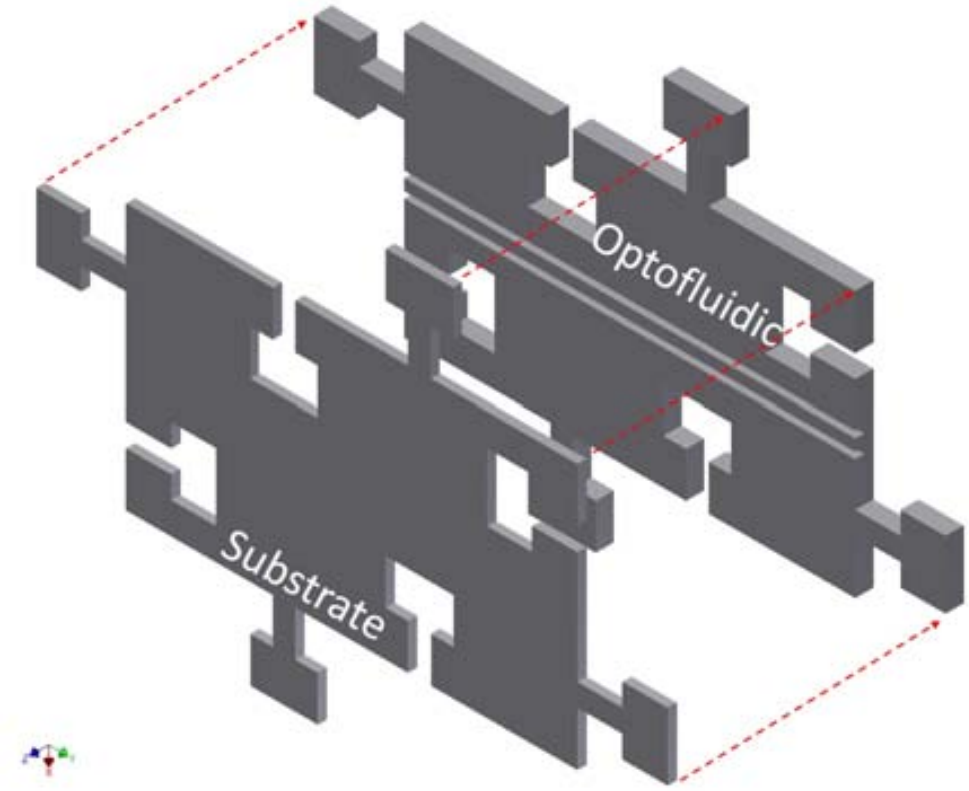

Figure 5.8: Bonding of the substrate and the optofluidic parts for the waveguide module.

5.3 Characterization

5.3.1 Jigsaw

In order to chose between different connectors shapes (5.5), three parameters are considered:

1. Peel off, *i.e.*, difficulty to peel off the replica from the master without structural damage.

2. Fluidic connection tightness, *i.e.*, leaking of the fluid through the connector.

3. Optical connection repeatability, *i.e.*, optical variations when the modules are separated and connected again.

Table 5.1: Connectors characterization.

Connector	Peel off	Fluidic tightness	Optical repeatability
cross	-	$> 60\%$	+
hook	-	$< 40\%$	-
rectangle	+	$> 70\%$	+
L	-	$< 30\%$	+

The results, shown in table 5.1, greatly varies between connectors. All of them but rectangle have peel off problems and some replicas are broken. Regarding fluidic tightness, the rectangle offers the best performance. Finally, optical operation of the connectors is more similar with good repeatability except for hook connector that shows a standard deviation bigger than 50%. With these results the chosen connector is the rectangular.

5.3.2 Light guides

First of all, an optical characterization of insertion and propagation losses of waveguides is needed. Characterization is done with an intensity measurement set up as detailed in section 3.5 using the $\lambda = 635$ nm laser source and 200 µm optical fibres. The fibres are connected to the optical I/O module. Between both I/O modules a different number of waveguide modules can be fitted. The schematic configuration is shown in Figure 5.9.

In order to calculate the insertion (L_i) and propagation (L_p) losses, three different longitudes are needed. The total length of the waveguide is increased by simply introducing more waveguide modules between the Optical I/O modules. For each length the measured intensity is recorded and ploted in Figure 5.10. The linear regression results are,

$$I = d \cdot (-12 \pm 2) \cdot 10^{-3} + (46 \pm 4) \cdot 10^{1}, \quad \text{with} \quad R^2 = 0.97.$$

Then, experimental results are $L_i = 5.45$ dB and $L_p = 3.06$ dB/cm.

Insertion losses are relatively high, mainly due to cylindrical lenses limitations. Cylindrical lenses are only able to collimate in the XY plane and therefore, most of the light is lost. Propagation loses are acceptable and similar to other PDMS waveguides with results of between 3.1 and 2.9 dB/cm [AfFM10].

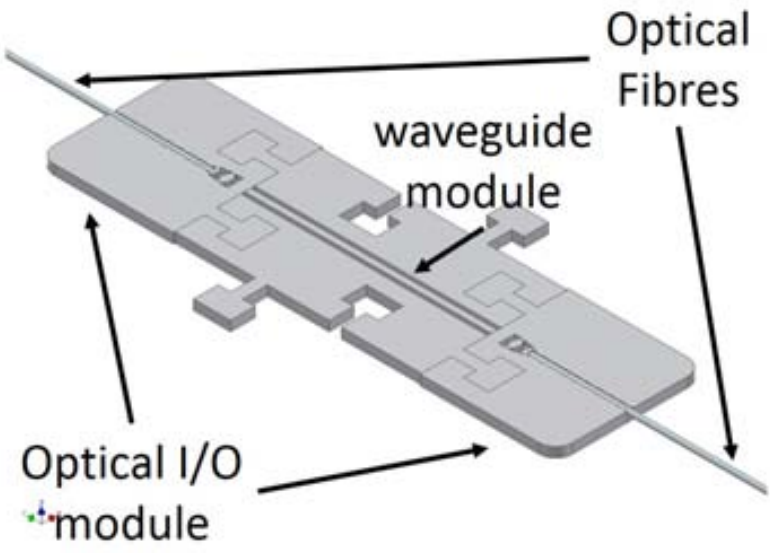

Figure 5.9: Configuration of a waveguide module between optical I/O modules.

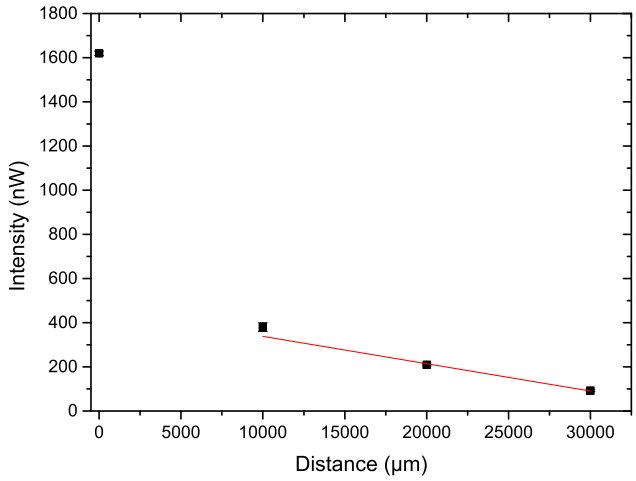

Figure 5.10: Experimental insertion and propagation losses using up to three waveguide modules.

5.3.3 Integrated filters

After that, a characterization of the filters is done. The setup is practically the same than for waveguides, only changing the waveguide modules for the filter module and substituting the powermeter for an spectophotometer (ocean optics QE65000).

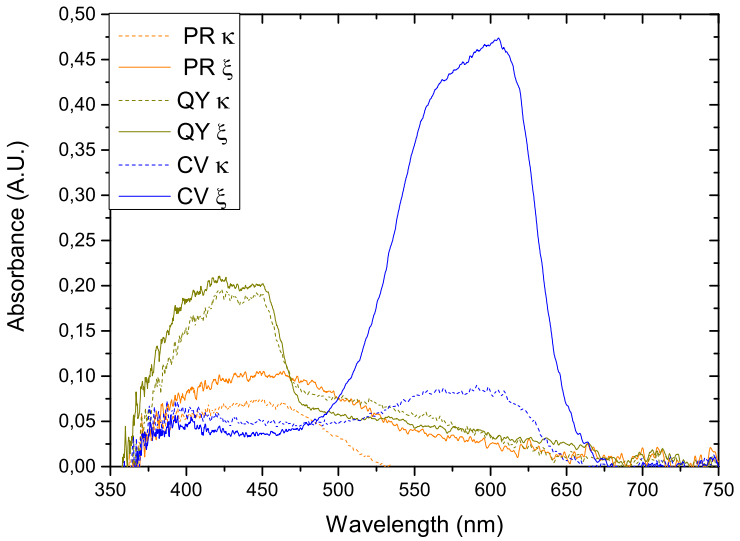

Figure 5.11: Filters absrobance, in arbitrary units, against wavelength.

Absorbance measurements can be seen in Figure 5.11. The absorbance peaks match the theoretical ones except for the PR, where a displacement from the theoretical 515 nm to 464 nm is observed. This displacement may be due to an inefficient pH control, with the consequent absorbance peak shift, or a defective PR sample, which will also explain the observed low absorbance values for this dye. For QY dye the absorbance for both filters length are really similar, which suggest that the filter, with the used concentration, has already achieved its maximum absorbance value on the shorter filter. On the other hand, CV filter has a huge change between κ and ξ filters. In fact, ξ filter achieve the maximum absorbance value.

The filters are demonstrated good optical capabilities and keep the fabrication requirements and costs low. Moreover, the filters can be easily

adapted to other polymers and dyes, increasing their flexibility.

5.3.4 Liquid state-emitter

Once the emitter is redesigned and filled with the solution specified in section 3.3.3, the characterization is performed using the emission mapping set-up, detailed in section 3.5 with $\lambda = 405$ nm light source. Excitation optical fibre is the smallest one, *i.e.*, 50 µm-core, in order to obtain the finest mapping resolution possible.

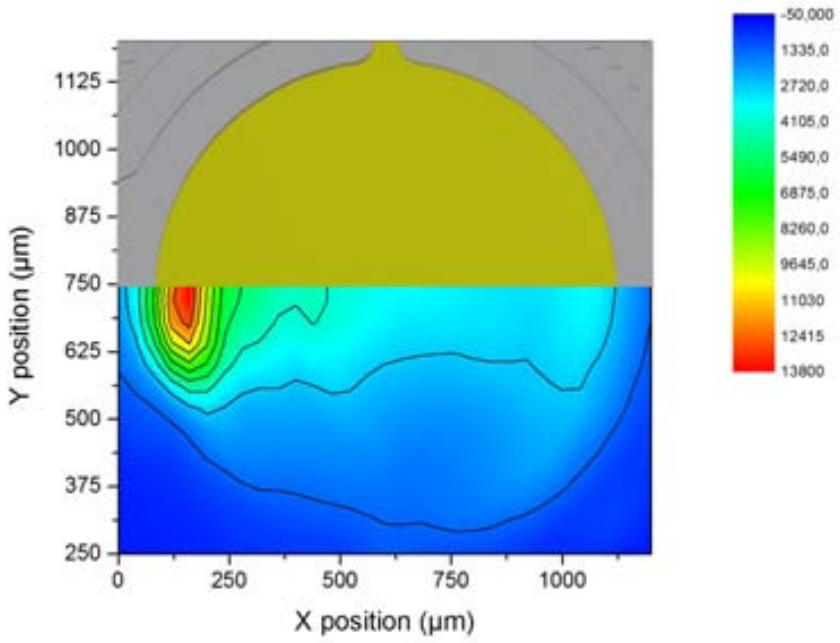

Figure 5.12: Recorded intensity (a.u.) at λ =479.6 nm. Scan using motor steps of 40 µm and spectrophotometer integration time of 400 ms/step. In the top half a CAD emitter design is over impressed.

Results of the intensity mapping, at fluorescence emission wavelength of $\lambda = 479.6$ nm, are plotted in Figure 5.12. As it can be seen, intensity distribution has a circular profile with a diameter of ∼1100 µm, which is consistent with emitter shape. Nevertheless, this circular intensity distribution is only a foggy shape, the maximum intensity peak is clearly located at the edge of the circle, at the closest region of the light recollec-

tion area. Such result indicates that only the closest region to the light recollection area contributes significantly to the output power. Therefore, the emitter dimensions could be reduced even more, reducing also the fluorophore volume needed.

5.3.5 Optofluidic Modular system

Once the optical modules have been characterized individually a more complex setup, with up to 4 modules combined together, is built to measure absorbance of a CV solution. The used modules are: two I/O optical modules, one I/O fluidic module and one MIR module, fitted as shown in Figure 5.13

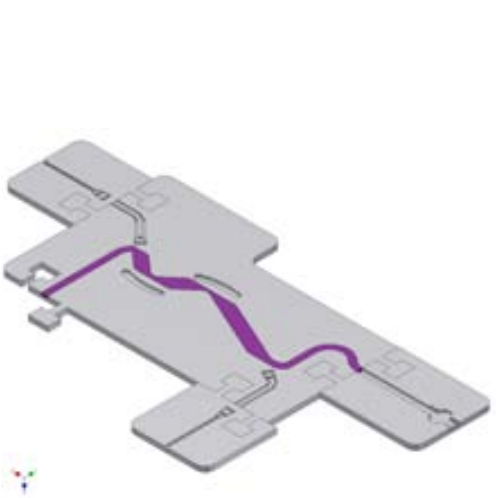

(a)

(b)

Figure 5.13: Scheme (a) and composed picture (b) of the final modular characterization.

A white light source (HL-2000, Ocean Optics) has been coupled to a 230 µm optical fiber, the optical fiber has been fixed into one of the I/O optical modules. An identical optical fiber has been fixed on the other I/O module and connected to an spectrophotometer (QE 65000, Ocean Optics).

Experimental results of absorbance measurements of different CV solutions are plotted in Figure 5.14

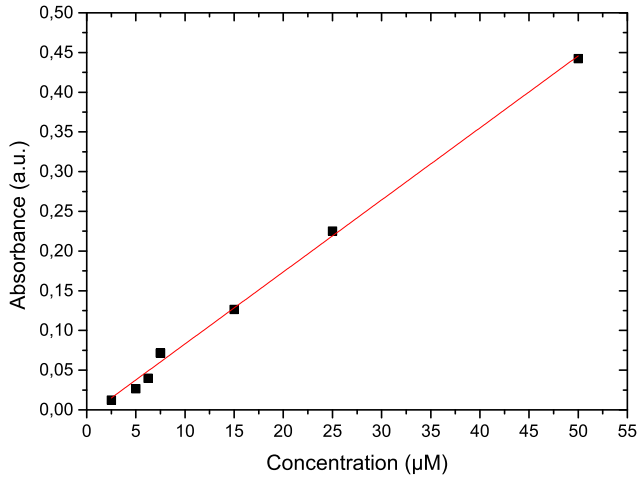

Figure 5.14: Absorbance measurements of CV at $\lambda = 600$ nm for different concentrations.

The obtained linear regression is,

$$A = C(9.1 \pm 0.2) \cdot 10^{-3} + (-8 \pm 5) \cdot 10^{-3}, \quad \text{with} \quad R^2 = 0.996.$$

The limit of detection obtained with the modular absorbance set up is LOD $= 1.53 \pm 0.04$µM, similar to that obtained with monolithical systems [LWB08]. These results validate the presented modular system for LOC applications.

6 | Micro Droplets

In this chapter, a highly integrated optofluidic system for spectrometric analysis of monodisperse microdroplets is presented. This chapter is the result of a short stage fellowship in Albanova University Centrum, Stockholm, Sweden, under the supervision of Prof. Dr. Helene Andersson-Svahn.

6.1 Microfluidic

Microdroplets are colloids resulting from the breakup of one liquid phase in another, typically in the presence of surfactants. A colloid can be easily achieved simply mixing oil and water. Nonetheless, monodispersity was not achieved until 2000 [UPW00], although, following a protocol not suitable for miniaturization.

In 2001, a new device to generate monodisperse microdroplets with a droplet size variation lower than 1% was presented [TRAQ01]. Water (aqueous phase) and oil with surfactant (oil phase) were mixed together in a T-juntion. Droplets were formed when the water pressure is lower than the oil pressure (more detailed explanation can be found in section2.2.2).

Since then, monodisperse microdroplets, microdroplets from now on, has been used in a wide range of applications for (bio)-chemical analysis. Microdroplets have three key features; (*i*) Monodispersity that allows quantitative and statistical measurements, (*ii*) high-throughput with typical droplet generation rates between 0.1 and 10kHz [MEM$^+$12] and (*iii*) compartmentalization, where reactions [MBB$^+$09], bacterial [BLKI08], human cells [WCD$^+$13] or even living organisms [CTLB$^+$08] could be isolated. Microdroplets have been used for single cell encapsulation, manipulation and analysis [JA12] as well. Microdroplets also offers an easy way to solve the mixing problem, as can be seen in Figure 6.1. Once

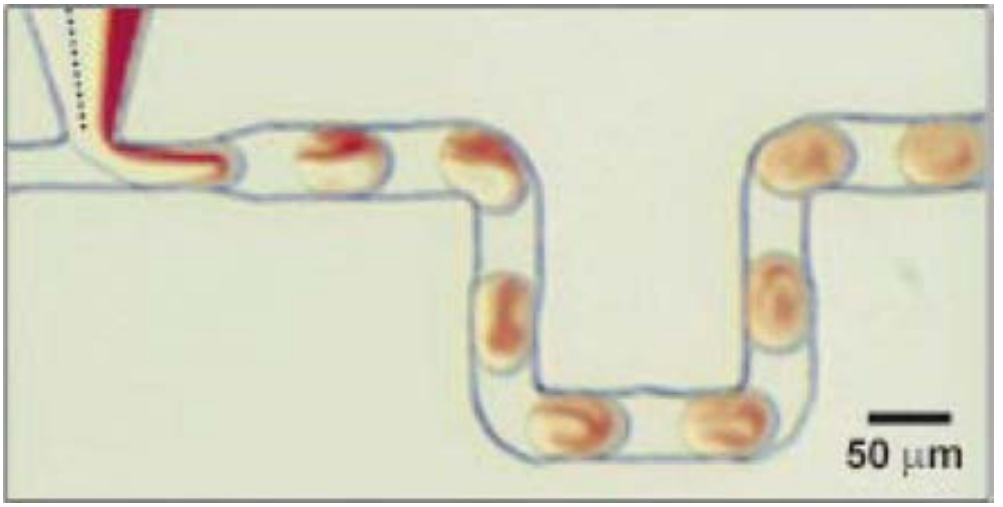

Figure 6.1: Reported mixing process for monodisperse microdroplets [SI03].

droplets are formed, a simple U-shaped microchannel of few micrometers long is enough to mix their content, as can be seen in Figure 7.2b.

Nowadays a myriad of tools for forming [vSKD+13], fusing [CDX+12] and sorting [HYSS12] microdroplets have been reported.

Regarding detection mechanism three main methods have been used:

Mass spectrometry is a label-free detection method for both, chemical and biological reactions [FWR+09]. However, integration of this method for microdroplets detection instead of continuous flow is challenging and increase the complexity and cost of the final LOC.

Electrochemical detection method is inexpensive and also label-free [FYE+12]. Nevertheless, it is hampered by the use of an electrochemically active reactant and only interacts with the droplet interface.

Fluorescence detection is a widely used method for droplet detection and allows sensitive, ulta-fast and localized information in a quantitative manner. Nevertheless, the setup requires an inverted microscope, labelled droplets to produce laser-induced fluorescence and usually a high speed CCD camera, making the setup bulky and relatively expensive. Therefore, a fast-response, label-free and inexpensive detection method is required.

The system here presented aims to improve current detection methods by defining a system able to perform optical detection, *i.e.,* fluorescence or absorbance measurements, with a couple of integrated optical fibres. Such system prevent the use of microscopes and then, reduce cost and size of the setup.

6.2 Design

In order to generate and measure single droplets (∼65 pL) at generation ratios between 40 and 1000 Hz two LOC are designed.

Both LOCs are based on a 3 layer master. The bottom layer has a thickness of 45 µm and is the droplet generation layer. This layer contains the T-junction to form the droplets. Droplet sizes are determined by the dimensions of this layer, which is designed to produce droplets of Ø= 50 µm. The droplet detection layer has a thickness of 90 µm and it contains the detection region. Since droplets are less dense than the surrounding liquid, they experience buoyancy forces. New droplet position, on top of the channel, should match the optical fibre core position, ensuring a good alignment between droplet and light, to maximize detection. Finally, the top layer is 125 µm thick and this is the layer for optical components such as collimation lenses, integrated filters and the insertion of optical fibres. For clarification purposes a schematic view of the device is shown in Figure 6.2.

These two LOCs are designed to make the device suitable for working in fluorescence or absorbance regimes and hence both LOCs have collimation cylindrical lenses to minimize diffraction losses. In fluorescence measurements (Figure 6.3a) the filtering of excitation light is a key issue, and for this reason integrated, polymer based, optical filters (sec. 4.1.3) are included in the device. Moreover, light injection and light recollection are placed at 90° to minimize the noise generated by the excitation light. This LOC is called $\pi/2$.

On the other hand, the absorbance measurements requires to collect as much light as possible in the output optical fibre. Therefore, 180° configuration is designed. This LOC is called π. Optical fibres are placed perpendicular to main channel in order to reduce the distance between the injection and recollection optical fibres, as it is shown in Figure 6.3b.

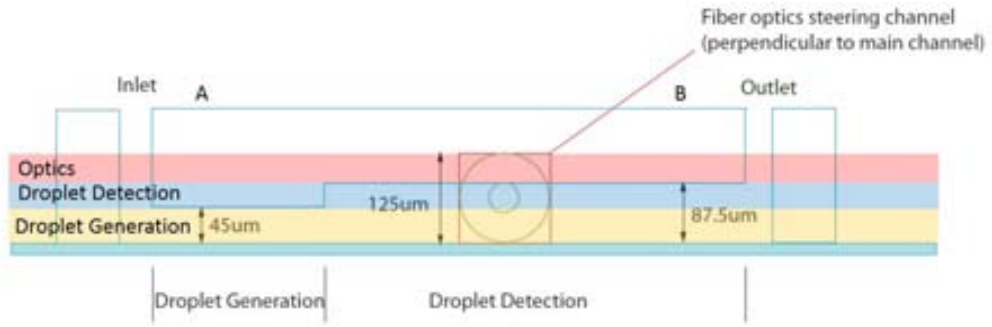

(a) Cross section of the LOC.

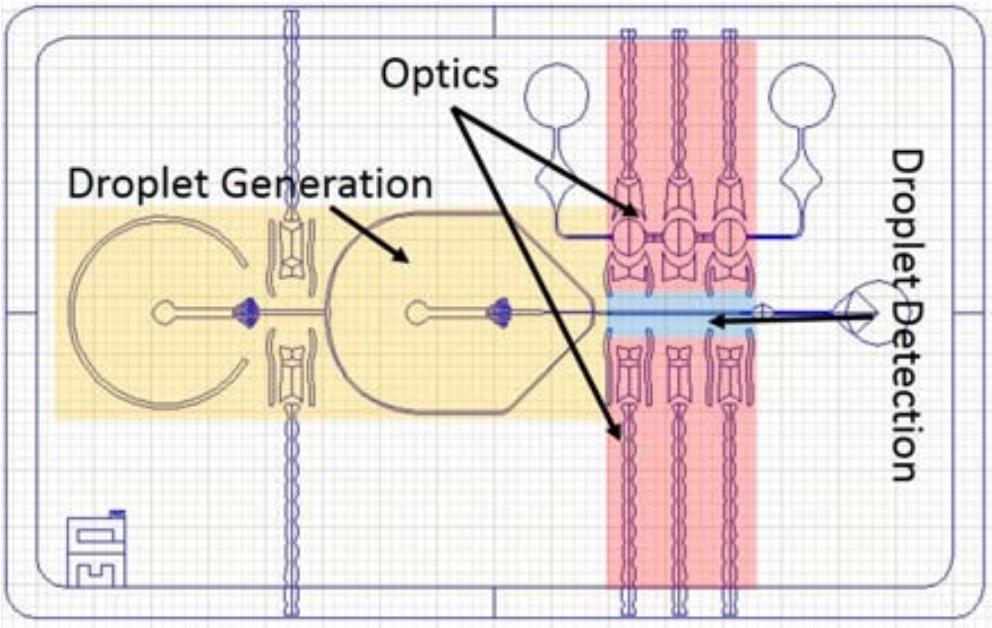

(b) Top view of the LOC.

Figure 6.2: Cross section and top view of the 3 layers master. Orange zone corresponds to droplet generation, with a thickness of 45 µm, blue zone is the droplet detection layer, with a total thickness of 90 µm and red zone delimits the optical layer, with a total thickness of 125 µm.

6.3 Fabrication

Droplet LOC master is the most complex and require 3 layers. Details of fabrication can be seen in section 3.3.1. In table 6.1 the main parameters are detailed for every layer.

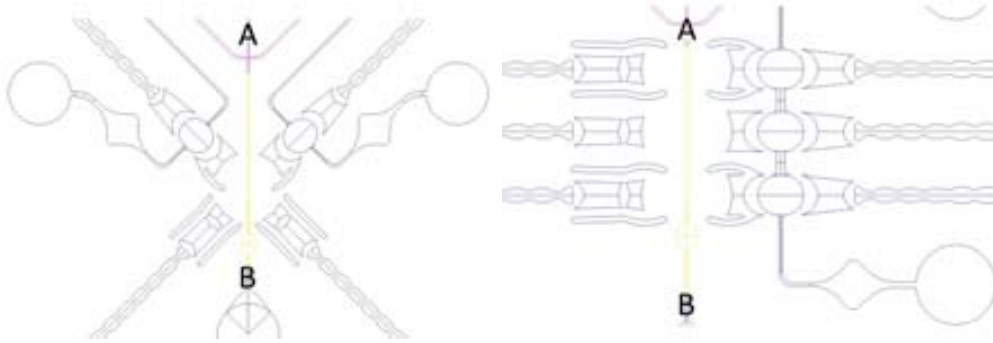

(a) Schematic view of X-LOC. (b) Schematic view of T-LOC.

Figure 6.3: Top view of X and T LOCs. The pink region is the droplet generation region (45 µm), yellow channel is the detection region (90 µm) and finally the blue parts are the optical layer (125 µm).

Table 6.1: Droplet genration master fabrication parameters for every layer. Development time of the wafer is $t = 7$min.

Layer	SU-8	ω (rpm)	t (h)	E (mJ/cm^2)
Generation	2025	1750	1	150
Interrogation	2025	2250	1	150
Optics	2025	2250	1	150

PDMS replicas are done following the same procedure reported in section 3.3.2 with a total PDMS thickness of 4 mm. This extra thickness ensures a good grip between the I/O reservoirs and the tubing, preventing fluid leaking and pressure changes. After that, openings (inlets and outlets) of 0.75 mm are done using Harris Uni-core biopsy punches. Finally, the inner surface of the LOC is treated by Aquapel (Pittsburgh Glass Works LLC, USA) to increase channel hydrophobicity and thus reducing, droplet coalescence.

6.4 Results & Discussion

In this section three main setups are considered. The first one, from now standard set up, consist of an inverted microscope, a laser excitation light source (Cobolt Calypso 491 nm, Sweden) and a Photomultiplier Tube (PMT) (Hamamatsu H5784-20, Japan). On the other hand, second and

third setups, also known as $\pi/2$ and π, are basically the spectral response set up (see section 3.5) using 125 µm optical fibres to connect the optical input and output and USB200+ spectrophotometer. The main difference between them is the relative position of the fibres, while for $\pi/2$ the fibres are orthogonal, for π the fibres are faced. In Figure 6.4 the π set up is clearly seen.

6.4.1 Standard set up versus new LOCs

A first set of experiments were designed to measure the speed, size and number of droplets. For the standard setup the aqueous phase is a 100 µM fluorescein solution, while for π and $\pi/2$ the aqueous phase is pure water. It is noteworthy that detection of unlabelled droplets, *i.e.,* pure water droplets, is not possible with the standard set up.

In accordance to Anna *et al.* [ABS03], the flow quotient between aqueous flow rate (Q_{aq}) and oil flow rate (Q_{oil}) may change droplet size and frequency. To reduce the number of parameters to consider it is fixed at $Q_{aq}/Q_{oil} = 0.1$. Droplet size depends on flow rate. In Figure 6.5, droplets of different sizes for different Q_{aq} are shown. For low Q_{aq} the experimental frequency is smaller than theoretical one, and hence, droplets size are bigger than the expected droplet size. Theoretical values are calculated assuming constant hydrodynamic resistance and constant droplet size (50 µm). These assumptions are a simplification [ABS03, XLTL08, VBvdE$^+$09] of the real case but give us a valuable approximation.

When comparing theoretical droplet generation frequency with experimental results, shown in Figure 6.6a, one can see that $Q_{aq} = 100$ µL/h is the most similar result between theoretical and experimental data, suggesting a droplet size very close to the expected 50 µm. On the other hand, droplets for flow rates lower than 100 µL/h are bigger than 50 µm and droplets generated at $Q_{aq} = 200$ µL/h are smaller than that.

Comparing the measured droplet frequency using the standard and the $\pi/2$ and π configuration setups, plotted in Figure 6.6b, one can see how all setups give similar results. The coincidence of the results validate our setups to optically detect unlabelled droplets for the first time.

However, is noteworthy that the flow rate limit for $\pi/2$ and π configurations is around 50 µL/h. At higher generation frequencies droplets are too fast to detect them with the presented setups. The observed

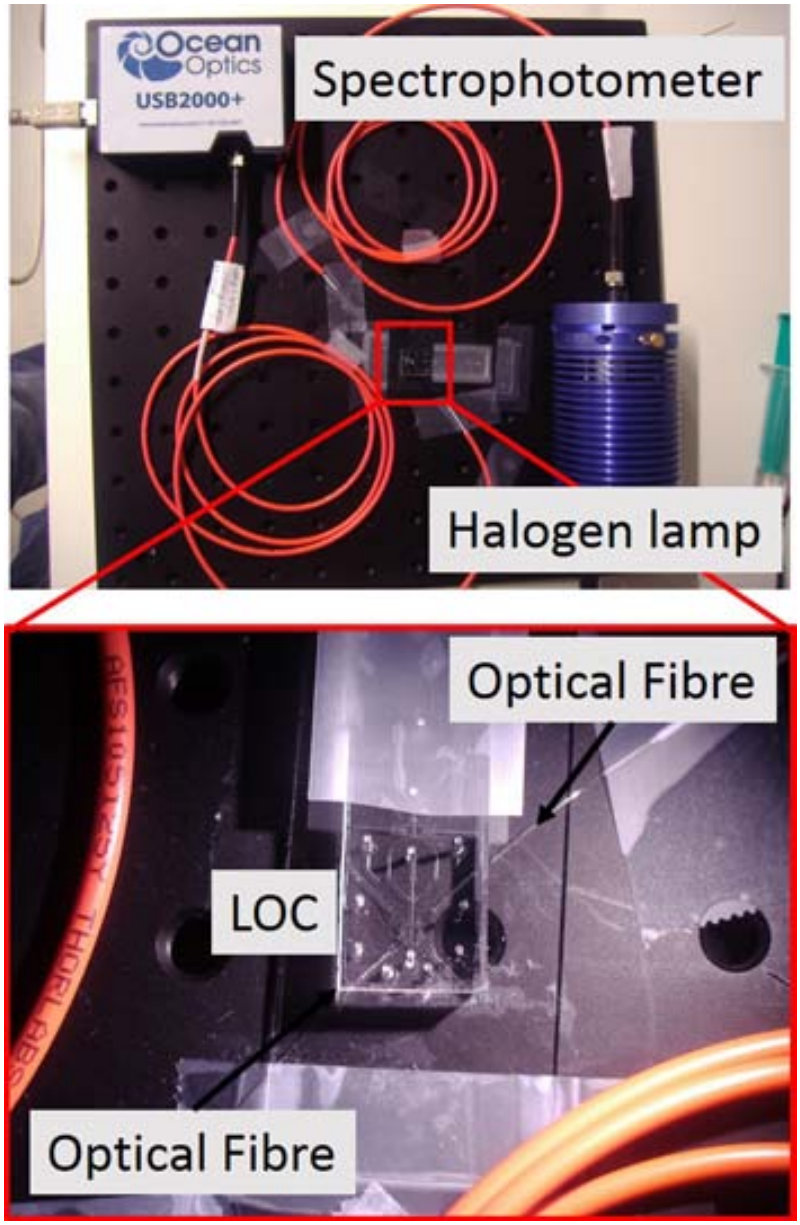

Figure 6.4: Droplet detection set up. Is the same picture showed in section 3.5.

flow rate limit is caused by two main reasons: (i) the spectrometer can only record an entire spectrum every 2 ms and then the theoretical detection limit is 500 droplets/s or, corresponding to aqueous flow rate of

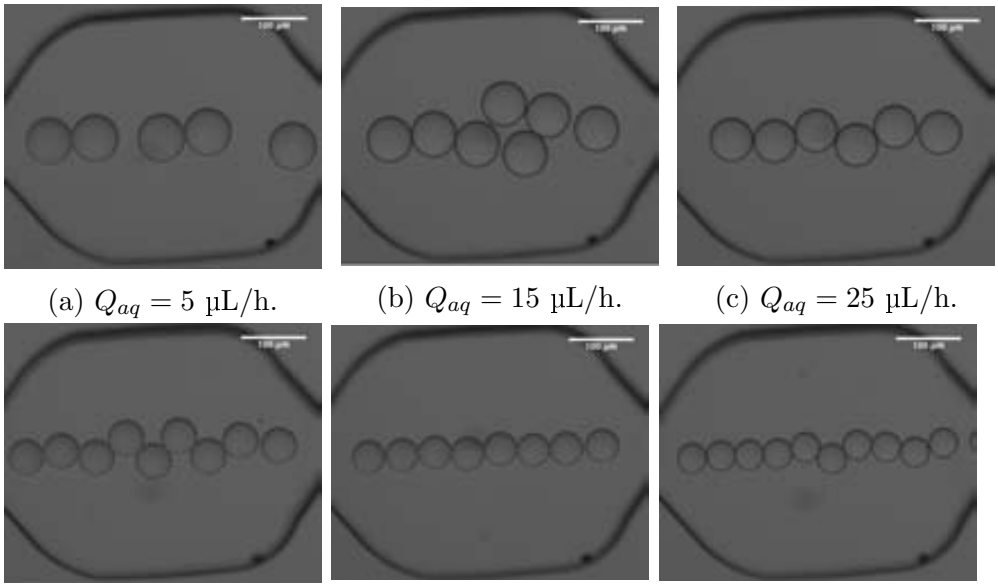

(a) $Q_{aq} = 5$ µL/h. (b) $Q_{aq} = 15$ µL/h. (c) $Q_{aq} = 25$ µL/h.

(d) $Q_{aq} = 50$ µL/h. (e) $Q_{aq} = 100$ µL/h. (f) $Q_{aq} = 200$ µL/h.

Figure 6.5: Pictures of the actual droplet size at different flow rates.

$Q_{aq} = 100$ µL/h, and (*ii*) the presented setups are not able to properly detect when more than one droplet is passing through the optical path. This situation can be seen in Figure 6.7. When a single droplet passes through the detection optical path on the π (Figure 6.7a), the measured intensity abruptly decays due to scattering produced in the aqueous/oil interface. In Figure 6.7b each intensisty valley corresponds to a single droplet measurement.

On the other hand, when more than one droplet are simultaneously placed on the detection optical path (Figure 6.7c) the measured intensity shows an average pattern (Figure 6.7d) and then single droplet detection is no longer possible. This circumstance limits the maximum droplet detection frequency.

In Figure 6.8 the measured intensity of the $\pi/2$ setup with pure water droplets can be seen. $\pi/2$ configuration has sharp peaks when the droplet is detected and a low background noise. These peaks in the $\pi/2$ LOC are due to excitation light scattered at the droplet oil/water interface. Significant differences in peaks intensity is observed, these differences may be due to uncontrolled screening position respect the droplet, *i.e.*, we do not know if the screening is taking place at the centre of the droplet,

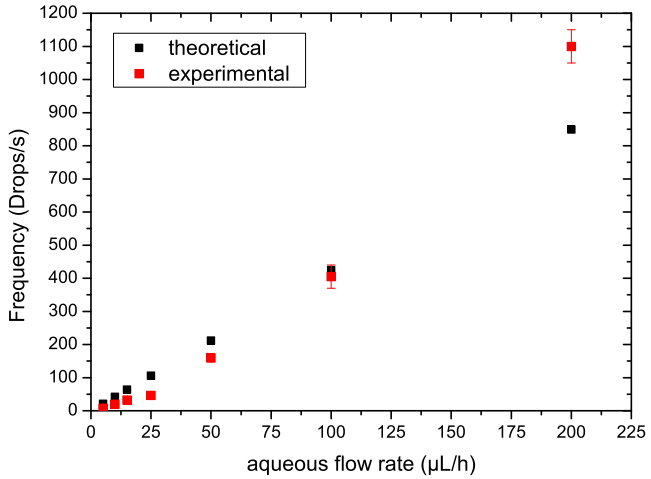

(a) Droplet generation frequency for different aqueous flow rates. The theoretical values are calculated assuming constant droplet size of 50 µm in diameter.

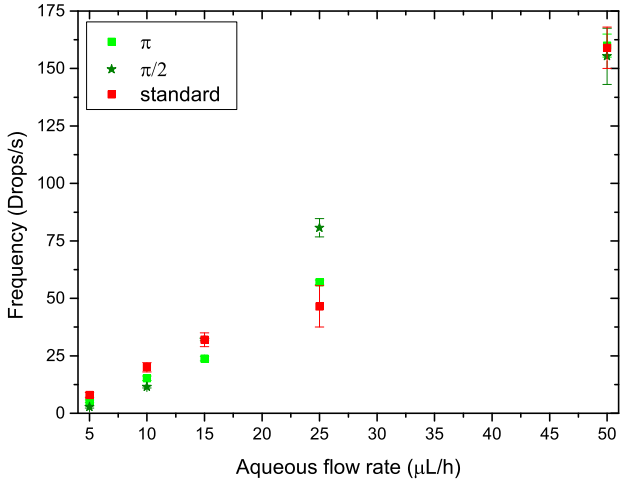

(b) Results of droplets generation frequencies at different flow rates for the three studied setups.

Figure 6.6: Frequency of droplet generation at different aqueous flow rates (Q_{aq}) detected by different setups.

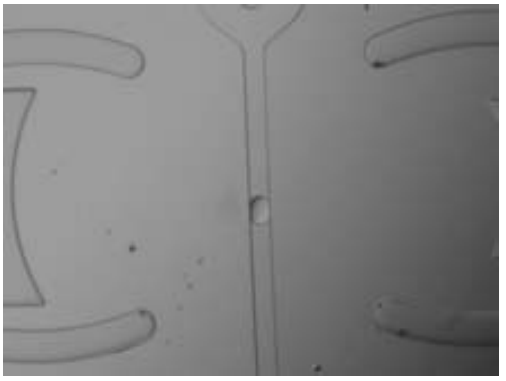

(a) A single drop passing through the detection optical path.

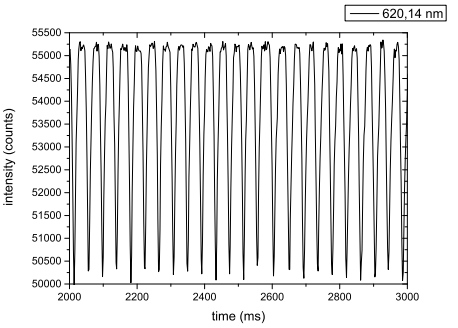

(b) Intensity results of water droplets detection at $\lambda = 620.14$ nm using the π configuration for a single droplet.

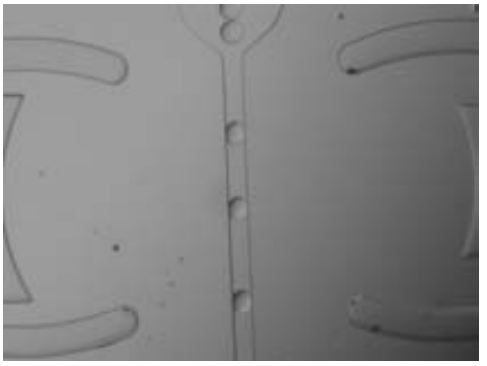

(c) Multiple drops passing simultaneously through the detection optical path.

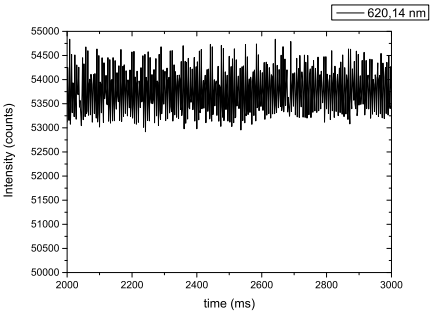

(d) Results of water droplets detection at $\lambda = 620.14$ nm using the π configuration for multiple droplets.

Figure 6.7: Pictures and typical recorded spectrum for single or multiple droplet detection.

with low scattering effects, or at the side, with scattering effects more noticeable. Summarizing, detection of pure water droplets for both, π and $\pi/2$ configurations, clearly suggest that we are detecting scattered light, validating a label-free, highly integrated optical detection mechanism.

6.4.2 pH measurements

Once the droplet detection is ensured on π and $\pi/2$ configurations our next goal is the detection of droplet content. In many biological appli-

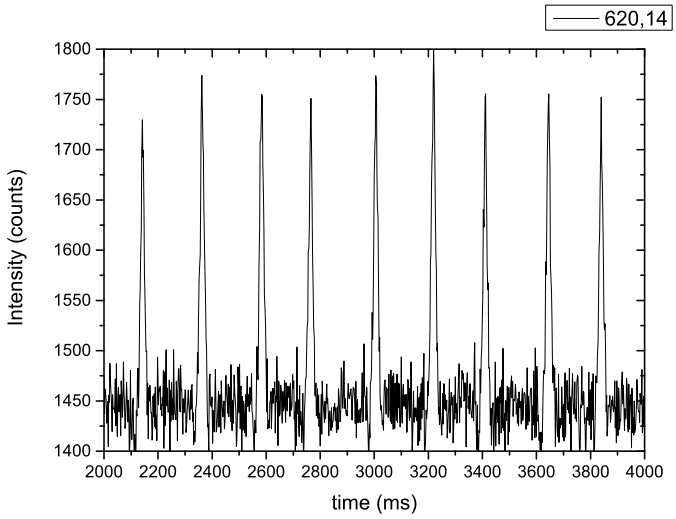

Figure 6.8: Intensity results of water droplets against time. Detection at $\lambda = 620.14$ nm using the $\pi/2$ configuration.

cations involving cell culture, pH of the medium is a key issue. Optical pH measurements are based in absorbance of a pH indicator and then, π configuration is the selected one. Firstly, a calibration curve for different bromothymol blue concentrations in continuous flow, as detailed in section 3.1, is performed. Continuous flow offers an important increase of interaction length when compared to single droplets, since the whole light beam width interacts with the solution. The results are shown in Figure 6.9, absorbance spectrum at three different concentrations, 250, 750 and 1000 µM, are plotted. Water is used as reference.

when calculating the linear regression of bromothymol blue absorbance ($\lambda = 620$nm) the equation obtained is:

$$A = C(25 \pm 2) \cdot 10^{-6} + (-3 \pm 1) \cdot 10^{-3}, \quad \text{with} \quad R^2 = 0.99.$$

with a limit of detection of LOD $= (12 \pm 1) \cdot 10$ µM. This result clearly suggest a linear relation between concentration and absorbance, in good agreement with Lambert-Beer's law (see sec. 2.1.3).

Once the linear correlation in continuous flow detection of droplet content is attempted. Light beam interaction with droplets is significantly smaller than in the continuous flow case. Hence, bigger LOD is expected. In order to calculate absorbance the reference signal is the flat region

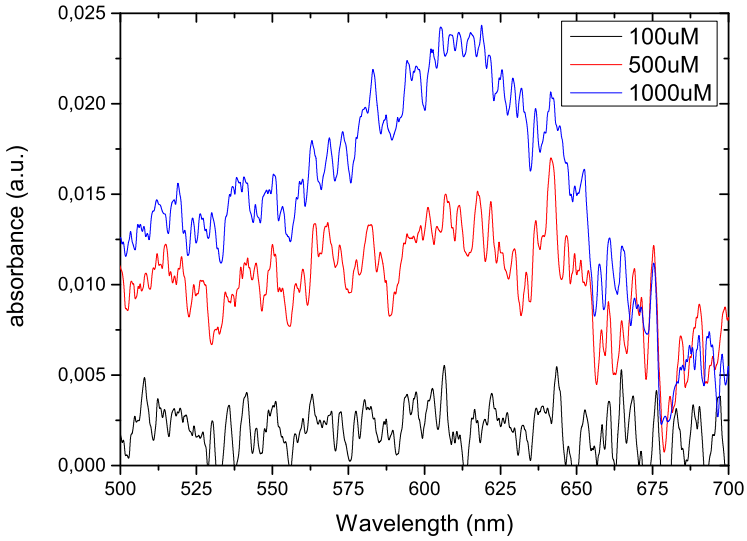

Figure 6.9: Absorbance results of bromothymol blue continuous flow at 3 different concentrations using π LOC.

between valleys observed in Figure 6.7b, which corresponds to no droplet situation, and intensity registered on the bottom of the valley links with the droplet measurement situation. The obtained linear regression is detailed below.

$$A = C(8 \pm 1) \cdot 10^{-6} + (12 \pm 1) \cdot 10^{-3}, \quad \text{with} \quad R^2 = 0.96.$$

obtaining a LOD $= (38 \pm 5) \cdot 10$ µM. As expected the results are worse than those in continuous flow. Nonetheless, strong linear correlation between bromothymol blue concentration and absorbance suggest that light absorption is taking place inside the droplets. However, LOD of our set up is 380 µM, far from state of the art results of few nM, but it provides the first experimental evidence of inner droplet medium quantification using a highly integrated optofluidic system.

7 | Fluidically Controled Optical Router

In this chapter a highly integrable fluidically controlled optical router (FCOR) for optofluidic systems is presented. Along the chapter, the prototyping process is explained. Already reported routers are analysed in order to improve them for LOC applications. After that, a new FCOR is designed and simulated. Then, the FCOR is fabricated using soft-lithography techniques and finally, it is characterized and combined with a previous LOC for multi-analyte detection. This work is the result of a collaboration between IMB-CNM, CSIC, and IMTEK, University of Freiburg.

7.1 Optical routers

Nowadays, LOC applications are becoming extremely sophisticated analysis platforms requiring statistical analysis [GLI+11], multiple control points [DVPA+11, WSK+14] (Figure 7.1) and several wavelengths in order to achieve a reliable analysis performance [DvWB+10, JWL13].

However, integration of many readout systems and light sources at different LOC points is very complex. For instance, Carlborg *et al.* [CGK+10] used diffraction gratings, MMI splitter and a set of 8 detectors to insert, split and detect light obtaining a simultaneous measure of up to 6 fluidic channels at once. However, diffraction gratings and MMI splitters are strongly wavelength dependent and require very precise fabrication technologies (sub-micron). Other groups used even more complex setups requiring several external optical elements such as beam splitters and lenses. Furthermore, their working wavelength is limited to the range between 700-850 nm [RDF+13]. An easily integrable optical

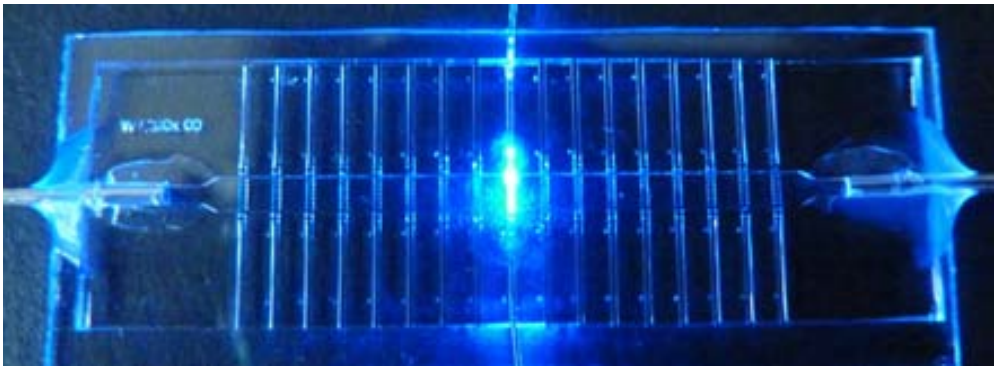

Figure 7.1: Picture of a LOC with 34 optical channels [DVPA+11].

router could solve these drawbacks providing an automatic way to switch between light sources, readout systems or control points.

Nonetheless, the overwhelming majority of optical routers are applied on telecommunications. Telecommunications routers have switching frequencies on the order of GHz, but they are not suitable for LOC applications due to their cost (∼1 k€), working wavelengths regime, focused at $\lambda = 1550$nm with a maximum wavelength range of $\Delta\lambda = \pm$ 50nm [WPW+02] and fabrication technologies, mainly limited to CMOS compatible devices.

Few commercial optical routers (e.g., OSWxx-yyyyE from Thorlabs or MPM-2000 Optical Multiplexer from Ocean Optics) are available at wavelengths outside telecommunications range, *i.e.*, at $\lambda = 1550$ nm. Their wavelength working range is of ∼200 nm in the spectral region included from 200 nm to 1650 nm, depending on the chosen model. Nonetheless, their switching frequencies are limited ($\leq$ 6.5 Hz). Moreover, these commercial routers are expensive and not integrable in LOC systems.

In the literature, several integrated optical routers and switches can be found. Regarding optofluidic switches, Nguyen *et al.* [NKGL07] used an hydrodynamic flow control to steer a liquid-core/liquid-cladding (L^2) waveguide and then, choosing the output optical channel. Seow *et al.* [SLL09] used hydrodynamic flow control to modify the reflection position and hence, switching between optical channels (Figure 7.2a). In both cases, 3 different fluidic flows, precisely controlled, were needed in order to obtain switching frequency of 3.3 and 1.56 Hz for Nguyen and Seow respectively.

Song *et al.* [SP11] presented a pneumatically tunable 2x2 optical

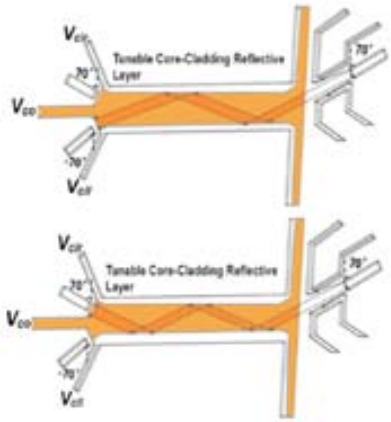

(a)

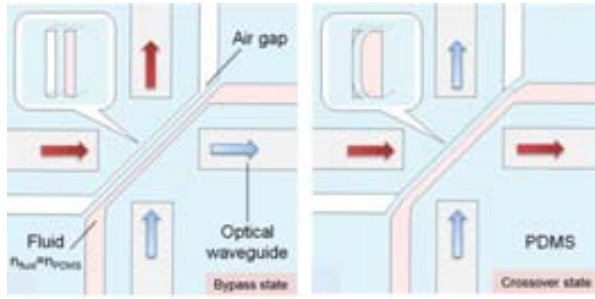

(b)

Figure 7.2: router schemes reported by (a) Seow *et al.* and (b) Song *et al.*

switch with a single fluidic flow control needed. They had two parallel channels in close proximity, one of them was filled with air, which serve as switchable air-gap mirror, and the other one with a liquid. When the liquid pressure was increased the PDMS wall starts to deform until the air-gap collapsed, Figure 7.2b. Song *et al.* achieved switching frequencies of 5 Hz.

Regarding optofluidical routers, Fouquet [Fou00] reported a 4x4 planar optofluidic router with fast switching frequencies of 1 kHz. The working principle was based in total internal reflection at air bubbles generated by thermal actuators. This router can be extended to 32x32 configuration. However, it was thermally controlled and the thermal actuator was fabricated on a separate system bonded to a silica waveguide chip, increasing the costs and technological complexity.

Groisman *et al.* [GZC+08] reported a 1x4 router based on RI changes of a liquid over a diffraction grating. This optofluidic router had a good switching frequency of $\sim$ 18.2 Hz. Nonetheless, RI change requires 4 liquids with different RI in order to allow the optical switching. Besides, the optical router worked in an out of plane configuration, complicating the integration in LOC applications.

Recently an optofluidic router based on EWOD has been presented [MKLZ13]. EWOD actuators are used to precisely control a water/oil interface which act as a mirror when the TIR conditions are fulfilled. Due

to EWOD actuators, LOC fabrication complexity, cost and response time highly increase, achieving switching frequencies between 0.3 and 0.6 Hz.

All reported optical routers require non-standard technologies dramatically increasing fabrication costs and time, thus preventing their integration in optofluidic systems. Consequently, an integrable, compact, large spectrum working range, fluidically controled optical router has been designed, fabricated and characterized in this thesis.

Router fabrication is based in soft-lithography and it is build entirely with PDMS and air, fulfilling the requirements of robustness, reliability, low cost and wide optical working regime. The working principle of the router is based on both, phaseguides (sec. 2.2.1) and air mirrors (sec. 2.1.1). In fact, phaseguides allow the formation of air mirrors. Each air mirror reflects the light to a specific output optical channel. Using phaseguides as mirrors, a final device fabricated using replica moulding and actuated using a single fluidic flow is here presented.

7.2 Design & Fabrication

7.2.1 Design

In Figure 7.3 a schematic view of the device can be seen. Cylindrical lenses are added to the structure in order to collimate the light, increasing the light amount reaching the output optical channel. Self-alignment systems are included to ensure the alignment between the optical fibres and the lenses. Output optical channels are numbered from right to left and the input optical channel is labelled as channel 0 (ch 0). On the other hand, fluidic input and output channels are labelled as inlet and outlet respectively. Embeded phaseguides can be seen in the main microfluidic chamber (Figure 7.3).

The presented router design addresses two main topics, optics and microfluidics. From a microfluidic point of view, phaseguides previously reported [VMA+06] are implemented. Detailed at the bottom left corner of Figure 7.3, a scheme of the phaseguides is shown. They are significantly taller (110 µm in a channel of 125 µm, 88%) than the ones presented by Vulto *et al.* (25%) and are suspended 10 µm over the glass substrate. Presented phaseguides limit the meniscus pinning effect to the bottom of the chamber, avoiding possible uncontrolled lensing effects.

Since the phaseguides are fixed elements, and hence, the incident light

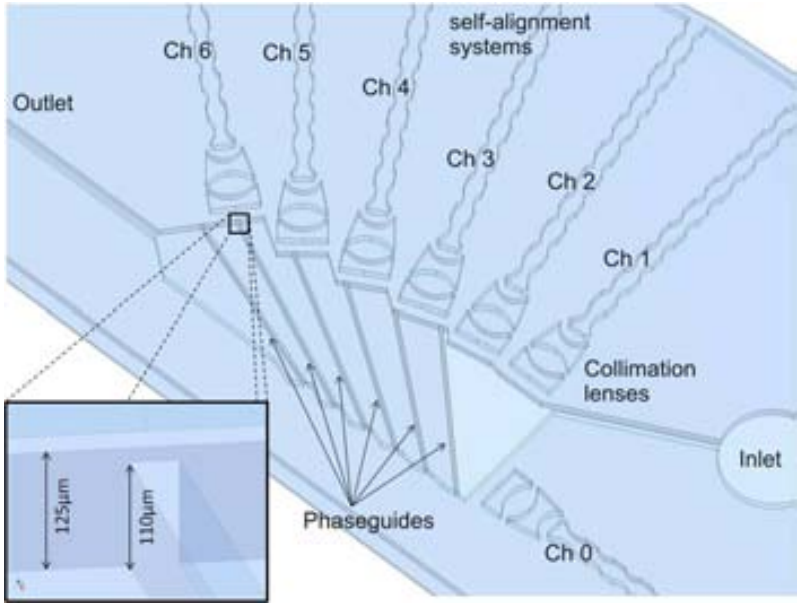

Figure 7.3: Schematic view of the LOC. The optical channels are numbered and the phaseguides clearly pointed.

angle is constant at each phaseguide, TIR conditions do not depend on the PDMS refractive index and are only limited by the RI of the liquid used to fill the chamber. A detailed scheme of the light behaviour on a phaseguide tilted 45° with respect to the incident light beam can be seen in Figure 7.4. The precise mathematical analysis is detailed in equation 7.1.

$$\left.\begin{aligned} n_l \sin 45^\circ &= n_{PDMS} \sin \beta_2 \\ n_{PDMS} \sin \beta_2 &= 1 \end{aligned}\right\} n_l = \frac{1}{\sin 45^\circ} = \sqrt{2} \approx 1.4142 \tag{7.1}$$

In order to demonstrate the described behaviour the first phaseguide angle is placed at 45°(channel 1). The rest of the phaseguide angles are bigger than the critical angle when the filling liquid is water ($\theta_c = 48.61$) and different enough to avoid light in more than one output optical channel at any time, thus avoiding cross-talking between channels. Hence, phaseguide angles are 50, 55, 60, 70 and 75°for channels from 2 to 6 respectively.

The presented design has two main advantages. Firstly, it reduces the fabrication costs and complexity allowing soft-lithography fabrication

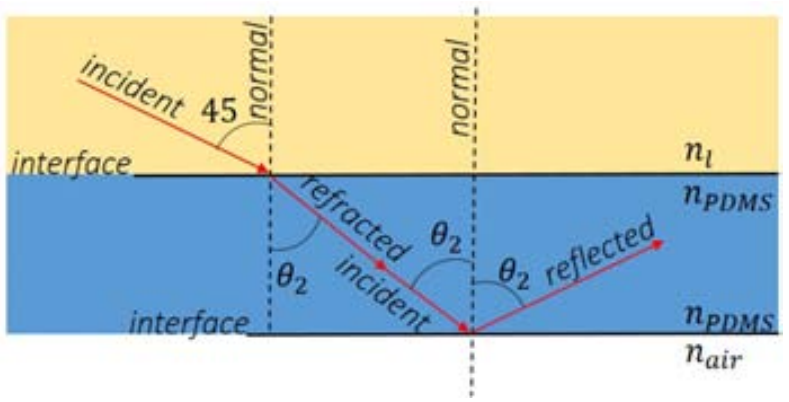

Figure 7.4: Schematic representation of the light behaviour on the first phaseguide (45°).

techniques, where only two photolithographic steps are required for the master definition. Secondly, the liquid/air meniscus is much smaller and attached to the bottom, far from the optical path. This is important because meniscus pinning effect generates hardly controlled liquid/air meniscus shape changes [GW05]. These meniscus shape changes could act as unstable lenses, preventing then a controlled and repetitive final FCOR.

From an optical point of view, different elements, *i.e.*, self-alignment systems, collimating lenses and air mirrors, detailed in section 4.1, has been included in the final design. In this case, the phaseguides play the role of air mirrors. Once the liquid achieve the breaking pressure and fills the next reservoir, the following phaseguide becomes the mirror interface. For simulating the optical performance of the developed FCOR, ray-tracing was performed for a single wavelength of $\lambda = 550$ nm, using the commercial tool ZEMAX. Cylindrical lenses at the input and output optical channels were modeled by biconic lens elements with constant radius of curvature. For PDMS, a refractive index of $n = 1.420$ was assumed [SBP+11].

The coupling efficiencies were calculated as follows. Using the non-sequential mode of ZEMAX, 100.000 rays were emitted from the end facet of the input fibre with a numerical aperture NA = 0.22, traced through the system taking into account Fresnel reflections losses at various interfaces, and the optical power at the end facet of the output fibre was detected, considering 0.22 as the NA of the output fibre. Coupling efficiencies are

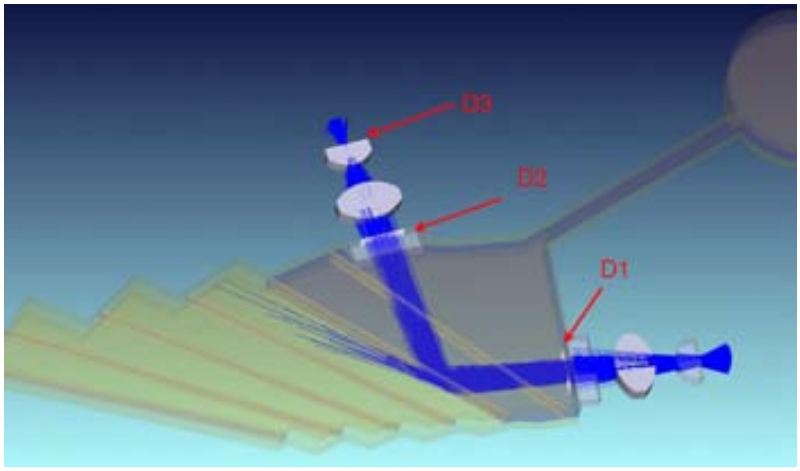

Figure 7.5: Simulated ray tracing propagation for channel 2 output.

very low due to the fabrication limitations (*i.e.*, cylindrical lenses). In other words, part of the optical efficiency has been sacrificed in order to keep the fabrications costs as low as possible.

Table 7.1: Simulated coupled efficiencies for every channel.

Ch.	Coupling efficiency (%)
1	$(1.7 \pm 0.1) \cdot 10^{-2}$
2	$(8.2 \pm 0.1) \cdot 10^{-2}$
3	$(6.8 \pm 0.2) \cdot 10^{-2}$
4	$(4.4 \pm 0.4) \cdot 10^{-2}$
5	$(3.9 \pm 0.3) \cdot 10^{-2}$
6	$(2.2 \pm 0.2) \cdot 10^{-2}$

Simulations also shows that for channel 2 the TIR conditions are not fulfilled and some of the incident rays are not reflected. This behaviour can be seen in Figure 7.5 as rays propagating through air once they have reached the second phaseguide. This fraction of refracted rays may be due to a non perfect collimation of the lenses, changing the incident angle and then the TIR conditions.

7.2.2 Fabrication

FCOR master fabrication is a two level master, the parameter of every layer are detailed on table 7.2. The phaseguide layer define the distance between the phaseguide and the glass substrate, while the optics layer define the total thickness of the lenses, self-alignment systems and microfluidic channel.

Table 7.2: FCOR master fabrication parameters for every layer. Development time of the wafer is $t = 4$min.

Layer	SU-8	ω (rpm)	t (min)	E (mJ/cm^2)
Phaseguide	2005	1750	20	110
Optics	2050	2250	60	150

7.3 Results

Results are divided in two parts, the first part is a complete characterization of the device and the second part is the use of the FCOR for parallel measurement of glucose and lactate in a real rat serum samples with a single microspectrophotometer.

7.3.1 Characterization

Characterization of the final device is performed starting with a test of air mirrors and phaseguides. In order to check them, two situations have been studied. Firstly, water at both sides of the phaseguide to switch off the desired optical channel and secondly, water on the incident light side and air on the other side to switch on the channel. Both situations are illustrated in Figure 7.6a and Figure 7.6b respectively.

The experimental set up consists of a laser light source ($\lambda = 532$ nm) connected to channel 0 and the powermeter as a readout system. In Figure 7.7 one can observe the measured intensity against the optical path length of four different data sets. These 4 data sets are: (i) Simulations results; Experimental results, (ii) Water in both sides of the phaseguide (labeled as W-W), *i.e.*, switch off situation. Then, two different regimes for the switch on situation, *i.e.*, air at the outer side of the phaseguide and

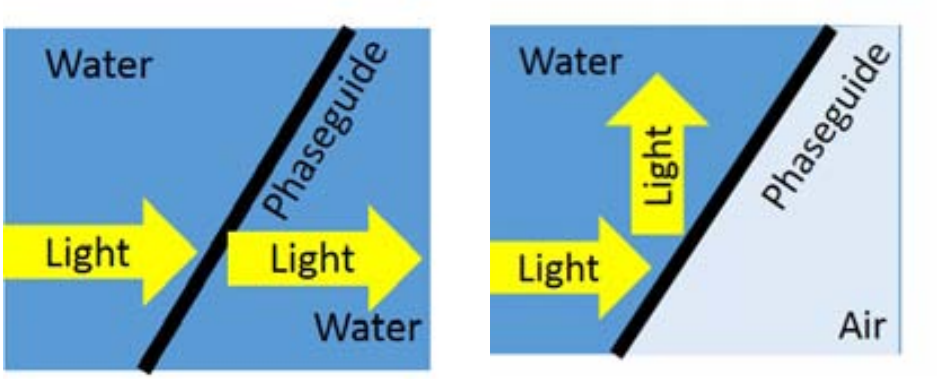

(a) (b)

Figure 7.6: Testing situations of phaseguides for (a) switch off and (b)switch on.

water in the inner, (*iii*) Maximum coupling and (*iv*) minimum coupling efficiencies.

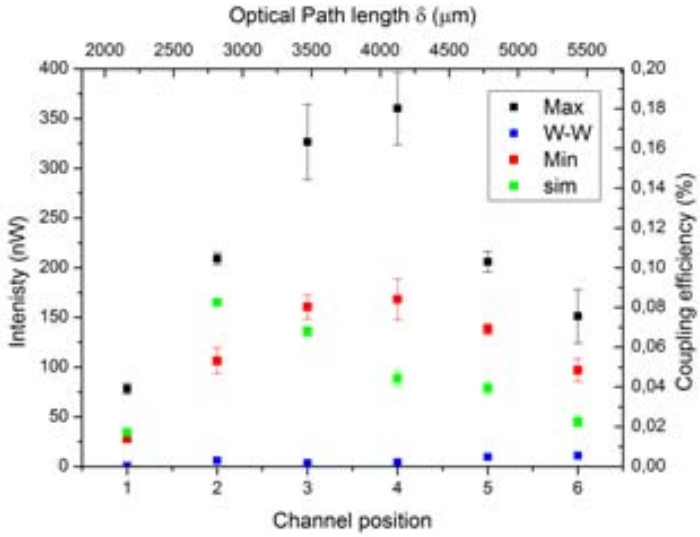

Figure 7.7: Intensity measured as function of output channel position for four different data sets. Error bars show the standard deviation of five repetitive measurements (95% confidence interval).

Experimentally we observe that once the liquid reaches the phaseguides, the maximum intensity value is obtained. Then, the liquid pres-

sure gradually increases until it reaches the breaking pressure. While the pressure increases, the valve of the output intensity has been measured to decreases. Such behaviour may be due to deformations of the phaseguide at higher pressures. For instance, overpressure could tilt the phaseguide, generating an slightly tilted mirror, which reduce the coupling efficiency.

In order to check this hypothesis, optical simulations with tilted phaseguides on channel 4 show coupling efficiencies of 0.44, 0.40, 0.38 and 0.22 % for tilting angles of 0, 1, 2 and 4º respectively. These 50% losses between the tilted and not-tilted situations matches with the experimental results (Figure 7.7), suggesting that this is indeed the case.

Both data sets, maximum and minimum, are obtained at different liquid pressures and then, one can avoid the tilting effects simply controlling the applied pressure. Therefore, from now, coupling efficiencies will be always at its maximum values *i.e.*, no tilting effects. Finally, W-W results show a perfect predictable result since the air mirrors were not active.

As explained in section 7.2.1 and predicted by simulations, the first optical channel ($\delta = 2225$ μm) shows the lower coupling efficiency. The low coupling efficiency is due to the non-fulfilled TIR conditions. Hence, the light reaching output channel is due to Fresnel reflection.

In order to check the theoretical result obtained from equation 7.1, *i.e.*, TIR condition only depends on the refractive index of the liquid used to fill the chamber, a battery of calcium chloride ($CaCl_2$) solutions at different concentrations, from 0 until 6 M, is used. $CaCl_2$ RI linearly depends on the concentration [Hay13] and provide a simple way to change the RI of the liquid. In our case RI that will ensure TIR is $n_l = 1.4142$. Meanwhile, the intensity of the laser light source ($\lambda = 532$ nm) has been continuously measured with the powermeter. As can be seen in Figure 7.8, measured intensities present an step function with a threshold value of 1.4099 ± 0.0002 RIU. The coincidence between theoretical and experimental results (difference of $4.3 \cdot 10^{-3}$ RIU or 0.3%) not only confirms the working principle of the air mirrors but also the robustness and precision of the whole system.

Finally, a determination of the switching time of our device is carried out. For this characterization two different lasers are connected through 105μm-core optical fibres ($\lambda_1 = 532$ nm for channel 4 and $\lambda_2 = 635$ nm for channel 1) and the channel 0 is connected to a microspectrophotometer. Then the router has been completely filled and emptied 5 times at each flow rate.

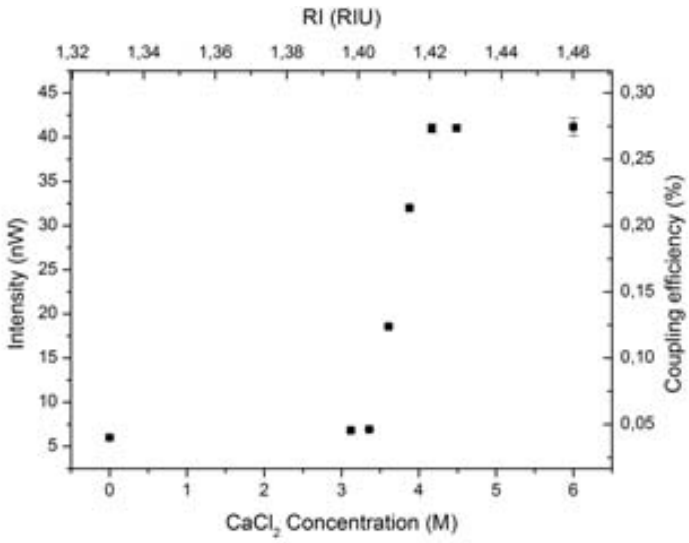

Figure 7.8: Channel 1 intensity response for different RI of the active liquid. Error bars show the standard deviation of five repetitive measurements (95% confidence interval).

The results are shown in Figure 7.9. The inset shows the intensity peaks of both wavelengths against time. Measuring the distance between peaks one can easily calculate the time needed to switch between optical channels. As can be seen, there is some background from 640 nm (channel 1) where the 537 nm peak (channel 4) is located. The slight differences between nominal and detected wavelengths, 5 nm, may be due to a non perfect microspectrometer calibration. This background, called cross-talk, is defined as:

$$\text{cross-talk} = -20 \cdot \log \frac{I_0}{I_1} \tag{7.2}$$

where I_0 is the intensity peak in channel 1 ($\lambda = 640$ nm) and I_1 is the background noise in channel 1 . The calculated cross-talk for this two channels is -12 $\pm$ 2 dB, which is an acceptable result with typical values on ranges between -16 and -21 dB [JYZ$^+$11, HQY$^+$11].

FCOR characterization has showed wide range of wavelength working regime and low cross-talk between channels validating the router for applications where multiplexing is a must.

Switching times (s) as function of flow rates (Q) are plotted in Fig-

ure 7.9. A two phase exponential decay regression is made

$$s = (28 \pm 4) \cdot 10 \cdot \mathrm{e}^{-(0.02 \pm 0.003)Q} + (152 \pm 9) \cdot 10 \cdot \mathrm{e}^{-(0.13 \pm 0.01)Q} + (49 \pm 5),$$

with $R^2 = 0.9994$. This result stablish a theoretical switching frequency limit (49 ± 5 ms or 20 ± 2 Hz), that may be due to fluidic resistance at the input microfluidic channel as well as to microfluidic chamber volume. With smaller volumes the switching frequency may be significantly improved.

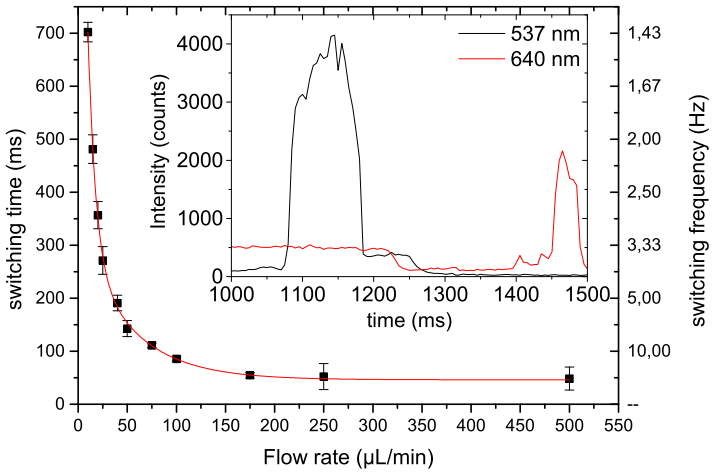

Figure 7.9: Switching time against flow rate. Inset the intensity as time function at input wavelengths Error bars show the standard deviation of five repetitive measurements (95% confidence interval).

Switching time experiment also demonstrates that FCOR can be used in both ways, as 1 to N channels in order to, for example, choose between several different readout devices (powemeter, spectrometer, etc.) as well as N to 1 to select among many different light sources with small crosstalk.

It is noteworthy that using two FCOR integrated in a LOC we are able to select the light source as well as the detection mechanism in an automatic and controlled way.

7.3.2 Parallel measurement of analytes in real rat serum samples

As prof of concept the router has been connectorized to 2 Multiple Internal Reflection (MIR) LOCs [LDJ+10] in order to provide a new method for parallel optical measurements of glucose and lactate in real rat serum samples. Lactate levels in blood indicates whether the organism has already consumed most of the glucose reserves and when the physical exercise regime changes from aerobic to anaerobic. Parallel measurements of glucose and lactate will provide clear image of this exercise regime change, and therefore when the studied subject should eat a glucose supplement or change reduce the physical effort. This method could be extended to simultaneously measure of as many oxidase-reductase enzymes as optical channels in the router. A detailed scheme of the setup is detailed in Figure 7.10. As it can be seen, with a single light source, two LOC systems can be used. Adding another FCOR at the output channels would allow the readout with a single equipment as well.

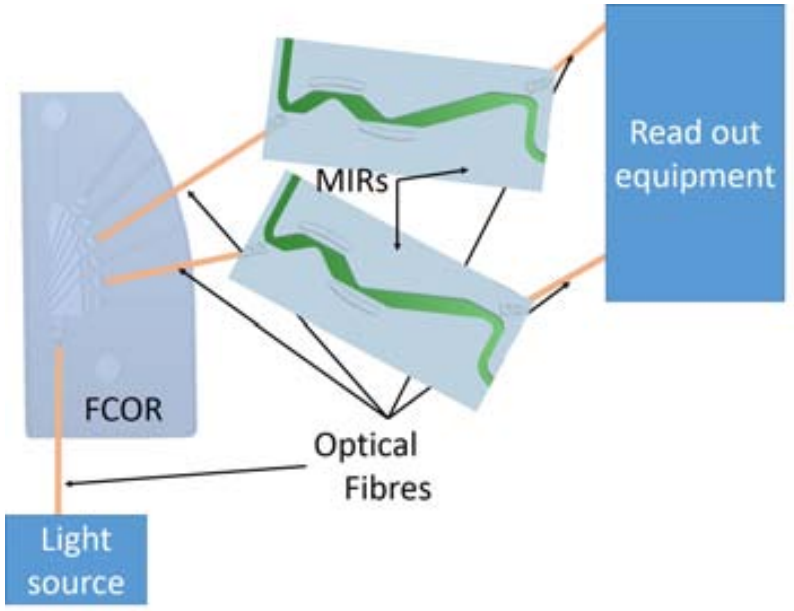

Figure 7.10: Illustration of the parallel measurement setup.

GOX and HRP are immobilized on the walls of one MIR LOC and LOX and HRP in the walls of the other. Immobilization of enzymes and

HRP is done following the protocol reported by Ibarlucea *et al.* [IFSD+11]. As the sample downstream propagates, a reaction between glucose or lactate (depending on the chip), the redox mediator (ABTS added to the rat serum), and the immobilized enzymes occurs. GOX catalyzes the oxidation of D-glucose by oxygen to produce D- gluconolactone and H_2O_2, while LOX catalyzes the oxidation of L-lactate by oxygen to produce piruvate and H_2O_2. H_2O_2 is the substrate for HRP, which catalyzes the reduction to H_2O with the concomitant oxidation of ABTS redox mediator to $ABTS^+$, that presents absorbance peaks at 420, 650, 740 and 835 nm. The chemical reactions during D-glucose and L-lactate detection using HRP and ABTS are graphically detailed in Figure 7.11. Hence, allowing parallel measurements of lactate and glucose, is an important step forwards.

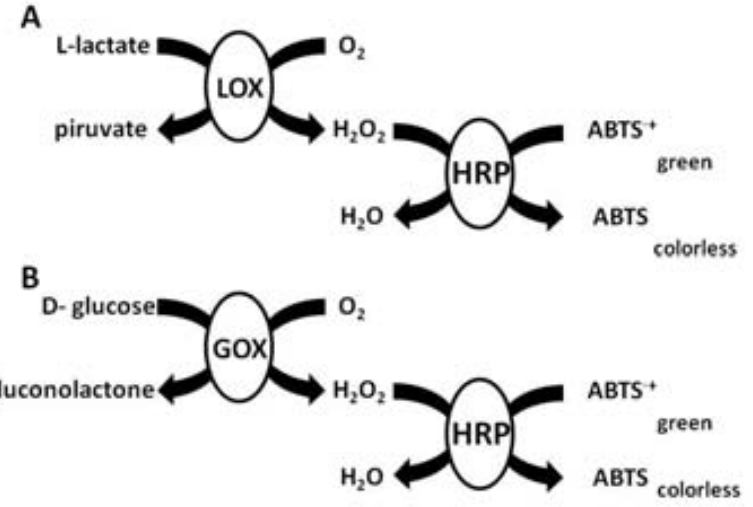

Figure 7.11: Schematic description of the chemical reactions for a) lactate and b) glucose detection.

In order to perform the parallel measurement of glucose and lactate in real rat serum sample previous calibration curves are required. Two sets of samples, one with different glucose concentration and the other with different lactate concentration, both of them with PBS medium and constant concentration of ABTS, are prepared. After that, the bio-functionalized MIR LOCs are connected though optical fibres to channels 3 and 4 of the FCOR. LOC connected to channel 3 measures the set of samples with different lactate concentrations while LOC connected to channel 4 measures

glucose samples. Afterwards, absorption is measured with a single laser source ($\lambda = 405$ nm). FCOR switches light output between channels 3 and 4. The readout is preformed by QE65Pro microspectrophotometer with integration time of 0.5 s. The calibrating linear fits can be observed in Figure 7.12.

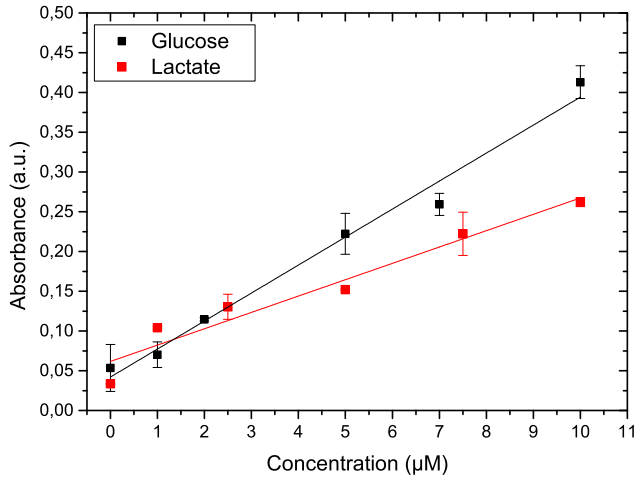

Figure 7.12: Absorbance as function of glucose and lactate concentration for calibrating purposes.

Linear regression equations for lactate and glucose are,

$$A_L = C_L \cdot (21 \pm 2) \cdot 10^{-3} + (6 \pm 1) \cdot 10^{-2}, \text{ with } R^2 = 0.93. \quad (7.3)$$

$$A_G = C_G \cdot (35 \pm 2) \cdot 10^{-3} + (4 \pm 1) \cdot 10^{-2}, \text{ with } R^2 = 0.98. \quad (7.4)$$

Equations 7.3 and 7.4 corresponds to lactate and glucose respectively with limits of detection of $\text{LOD}_L = 1.4 \pm 0.1$ µM and $\text{LOD}_G = (8.6 \pm 0.5) \cdot 10^{-1}$µM.

These calibrations are used to determine the concentration of glucose and lactate of real rat serum sample. They also demonstrate that even with the small coupling efficiencies previously reported, we are able to detect concentrations of µM for both, glucose and lactate with integration times of 0.5 s. As it can be seen in table 7.3, resolution of proposed glucose and lactate parallel measurement is good enough for biological samples and the results show a good agreement with previously reported results and commercial available kit results.

Table 7.3: Experimental results comparing commercial kits with the proposed parallel setup.

	commercial (mM)	parallel (mM)
Glucose	6.7	6.8 ± 0.6
Lactate	6.7 ± 0.4 [VGdM08]	6 ± 3

Therefore, FCOR has enough sensitivity and switching frequency to be used in (bio)chemical applications.

8 | Conclusions & Future work

In this last chapter a summary of the main results presented on this PhD thesis, followed by the future work that can be done in order to improve LOCs performance.

8.1 Conclusions

Microfluidic systems and specially LOCs are changing the landscape of several, well established, disciplines such as, engineering, biology, chemistry, medicine and pharmacy among others. The ongoing changes will have impact soon in everyday life, although, design and fabrication complexity are preventing major acceptance of this new technology. Integration of several optofluidic elements in more advanced LOCs has been achieved using developments of already existing soft-lithographic technologies. Integration of all these elements using a single, well established and low cost technology is an important step towards minutarization of detection elements in disposable LOC systems.

Along the thesis, several optics and fluidics elements have been succesfully integrated in fully functional optofluidic systems. Integration of these elements using soft-lithography fabrication technique and PDMS as constituent material ensures low-cost, disposable and flexible LOCs systems. Developed elements are individually characterized and LOCs are characterized and tested as (bio)chemical tools to overcome unsolved issues of the present state of the art in LOC applications.

Design, optimization, fabrication and characterization of individual optical elements have been outlined in Chapter 4. Optical elements have been divided in two categories, passive and active elements. Passive elements are those which do not require an energy source to work. Firstly, the most simple elements, *i.e.*, collimation lenses and self-alignment struc-

tures, necessary to create more complex structures. Such elements usually were published previously, but our development and optimization of elements as well as auxiliary structures, *e.g.*, stoppers and self-alignment channels, built using a single technology with no increase of fabrication steps, provide a robust approach to create more complex structures.

Air mirrors and lenses have been combined to create beam splitters. It is noteworthy that reported beam splitters are limited to 2D collimation of the beam and hence, propagation losses increase dramatically as the optical path increment. However, the optical characterization of the beam splitters have showed high optical losses associated to beam division, 7.8± 1.2 dB. These losses do not proper differentiate between propagation or beam division and then it is difficult to compare with previosuly reported beam splitters. The major issue of the BS is the deviation of output power between channels. This result suggests that some misalignment in the fibre position, the lens collimation or the waveguide geometry has occurred.

Using previously developed MIMIC variations a new passive optical element, *i.e.*, an absorbance based integrated filter, have been designed, fabricated and characterized. PDMS doped with three different pigments have been used to create filters with stopbands along the whole visible spectrum.

Finally, an active element, an integrated emitter, has been redesigned using TracePro simulation software. Simulation results suggest there are dead volumes inside the emitter chamber. Then, size reduction and shape change have been proposed.

Integration of many of the these optical plus some fluidic elements have been explained in Chapter 5. Firstly, different connectors between modules have been designed and tested considering three parameters, peel off, fluidic tightness and optical repeatability. Using these parameters the best connector, *i.e.*, rectangle, has been chosen. The previously redesigned integrated emitter has been manufactured and characterized. Its behaviour matches with simulations results and suggest a further size reduction is not only possible but also recommendable. All the modules have been fabricated from two PDMS replicas, the substrate and the optofluidic, bonded together. Each module is elastic and can be assembled with other modules in any substrate, modules connections are not permanent and can be plug and unplug with no previous knowledge in microfluidics or LOC. Hence, presented modular system have enough flex-

ibility to create LOC on demand to researchers without the background required to design and manufacture LOC systems from scratch. In order to prove it several modules are tested together in a crystal violet concentration determination. LOD of 1.53 ± 0.04 µM has been obtained. This result is similar to that obtained with monolithic chips [LWB08], proving its capabilities in sensing applications.

In Chapter 6 previously reported collimation lenses have been monolithically integrated in an state of the art microfluidic systems, *i.e.*, monodisperse microdroplets generator. Two different optical configurations have been proposed in order to make possible fluorescence and absorbance measurement of droplets. Both configurations have been tested and compared to previous set up with equivalent results. Droplets have been detected in both configurations with no need of bulky and expensive equipments, *i.e.*, inverted microscope, laser light source and PMT. In addition, proposed configurations can detect unlabelled droplets, a feature that was not possible with the previous set up, with the same precision and reliability. However, due to our collimation lenses and readout equipment, the droplet generation rate is limited to 50 µl/hwhich is ∼160 drops/s. Finally, screening of droplet inner medium has been experimentally proved for first time in optofluidic system.

In Chapter 7, a compact and integrable FCOR has been build using soft-lithographic techniques and made entirely of PDMS and air ensuring low-cost and robustness. A recently developed microfluidic tool, *i.e.*, phaseguides [VPM+11], has been exploited to create a fluidically controlled optical router with a movable mirror without mobile parts. The LOC is repetitive, as shows the standard deviation of the measurements, and has a good durability (non appreciable degradation or performance deterioration for weeks, in the whole visible spectrum). Furthermore, FCOR has a switching frequency of 20 ± 2 Hz at flow rate of 175μL/min and a small cross-talk (-12 ± 2 dB) between channels, with no movable parts, providing a great robustness to the chip.

Finally, FCOR has been integrated in a previously reported LOC performing parallel measurements of glucose and lactate with a single light source. After setup calibration, the FCOR allows parallel measurement of glucose and lactate showing good agreement with previous results. Validating then, the FCOR for parallel analysis.

8.2 Future work

Despite the good behaviour of the presented systems several changes are here proposed in order to improve the final optofluidic systems.

8.2.1 Modular system

The main problem in the modular system is the connectors reliability. Even though four configurations have been tested the fluidic connections have leaks in a no negligible number of cases. This is a major problem for LOC applications and has to be addressed before further development in optofluidic elements and applications. PDMS elasticity could be combined with thermoplastics stiffness to generate a tighter fluidic connections. The idea is to bond PDMS optofluidic elements to a thermoplastic substrate. In such design, the substrate is rigid and provides a strong connection with no bending of the female/male connectors while the fluidic PDMS channels allow certain flexibility in alignment and pressure requirements. In Figure 8.1 an schematic representation fo this configuration can be seen. Using thermoplastic fabrication techniques is relatively easy to generate tilted profiles to ensure vertical alignment. Such profiles and elasticity of PDMS on top of the structure should increase both optical repetitivity and fluidic tightness. Moreover, rigid substrates made using mass production technologies,*i.e.*, hot embossing or injection moulding, could reduce production costs even more.

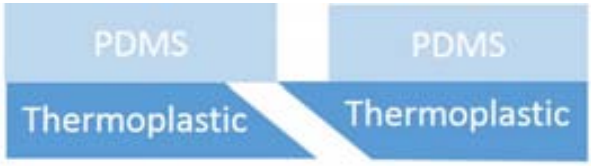

Figure 8.1: Cross section of the modular system with a thermoplastic substrate and PDMS optofluidic parts.

In order to reduce optical losses and increase repetitivity, more robust waveguides should also be implemented. Using the previously developed MIMIC variation a good alternative could be thermoplastic waveguides, embedded in the PDMS structures. It is important to chose thermoplastics with RI substantially higher than PDMS in order to ensure light confinement. Another alternative could be the use of PDMS at different

ratios of base elastomer and curing agent. This approach have the advantatge that changing the ratio also change the refractive index [CQSW13] of the final waveguide and do not require different materials.

8.2.2 Droplets

The presented designs for droplet detection with collimation lenses presents two main drawbacks: Firstly, the optical beam width is between 520 and 700 µm depending on the used chip, allowing multiple droplets passing simultaneously through the optical path and complicating droplet detection at certain flow threshold. Secondly, the distance between the optical fiber and the microfluidic channel is 2000 µm for collimation lenses without integrated filter and 2950 µm for lenses with integrated filter. These distances increases intrinsic optical losses, specially vertical divergence, and reduce chips' sensitivity.

In order to increase droplet detection sensitivity deeper simulations have been made using TracePro. These simulation determine the exact behaviour of light in the structure. In Figure 8.2, a ray tracing simulation can be observed. The simulated droplet size is 50 µm in diameter and materials RI are: $n_{oil} = 1.295$, $n_{\mathrm{H_2O}} = 1.333$ and $n_{PDMS} = 1.42$.

As can be seen a the microdroplet acts as a microlens with a focal point at 260 µm. Since droplets are spherical, focalization occurs in all 3 dimensions instead of 2 dimensional optics of our cylindrical lenses. This light behaviour has been observed for the first time and suggest a complete new way to use droplets as an active optical element to improve chip performance. Such lenses will change their focal distance depending on the droplet characteristics, *e.g.*, size and refractive index contrast. Providing a valuable tool droplet screening. Moreover, 3D focalization may increase the amount of light reaching the detector, and then increasing sensitivity and LOD.

Besides using droplet as active optical element, optical fibers with smaller core and width and with lower NA are also recommendable to minimize beam width at the interaction point. Increasing then, the amount of light interacting with the droplet.

In order to increase the interaction length a narrow zig-zag detection path could be implemented. This channel, should be significantly narrower than droplet diameter to squeeze the droplet, which will be no longer spherical. Then, light will propagate along these narrow and long

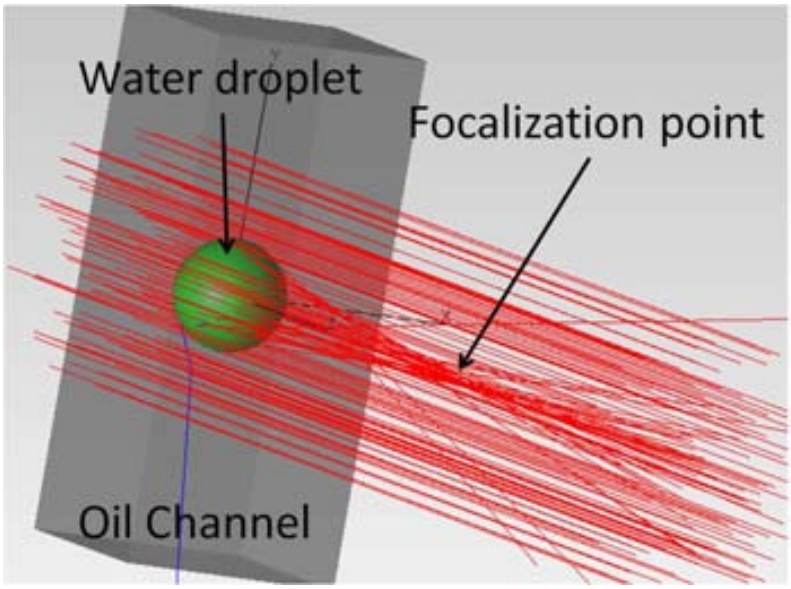

Figure 8.2: Ray tracing simulation of T-conf usign TracePro software. Droplet diameter is 50 µm and focal point is located at 360 µm.

droplets, increasing the interaction path. For instance, a channel width of 10 µm will produce an interaction length of ∼250 µm. Five times bigger than spherical droplets.

8.2.3 FCOR

FCOR is a robust and versatile optofluidic element to be integrated in more complex LOCs, as has been proved. Nevertheless, minor improvements are here proposed. Once the working principle has been proved, the first and second phaseguides should increase their incidence angle to fulfil TIR conditions. This redesign of the FCOR should be used to obtain the same path length in the optical channels. With equal path lengths, similar coupling efficiencies in all the channels would be obtained.

Regarding FCOR switching frequency, it is limited by the inner volumes, then a reduction of the chamber size will increase velocity. Furthermore, a wider fluidic channel may also increase switching frequency.

PDMS elasticity is a drawback in FCOR with probable bending of the phaseguides, generating another element that should be controlled. Moving from PDMS to more rigid materials could solve this problem and

also allow the use of mass production technologies. Moreover, integration of FCOR in more complex LOCs also require the implementation of robust waveguides. As explained in the modular section they can be easily integrated using the previously developed MIMIC technique.

A | Glossary of acronyms

***A*,** Absorbance.

ABTS, 2,2'azino-bis (3-ethylbenzthiazoline-6-sulfonic acid).

ARROW, anti-resonant reflecting optical waveguide.

AWG, arrayed waveguide grating.

$\boldsymbol{\beta_i}$**,** angle formed between the surface normal and the i light beam direction.

BS, Beam splitter

CAD, Computer-aided design.

COC, Cyclic Olefin copolymer.

COP, Cyclic Olefin Polymer.

CV, Crystal violet.

DMSO, Dimethyl sulfoxide.

***E*,** ultraviolet light dose.

ELISA, Enzyme-linked immunosorbent assay.

$\boldsymbol{\epsilon}$**,** molar absorptivity.

EWOD, Electro wetting on dielectrics.

FCOR, Fluidically controlled optical router.

GOX, glucose oxidase.

HDT, Heat distortion temperature.

HRP, horseradish peroxidase.

IC, Integrated Circuit.

IUPAC, International Union of Pure and Applied Chemistry.

$\boldsymbol{L^2}$**,** Liquid-core liquid-cladding.

LIGA, Lithography, electroplating and moulding process.

LOC, Lab on a Chip.

LOD, limit of detection.

LOX, lactate oxidase.

µCP, microcontact printing.

µPAD, microfluidic paper-based analytical devices.

µTAS, micro Total Analysis System.

µTM, microtransfer moulding.

MEMS, Micro electro mechanical systems.

MIMIC, micromoulding in capillaries.

MIR, multiple internal reflection.

MMI, multimode interference.

$\boldsymbol{n_i}$**,** refractive index of the medium i.

NA, Numerical aperture.

NIR, near infra red.

PC, Polycarbonate.

PCR, Polymerase chain reaction.

PDMS, Polydimethylsiloxane.

PEB, Post exposure bake.

PEG, polyethylene glycol.

PEEK, Polyether ether ketone.

PFPE, perfluorinated polyethers.

Ph-LOC, Photonic lab on a chip.

PhTMO, Phenyltrimethoxysilane.

PI, Polyimide.

PMMA, Poly(methyl methacrylate).

POC, Point of care.

PP, Polypropylene.

PR, Phenol red.

PS, Polystyrene.

$\boldsymbol{Q}$**,** flow rate.

QD, quantum dot.

QY, Quinoline yellow.

Re, Reynolds number.

RI, refractive index.

SAMIM, solvent-assisted micromoulding.

$\boldsymbol{T}$**,** Transmittance.

$\boldsymbol{T_p}$**,** Transmittance at the passband.

$\boldsymbol{T_s}$**,** Transmittance at the stopband.

$\boldsymbol{\tau_d}$**,** Decomposition temperature.

$\boldsymbol{\tau_g}$**,** Glass transition temperature.

TIR, Total internal reflection.

UV, Ultraviolet.

$\boldsymbol{\omega}$**,** spinning velocity.

Bibliography

[ABS03] Shelley L. Anna, Nathalie Bontoux, and Howard A Stone. Formation of dispersions using "flow focusing" in microchannels. *Applied Physics Letters*, 82(3):364, 2003. No citations.

[AfFM10] Seyed M Azmayesh-fard, E Flaim, and J N McMullin. PDMS biochips with integrated waveguides. *Journal of Micromechanics and Microengineering*, 20(8):087002, August 2010. No citations.

[AM89] Wolfgang Arden and Karl Heinz Mueller. Light vs X-rays: how fine can we get. *Semiconductor International*, 12(10):128–131, 1989. No citations.

[BA11] H. Baez and M. I. Alayo. Integration of a micro-incandescent lamp and an interferometric filter for optical applications. In Ferechteh H. Teherani, David C. Look, and David J. Rogers, editors, *SPIE OPTO*, pages 79401I–79401I–9. International Society for Optics and Photonics, February 2011. No citations.

[BD90] J Brook and R Daendliker. Holographic Photolithography for submicron VLSI structures. *Microelectronic Engineering*, 11:127–131, 1990. No citations.

[BDB+06] Romeo Bernini, E De Nuccio, F. Brescia, Aldo Minardo, L. Zeni, Pasqualina M Sarro, R. Palumbo, M. R. Scarfi, and Elbano De Nuccio. Development and characterization of an integrated silicon micro flow cytometer. *Analytical and bioanalytical chemistry*, 386(5):1267–72, November 2006. No citations.

[BG00] Holger Becker and Claudia Gärtner. Polymer microfabrication methods for microfluidic analytical applications General. *Electrophoresis*, 21:12–26, 2000. No citations.

[BJB+06] S Balslev, A M Jorgensen, B Bilenberg, Klaus B Mogensen, Detlef Snakenborg, O Geschke, Jörg P Kutter, and A Kristensen. Lab-on-a-chip with integrated optical transducers. *Lab on a chip*, 6(2):213–7, March 2006. No citations.

[BLKI08] James Q Boedicker, Liang Li, Timothy R Kline, and Rustem F Ismagilov. Detecting bacteria and determining their susceptibility to antibiotics by stochastic confinement in nanoliter droplets using plug-based microfluidics. *Lab on a chip*, 8(8):1265–72, August 2008. No citations.

[BMG94] M Baciocchit, R Maggiorat, and M Gentili. HIGH RESOLUTION FRESNEL ZONE PLATES FOR SOFT X-RAYS. *Microelectronic Engineering*, 23:101–104, 1994. No citations.

[BMV+13] Marko Brammer, Christof Megnin, Achim Voigt, Manfred Kohl, and Timo Mappes. Modular Optoelectronic Microfluidic Backplane for Fluid Analysis Systems. *Journal of Microelectromechanical Systems*, 22(2):462–470, April 2013. No citations.

[BP08] Ali Asgar S Bhagat and Ian Papautsky. Enhancing particle dispersion in a passive planar micromixer using rectangular obstacles. *Journal of Micromechanics and Microengineering*, 18(8):085005, August 2008. No citations.

[BTZS08] Romeo Bernini, Genni Testa, Luigi Zeni, and Pasqualina M Sarro. Integrated optofluidic Mach–Zehnder interferometer based on liquid core waveguides. *Applied Physics Letters*, 93(1):011106, 2008. No citations.

[BVW81] W L Brown, T Venkatesan, and A Wagner. Ion beam lithography. *Nuclear instruments and methods*, 191:157–168, 1981. No citations.

[CC06] Charles J Choi and Brian T Cunningham. Single-step fabrication and characterization of photonic crystal biosensors with polymer microfluidic channels. *Lab on a chip*, 6(10):1373–80, October 2006. No citations.

[CCD+09] S Chibbaro, E Costa, D I Dimitrov, F Diotallevi, A Milchev, D Palmieri, G Pontrelli, and S Succi. Capillary filling in microchannels with wall corrugations: a comparative study of the Concus-Finn criterion by continuum, kinetic, and atomistic approaches. *Langmuir : the ACS journal of surfaces and colloids*, 25(21):12653–60, December 2009. No citations.

[CCM+01] M L Chabinyc, Daniel T Chiu, J Cooper Mcdonald, a D Stroock, J F Christian, a M Karger, and George M Whitesides. An integrated fluorescence detection system in poly(dimethylsiloxane) for microfluidic applications. *Analytical chemistry*, 73(18):4491–8, September 2001. No citations.

[CDX+12] Ran Chen, Peng-fei Dong, Jian-hong Xu, Yun-dong Wang, and Guang-Sheng Luo. Controllable microfluidic production of gas-in-oil-in-water emulsions for hollow microspheres with thin polymer shells. *Lab on a chip*, June 2012. No citations.

[CFF03] S Camou, H Fujita, and T Fujii. PDMS 2D optical lens integrated with microfluidic channels: principle and characterization. *Lab on a chip*, 3(1):40–5, February 2003. No citations.

[CGK+10] C F Carlborg, K B Gylfason, A Kaźmierczak, F Dortu, M J Bañuls Polo, A Maquieira Catala, G M Kresbach, H Sohlström, T Moh, L Vivien, J Popplewell, G Ronan, C a Barrios, G Stemme, and W van der Wijngaart. A packaged optical slot-waveguide ring resonator sensor array for multiplex label-free assays in labs-on-chips. *Lab on a chip*, 10(3):281–90, February 2010. No citations.

[CHC+10] Carl Fredrik Carlborg, Tommy Haraldsson, Matteo Cornaglia, Göran Stemme, and Wouter van der Wijngaart.

A High-Yield Process for 3-D Large-Scale Integrated Microfluidic Networks in PDMS. *Journal of Microelectromechanical Systems*, 19(5):1050–1057, October 2010. No citations.

[CLC+11] Curtis D. Chin, Tassaneewan Laksanasopin, Yuk Kee Cheung, David Steinmiller, Vincent Linder, Hesam Parsa, Jennifer Wang, Hannah Moore, Robert Rouse, Gisele Umviligihozo, Etienne Karita, Lambert Mwambarangwe, Sarah L Braunstein, Janneke van de Wijgert, Ruben Sahabo, Jessica E Justman, Wafaa El-Sadr, and Samuel K Sia. Microfluidics-based diagnostics of infectious diseases in the developing world. *Nature medicine*, 17(8):1015–9, August 2011. No citations.

[CNKH08] D.K. Cai, A. Neyer, R. Kuckuk, and H.M. Heise. Optical absorption in transparent PDMS materials applied for multimode waveguides fabrication. *Optical Materials*, 30(7):1157–1161, March 2008. No citations.

[Col90] Ed Colgate. An investigation of electrowetting-based microactuation. *Journal of Vacuum Science & Technology A: Vacuum, Surfaces, and Films*, 8(4):3625, July 1990. No citations.

[CQSW13] Ziliang Cai, Weiping Qiu, Guocheng Shao, and Wanjun Wang. A new fabrication method for all-PDMS waveguides. *Sensors and Actuators A: Physical*, 204:44–47, December 2013. No citations.

[CRID+12] Ester Carregal-Romero, Bergoi Ibarlucea, Stefanie Demming, Stephanus Büttgenbach, César Fernández-Sánchez, and Andreu Llobera. Integrated polymeric light emitter for disposable photonic lab on a chip systems. In *16th International Conference on Miniaturized Systems for Chemistry and Life Sciences*, pages 1972–1974, 2012. No citations.

[CRLC+12] Ester Carregal-Romero, Andreu Llobera, Victor J Cadarso, Margarita Darder, Pilar Aranda, Carlos Domínguez, Eduardo Ruiz-Hitzky, and César Fernández-Sanchez. One-

step patterning of hybrid xerogel materials for the fabrication of disposable solid-state light emitters. *ACS applied materials & interfaces*, 4(9):5029–37, September 2012. No citations.

[CTLB+08] Jenifer Clausell-Tormos, Diana Lieber, Jean-christophe Baret, Abdeslam El-Harrak, Oliver J Miller, Lucas Frenz, Joshua Blouwolff, Kartherine J Katherine J Humphry, Sarah Köster, Honey Duan, Christian Holtze, David Alain Weitz, Andrew D Griffiths, and Christoph a Merten. Droplet-Based Micro Fluidic Platforms for the Encapsulation and Screening of Mammalian Cells and Multicellular Organisms. *Chemistry & Biology*, 15(5):427–437, May 2008. No citations.

[CW91] Manoj K. Chaudhury and George M. Whitesides. Direct measurement of interfacial interactions between semispherical lenses and flat sheets of poly(dimethylsiloxane) and their chemical derivatives. *Langmuir*, 7(5):1013–1025, May 1991. No citations.

[CWH+12] Yi-Wen Chen, Hong Wang, Mateusz Hupert, Makgorzata Witek, Udara Dharmasiri, Maneesh R Pingle, Francis Barany, and Steven a Soper. Modular microfluidic system fabricated in thermoplastics for the strain-specific detection of bacterial pathogens. *Lab on a chip*, 12(18):3348–55, September 2012. No citations.

[CWK+13] Yue Chen, Ting-Hsiang Wu, Yu-Chun Kung, Michael a Teitell, and Pei-Yu Chiou. 3D pulsed laser-triggered high-speed microfluidic fluorescence-activated cell sorter. *The Analyst*, 138(24):7308–15, November 2013. No citations.

[DABJ06] Liang Dong, Abhishek K Agarwal, David J Beebe, and Hongrui Jiang. Adaptive liquid microlenses activated by stimuli-responsive hydrogels. *Nature*, 442(7102):551–4, August 2006. No citations.

[DAS07] Marc Dandin, Pamela Abshire, and Elisabeth Smela. Optical filtering technologies for integrated fluorescence sensors. *Lab on a chip*, 7(8):955–77, August 2007. No citations.

[DM98] Sukhtej S Dhingra and Eva Marand. Mixed gas transport study through polymeric membranes. *Journal of Membrane Science*, 141(November 1997):45–63, 1998. No citations.

[DUB+12] Bachir El Debs, Ramesh Utharala, Irina V Balyasnikova, Andrew D Griffiths, and Christoph A Merten. Functional single-cell hybridoma screening using droplet-based microfluidics. *PNAS*, 109(29):11570–11575, 2012. No citations.

[DVPA+11] Stefanie Demming, Jordi Vila-Planas, Sobehir Aliasghar Zadeh, Astrid Edlich, Ezequiel Franco-Lara, Rolf Radespiel, Stephanus Büttgenbach, and Andreu Llobera. Poly(dimethylsiloxane) photonic microbioreactors based on segmented waveguides for local absorbance measurement. *Electrophoresis*, 32(3-4):431–9, February 2011. No citations.

[DvWB+10] Chaitanya Dongre, Jasper van Weerd, Nicola Bellini, Roberto Osellame, Giulio Cerullo, Rob van Weeghel, Hugo J W M Hoekstra, and Markus Pollnau. Dual-point dual-wavelength fluorescence monitoring of DNA separation in a lab on a chip. *Biomedical optics express*, 1(2):729–735, January 2010. No citations.

[ESD05] Nicholas Edmonds, Doug Stark, and Jesse Davis. MASS : MODULAR ARCHITECTURE FOR SENSOR SYSTEMS. *IEEE*, 00(C):393–397, 2005. No citations.

[FLKY10] Elain Fu, Barry Lutz, Peter Kauffman, and Paul Yager. Controlled reagent transport in disposable 2D paper networks. *Lab on a chip*, 10(7):918–20, April 2010. No citations.

[Fou00] J.E. Fouquet. Compact optical cross-connect switch based on total internal reflection in a fluid-containing planar lightwave circuit. *Optical Fiber Communication Conference. Technical Digest Postconference Edition. Trends in Optics and Photonics*, 37:204–206, 2000. No citations.

[FSGHL05] T.M. Floyd-Smith, J P Golden, P B Howell, and F S Ligler. Characterization of passive microfluidic mixers fabricated using soft lithography. *Microfluidics and Nanofluidics*, 2(2):180–183, December 2005. No citations.

[FWR+09] Luis M Fidalgo, Graeme Whyte, Brandon T Ruotolo, Justin L P Benesch, Florian Stengel, Chris Abell, Carol V Robinson, and Wilhelm T S Huck. Coupling microdroplet microreactors with mass spectrometry: reading the contents of single droplets online. *Angewandte Chemie (International ed. in English)*, 48(20):3665–8, January 2009. No citations.

[FYE+12] Mao Fukuyama, Yumi Yoshida, Jan C. T. Eijkel, Albert Berg, and Akihide Hibara. Time-resolved electrochemical measurement device for microscopic liquid interfaces during droplet formation. *Microfluidics and Nanofluidics*, 14(6):943–950, December 2012. No citations.

[FZYZ12] Guang-Liang Fu, Hong-Yu Zhang, Yi-Qiao Yan, and Cui-Hua Zhao. p-Quaterphenyls laterally substituted with a dimesitylboryl group: a promising class of solid-state blue emitters. *The Journal of organic chemistry*, 77(4):1983–90, February 2012. No citations.

[GCS98] C. González, S.D. Collins, and R.L. Smith. Fluidic interconnects for modular assembly of chemical microsystems. *Sensors and Actuators B: Chemical*, 49(1-2):40–45, June 1998. No citations.

[GJM+99] B.L Gray, D Jaeggi, N.J Mourlas, B.P van Drieënhuizen, K.R Williams, N.I Maluf, and G.T.a Kovacs. Novel interconnection technologies for integrated microfluidic systems. *Sensors and Actuators A: Physical*, 77(1):57–65, September 1999. No citations.

[GLI+11] Manuel Gutiérrez, Andreu Llobera, Andrey Ipatov, Jordi Vila-Planas, Santiago Mínguez, Stefanie Demming, Stephanus Büttgenbach, Fina Capdevila, Carme Domingo, and Cecilia Jiménez-Jorquera. Application of an e-tongue

to the analysis of monovarietal and blends of white wines. *Sensors (Basel, Switzerland)*, 11(5):4840–57, January 2011. No citations.

[GLY11] Hongwei Gai, Yongjun Li, and Edward S Yeung. Optical Detection Systems on Microfluidic Chips. In *Microfluidics Technologies and applications*, number April, chapter Chapter 07, pages 171–201. 2011. No citations.

[GSK+09] Neus Godino, Detlef Snakenborg, Jörg P. Kutter, Jenny Emnéus, Mikkel Fougt Hansen, F. Xavier Muñoz, and F. Javier del Campo. Construction and characterisation of a modular microfluidic system: coupling magnetic capture and electrochemical detection. *Microfluidics and Nanofluidics*, 8(3):393–402, July 2009. No citations.

[GSSW03] F Goldschmidtboeing, R Schlosser, S Schonhardt, and P Woias. CAPILLARY FILLING OF MICRO-RESERVOIRS WITH VARIOUS CROSS SECTIONS. In *Transducers*, pages 12–15, 2003. No citations.

[GW05] Frank Goldschmidtboeing and Peter Woias. STRATEGIES FOR VOID-FREE LIQUID-FILLING OF MICRO CAVITIES. In *Transducers*, pages 1561–1564, 2005. No citations.

[GYLW03] P Grodzinski, J Yang, R H Liu, and M D Ward. BioMEMs and BioMedical Nanotechnology : Section Editor Dr Mauro Ferrari A Modular Micro uidic System for Cell Preconcentration and Genetic Sample Preparation. *BioMEMS and BioMedical Nanotechnology*, 5(4):303–310, 2003. No citations.

[GZ91] W Groh and A Zimmermann. What Is the Lowest Refractive Index of an Organic Polymer? *Macromolecules*, 24:6660–6663, 1991. No citations.

[GZC+08] Alex Groisman, Steve Zamek, Kyle Campbell, Lin Pang, Uriel Levy, and Yeshaiahu Fainman. Optofluidic 1x4 switch. *Optics express*, 16(18):13499–508, September 2008. No citations.

[Hay13] William M. Haynes. *CRC Handbook of Chemistry and Physics, 94th Edition*. CRC Press, 2013. No citations.

[HC14] Jong Il Hong and Byoung-Yong Chang. Development of the Smartphone-based Colorimetry for Multi-analyte Sensing Arrays. *Lab on a Chip*, 2014. No citations.

[Hec01] Eugene Hecht. *Optics*. 2001. No citations.

[Hei73] R. D. Heidenreich. Fundamental aspects of electron beam lithography. I. Depth-dose response of polymeric electron beam resists. *Journal of Applied Physics*, 44(9):4039, 1973. No citations.

[Hes09] Volker Hessel. Novel Process Windows - Gates to maximizing process intensification via flow chemistry. *Chemical Engineering & Technology*, 32(11):1641, 2009. No citations.

[HGI91] Adam Hulanicki, Stanislaw Glab, and Folke Ingman. CHEMICAL SENSORS DEFINITIONS AND CLASSIFICATION. *Pure and applied chemistry*, 63(9):1247–1250, 1991. No citations.

[HH11] James T Heeres and Paul J Hergenrother. High-throughput screening for modulators of protein-protein interactions: use of photonic crystal biosensors and complementary technologies. *Chemical Society reviews*, 40(8):4398–410, August 2011. No citations.

[HHJ+12] Tobias W Hofmann, Siegfried Hänselmann, Jan-Wilhelm Janiesch, Anne Rademacher, and Christian H J Böhm. Applying microdroplets as sensors for label-free detection of chemical reactions. *Lab on a chip*, 12(5):916–22, March 2012. No citations.

[HHL05] Volker Hessel, C Hofmann, and P Lo. Aqueous Kolbe - Schmitt Synthesis Using Resorcinol in a Microreactor Laboratory Rig under High-p , T Conditions Abstract :. *organic process research & development*, 9(4):479–489, 2005. No citations.

[HJW+92] J M Heaton, R M Jenkins, D R Wight, J T Parker, J C H Birbeck, and K P Hilton. Novel I-to-N way integrated optical beam splitters mixing in GaAs / AIGaAs multimode waveguides using symmetric mode. *Scanning*, pages 1754–1756, 1992. No citations.

[HJW+10] Ting-Fu Hong, Wei-Jhong Ju, Ming-Chang Wu, Chang-Hsien Tai, Chien-Hsiung Tsai, and Lung-Ming Fu. Rapid prototyping of PMMA microfluidic chips utilizing a CO2 laser. *Microfluidics and Nanofluidics*, 9(6):1125–1133, May 2010. No citations.

[HMF+92] D Jed Harrison, Andreas Manz, Zhonghui Fan, Hans Ludi, and H Michael Widmers. Capillary Electrophoresis and Sample Injection Systems Integrated on a Planar Glass Chip. *Analytical chemistry*, 7(20):249–255, 1992. No citations.

[HMM+10] Dongeun Huh, Benjamin D Matthews, Akiko Mammoto, Martín Montoya-Zavala, Hong Yuan Hsin, and Donald E Ingber. Reconstituting organ-level lung functions on a chip. *Science (New York, N.Y.)*, 328(5986):1662–8, June 2010. No citations.

[HQY+11] Ting Hu, Huiye Qiu, Ping Yu, Chen Qiu, Wanjun Wang, Xiaoqing Jiang, Mei Yang, and Jianyi Yang. optical router for networks-on-chip. 36(23):4710–4712, 2011. No citations.

[HSH+13] Kyung Heon Lee, Kang Soo Lee, Jin Ho Jung, Cheong Bong Chang, and Hyung Jin Sung. Optical mobility of blood cells for label-free cell separation applications. *Applied Physics Letters*, 102(14):141911, 2013. No citations.

[HW12] Hamish C Hunt and James S Wilkinson. Kinoform microlenses for focusing into microfluidic channels. *Optics express*, 20(9):9442–57, April 2012. No citations.

[HWC+06] Oliver Hofmann, Xuhua Wang, Alastair Cornwell, Stephen Beecher, Amal Raja, Donal D C Bradley, Andrew J DeMello, and John C Demello. Monolithically integrated dye-doped PDMS long-pass filters for disposable on-chip

fluorescence detection. *Lab on a chip*, 6(8):981–987, 2006. No citations.

[HYSS12] Yu Harada, Dong Hyun Yoon, Tetsushi Sekiguchi, and Shuichi Shoji. Size-oriented passive droplet sorting by using surface free energy with micro guide groove. In *2012 IEEE 25th International Conference on Micro Electro Mechanical Systems (MEMS)*, pages 1105–1108. IEEE, January 2012. No citations.

[IAMC02] E Igata, M Arundell, H Morgan, and J M Cooper. Interconnected reversible lab-on-a-chip technology. *Lab on a chip*, 2(2):65–9, May 2002. No citations.

[IFSD+11] Bergoi Ibarlucea, César Fernández-Sánchez, Stefanie Demming, Stephanus Büttgenbach, and Andreu Llobera. Selective functionalisation of PDMS-based photonic lab on a chip for biosensing. *The Analyst*, 136(17):3496–502, September 2011. No citations.

[IH93] K. Ikuta and K. Hirowatari. Real three dimensional micro fabrication using stereo lithography and metal molding. In *Proceedings IEEE Micro Electro Mechanical Systems*, pages 42–47. IEEE, 1993. No citations.

[JA12] Haakan N Joensson and Helene Andersson Svahn. Droplet microfluidics–a tool for single-cell analysis. *Angewandte Chemie (International ed. in English)*, 51(49):12176–92, December 2012. No citations.

[JDAS06] Honghao Ji, Marc Dandin, Pamela Abshire, and Elisabeth Smela. Integrated Fluorescence Sensing for Lab-on-a-chip Devices. In *2006 IEEE/NLM Life Science Systems and Applications Workshop*, pages 1–2. IEEE, July 2006. No citations.

[JJ04] Ju-seog Jang and Bahram Javidi. Three-dimensional integral imaging of micro-objects. *Optics Letters*, 29(11):1230–1232, 2004. No citations.

[JRGL01] T J Johnson, D Ross, M Gaitan, and L E Locascio. Laser modification of preformed polymer microchannels: application to reduce band broadening around turns subject to electrokinetic flow. *Analytical chemistry*, 73(15):3656–61, August 2001. No citations.

[JS10] Kyung-Jin Jang and Kahp-Yang Suh. A multi-layer microfluidic device for efficient culture and analysis of renal tubular cells. *Lab on a chip*, 10(1):36–42, January 2010. No citations.

[JWC+14] Jing Jiang, Xinhao Wang, Ran Chao, Yukun Ren, Chengpeng Hu, Zhida Xu, and Gang Logan Liu. Smartphone based portable bacteria pre-concentrating microfluidic sensor and impedance sensing system. *Sensors and Actuators B: Chemical*, 193:653–659, March 2014. No citations.

[JWL13] Hai Jiang, Xuan Weng, and Dongqing Li. Dual-wavelength fluorescent detection of particles on a novel microfluidic chip. *Lab on a chip*, 13(5):843–50, March 2013. No citations.

[JYZ+11] Ruiqiang Ji, Lin Yang, Lei Zhang, Yonghui Tian, Jianfeng Ding, Hongtao Chen, Yangyang Lu, Ping Zhou, and Weiwei Zhu. Microring-resonator-based four-port optical router for photonic networks-on-chip. *Optics express*, 19(20):18945–55, September 2011. No citations.

[JZL+11] Am Jang, Zhiwei Zou, Kang Kug Lee, Chong H Ahn, and Paul L Bishop. State-of-the-art lab chip sensors for environmental water monitoring. *Measurement Science and Technology*, 22(3):032001, March 2011. No citations.

[KBMTD07] Myra Kitron-Belinkov, Abraham Marmur, Thomas Trabold, and Gayatri Vyas Dadheech. Groovy drops: effect of groove curvature on spontaneous capillary flow. *Langmuir : the ACS journal of surfaces and colloids*, 23(16):8406–10, July 2007. No citations.

[KM12] Y Kanno and N Miki. Development of a Nanotechnology-Based Dialysis Device, 2012. No citations.

[KME+13] Takashi Kasahara, Shigeyuki Matsunami, Tomohiko Edura, Juro Oshima, Chihaya Adachi, Shuichi Shoji, and Jun Mizuno. Fabrication and performance evaluation of microfluidic organic light emitting diode. *Sensors and Actuators A: Physical*, 195:219–223, June 2013. No citations.

[KVBA98] James Knight, Ashvin Vishwanath, James Brody, and Robert H Austin. Hydrodynamic Focusing on a Silicon Chip: Mixing Nanoliters in Microseconds. *Physical Review Letters*, 80(17):3863–3866, April 1998. No citations.

[KW93] Amit Kumar and George M Whitesides. Features of gold having micrometer to centimeter dimensions can be formed through a combination of stamping with an elastomeric stamp and an alkanethiol "ink" followed by chemical etching. *Applied Physics Letters*, 63(14):2002, 1993. No citations.

[KWBC09] O. Klais, F. Westphal, W. Benaïssa, and D. Carson. Guidance on Safety/Health for Process Intensification including MS Design; Part I: Reaction Hazards. *Chemical Engineering & Technology*, 32(11):1831–1844, November 2009. No citations.

[KXW95] Enoch Kim, Younan Xia, and George M Whitesides. Polymer microstructures formed by moulding in capillaries. *Nature*, 376(6541):581–584, August 1995. No citations.

[KXZW97] Enoch Kim, Younan Xia, Xiao-mei Zhao, and George M Whitesides. Solvent- Assisted Microcontact Molding: A Convenient Method for Fabricating Three-Dimensional Structures on Surfaces of Polymer. *Advanced Materials*, 9(8):651–654, 1997. No citations.

[LAJ12] Ye Liu, Bader Aldalali, and Hongrui Jiang. Lateral tunable liquid microlenses for enhanced fluorescence emission in microfluidic channels. *Journal of Micromechanics and Microengineering*, 22(10):105010, October 2012. No citations.

[LCM+09] Tassaneewan Laksanasopin, Curtis D. Chin, Hannah Moore, Jennifer Wang, Yuk Kee Cheung, and Samuel K. Sia. Microfluidic point-of-care diagnostics for resource-poor environments. In Thomas George, M. Saif Islam, and Achyut K. Dutta, editors, *Proceedings of SPIE*, volume 7318, pages 73180E–73180E–6, May 2009. No citations.

[LCZ+04] J. Liu, B. Cai, J. Zhu, G. Ding, X. Zhao, C Yang, and Danping Chen. Process research of high aspect ratio microstructure using SU-8 resist. *Microsystem Technologies*, 10(4):265–268, May 2004. No citations.

[LDF+97] H. Lorenz, M. Despont, N. Fahrni, N LaBianca, P. Renaud, and P. Vettiger. SU-8 : a low-cost negative resist for. *Journal of Micromechanics and Microengineering*, 97:121–124, 1997. No citations.

[LDJ+10] Andreu Llobera, Stefanie Demming, Haakan N Joensson, Jordi Vila-planas, Helene Andersson-Svahn, and Stephanus Büttgenbach. Monolithic PDMS passband filters for fluorescence detection. *Lab on a chip*, 10(15):1987–92, August 2010. No citations.

[LDWB07] Andreu Llobera, Stefanie Demming, R Wilke, and Stephanus Büttgenbach. Multiple internal reflection poly(dimethylsiloxane) systems for optical sensing. *Lab on a chip*, 7:1560–1566, 2007. No citations.

[Lee07] Seung Seok Woo Lee. Shrinkage ratio of PDMS and its alignment method for the wafer level process. *Microsystem Technologies*, 14(2):205–208, May 2007. No citations.

[LES96] M. Leemann, G. Eigenberger, and H. Strathmann. Vapour permeation for the recovery of organic solvents from waste air streams: separation capacities and process optimization. *Journal of Membrane Science*, 113(2):313–322, May 1996. No citations.

[LGVK09] Wei Li, Jesse Greener, Dan Voicu, and Eugenia Kumacheva. Multiple modular microfluidic (M3) reactors

for the synthesis of polymer particles. *Lab on a chip*, 9(18):2715–21, September 2009. No citations.

[LL07] Seok Woo Lee and Seung S. Lee. Focal tunable liquid lens integrated with an electromagnetic actuator. *Applied Physics Letters*, 90(12):121129, 2007. No citations.

[LLDM+11] Sean M Langelier, Eric Livak-Dahl, Anthony J Manzo, Brian N Johnson, Nils G Walter, and Mark a Burns. Flexible casting of modular self-aligning microfluidic assembly blocks. *Lab on a chip*, 11(9):1679–87, May 2011. No citations.

[LLR+95] K Y Lee, N LaBianca, S A Rishton, S Zolgharnain, J D Gelorme, J Shaw, and H P Chang. Micromachining applications of a high resolution ultrathick photoresist. *Journal of Vacuum Science & Technology B: Microelectronics and Nanometer Structures*, 13(6):3012, November 1995. No citations.

[LSF04] E Leclerc, Y Sakai, and T Fujii. Perfusion culture of fetal human hepatocytes in microfluidic environments. *Biochemical Engineering Journal*, 20(2-3):143–148, August 2004. No citations.

[LSL+12] Yang Liao, Jiangxin Song, En Li, Yong Luo, Yinglong Shen, Danping Chen, Ya Cheng, Zhizhan Xu, Koji Sugioka, and Katsumi Midorikawa. Rapid prototyping of three-dimensional microfluidic mixers in glass by femtosecond laser direct writing. *Lab on a chip*, 12(4):746–9, February 2012. No citations.

[LVS82] M.D. Levenson, N.S. Viswanathan, and R.A. Simpson. Improving resolution in photolithography with a phase-shifting mask. *IEEE Transactions on Electron Devices*, 29(12):1828–1836, December 1982. No citations.

[LWB04] Andreu Llobera, R Wilke, and Stephanus Büttgenbach. Poly(dimethylsiloxane) hollow Abbe prism with microlenses for detection based on absorption and refractive index shift. *Lab on a Chip*, 4:24–27, 2004. No citations.

[LWB05] Andreu Llobera, R Wilke, and Stephanus Büttgenbach. Optimization of poly(dimethylsiloxane) hollow prisms for optical sensing. *Lab on a Chip*, 5:506–511, 2005. No citations.

[LWB08] Andreu Llobera, R Wilke, and Stephanus Büttgenbach. Enhancement of the response of poly(dimethylsiloxane) hollow prisms through air mirrors for absorbance-based sensing. *Talanta*, 75:473–479, 2008. No citations.

[Mac10] H. Angus Macleod. *Thin-Film Optical Filters, Fourth Edition (Series in Optics and Optoelectronics)*. CRC Press, 2010. No citations.

[MBB+09] Laurent Mugherli, Olga N Burchak, Larissa a Balakireva, Aline Thomas, François Chatelain, and Maxim Y Balakirev. In situ assembly and screening of enzyme inhibitors with surface-tension microarrays. *Angewandte Chemie (International ed. in English)*, 48(41):7639–44, January 2009. No citations.

[MEA+87] Kary B Mullis, Henry A Erlich, Norman Arnheim, T Horn Glenn, Randall K Saiki, and Stephen J Scharf. Process for Amplifying, detecting, and/or-cloning nucleic acid sequences, 1987. No citations.

[MELVP+13] Ricard Menchon-Enrich, Andreu Llobera, Jordi Vila-Planas, Víctor Javier Cadarso, Jordi Mompart, and Veronica Ahufinger. Light spectral filtering based on spatial adiabatic passage. *Light: Science & Applications*, 2(8):e90, August 2013. No citations.

[MEM+12] Oliver J Miller, Abdeslam El, Thomas Mangeat, Jean-christophe Baret, Lucas Frenz, Bachir El, Estelle Mayot, Michael L Samuels, Eamonn K Rooney, Pierre Dieu, Martin Galvan, Darren R Link, and Andrew D Griffiths. High-resolution dose-response screening using droplet-based microfluidics. *PNAS*, 109(2):378–383, 2012. No citations.

[MGW90] Andreas Manz, N Graber, and H Michael Widmers. Miniaturized total chemical analysis systems: A novel concept

for chemical sensing. *Sensors and Actuators B: Chemical*, 1(1-6):244–248, January 1990. No citations.

[Mil69] Stewart E Miller. Integrated optics: An Introduction. *The bell system technical journal*, pages 2059–2069, 1969. No citations.

[MKLZ13] Philipp Müller, Daniel Kopp, Andreu Llobera, and Hans Zappe. Optofluidic router based on tunable liquid-liquid mirrors. *Lab on a chip*, pages 11–15, November 2013. No citations.

[MPC+08] Andres W Martinez, Scott T Phillips, Emanuel Carrilho, Samuel W Thomas, Hayat Sindi, and George M Whitesides. Simple telemedicine for developing regions: camera phones and paper-based microfluidic devices for real-time, off-site diagnosis. *Analytical chemistry*, 80(10):3699–707, May 2008. No citations.

[MPC+11] Philip Measor, Brian S Phillips, Aiqing Chen, Aaron R Hawkins, and Holger Schmidt. Tailorable integrated optofluidic filters for biomolecular detection. *Lab on a chip*, 11(5):899–904, March 2011. No citations.

[MPW08] Andres W Martinez, Scott T Phillips, and George M Whitesides. Three-dimensional microfluidic devices fabricated in layered paper and tape. *Proceedings of the National Academy of Sciences of the United States of America*, 105(50):19606–11, December 2008. No citations.

[MS96] C.R.K. Marrian and E.S. Snow. Proximal probe lithography and surface modification. *Microelectronic Engineering*, 32(1-4):173–189, September 1996. No citations.

[MW06] A D McNaught and A Wilkinson. IUPAC Gold Book, 2006. No citations.

[NGL+12] Pavel Neuži, Stefan Giselbrecht, Kerstin Länge, Tony Jun Huang, and Andreas Manz. Revisiting lab-on-a-chip technology for drug discovery. *Nature reviews. Drug discovery*, 11(8):620–32, August 2012. No citations.

[Ngu10] Nam-Trung Nguyen. Micro-optofluidic Lenses: A review. *Biomicrofluidics*, 4(3):1–15, January 2010. No citations.

[NHM+14] Shuai Nie, W Hampton Henley, Scott E Miller, Huaibin Zhang, Kathryn M Mayer, Patty J Dennis, Emily a Oblath, Jean Pierre Alarie, Yue Wu, Frank G Oppenheim, Frédéric F Little, Ahmet Z Uluer, Peidong Wang, J Michael Ramsey, and David R Walt. An automated integrated platform for rapid and sensitive multiplexed protein profiling using human saliva samples. *Lab on a chip*, 14(6), January 2014. No citations.

[NKGL07] Nam-Trung Nguyen, Tian-Fook Kong, Jun-Hui Goh, and Cassandra Lee-Ngo Low. A micro optofluidic splitter and switch based on hydrodynamic spreading. *Journal of Micromechanics and Microengineering*, 17(11):2169–2174, November 2007. No citations.

[NMB+13] Krishnamurthy V Nemani, Karen L Moodie, Jeoffry B Brennick, Alison Su, and Barjor Gimi. In vitro and in vivo evaluation of SU-8 biocompatibility. *Materials science & engineering. C, Materials for biological applications*, 33(7):4453–9, October 2013. No citations.

[Nor95] David J Norris. *Measurement and Assignment of the Size-Dependent Optical Spectrum in Cadmium Selenide (CdSe) Quantum dots.* PhD thesis, Massachusetts Institute of Technology, 1995. No citations.

[NTC+09] Ming Ni, Wen Hao Tong, Deepak Choudhury, Nur Aida Abdul Rahim, Ciprian Iliescu, and Hanry Yu. Cell culture on MEMS platforms: a review. *International journal of molecular sciences*, 10(12):5411–41, December 2009. No citations.

[OLF+10] Jennifer L Osborn, Barry Lutz, Elain Fu, Peter Kauffman, Dean Y Stevens, and Paul Yager. Microfluidics without pumps: reinventing the T-sensor and H-filter in paper networks. *Lab on a chip*, 10(20):2659–65, October 2010. No citations.

[OOI+07] Yasuo Ohtera, Teppei Onuki, Yoshihiko Inoue, Shojiro Kawakami, and Life Fellow. Multichannel Photonic Crystal Wavelength Filter Array for Near-Infrared Wavelengths. *Journal of Lightwave Technology*, 25(2):499–503, 2007. No citations.

[PB08] Amy L Paguirigan and David J Beebe. Microfluidics meet cell biology: bridging the gap by validation and application of microscale techniques for cell biological assays. *BioEssays : news and reviews in molecular, cellular and developmental biology*, 30(9):811–21, September 2008. No citations.

[PB09] Om Prakash Parida and Navakant Bhat. CHARACTERIZATION OF OPTICAL PROPERTIES OF SU-8 AND FABRICATION OF OPTICAL COMPONENETS. In *International conference on optics and photonics*, pages 4–7, 2009. No citations.

[PLK11] Hyoung-Jun Park, Kwon-Seob Lim, and Hyun Seo Kang. Low-cost 12 plastic optical beam splitter using a V-type angle polymer waveguide for the automotive network. *Optical Engineering*, 50(7):075002, July 2011. No citations.

[PLMY13] Tu San Park, Wenyue Li, Katherine E McCracken, and Jeong-Yeol Yoon. Smartphone quantifies Salmonella from paper microfluidics. *Lab on a chip*, 13(24):4832–40, December 2013. No citations.

[PM94] P Pantelis and D J McCartney. Polymer microlens arrays. *Pure and applied optics*, 3:103–108, 1994. No citations.

[PPF03] Phil Paik, Vamsee K Pamula, and Richard B Fair. Rapid droplet mixers for digital microfluidic systems. *Lab on a chip*, 3(4):253–9, November 2003. No citations.

[PTC+02] Duy Pham, Livia Tonge, Jinan Cao, Jon Wright, Michal Papiernik, Erol Harvey, and Dan Nicolau. Effects of polymer properties on laser ablation behaviour. *Smart Materials and Structures*, 11(5):668–674, October 2002. No citations.

[QHW+10] Lingling Qiao, Fei He, Chen Wang, Ya Cheng, Koji Sugioka, and Katsumi Midorikawa. A microfluidic chip integrated with a microoptical lens fabricated by femtosecond laser micromachining. *Applied Physics A*, 102(1):179–183, October 2010. No citations.

[RB08] Minsoung Rhee and Mark a Burns. Microfluidic assembly blocks. *Lab on a chip*, 8(8):1365–73, August 2008. No citations.

[RDF+13] S. Rampazzi, G. Danese, L. Fornasari, F. Leporati, F. Marabelli, N. Nazzicari, and a. Valsesia. Lab on Chip: Portable Optical Device for On-site Multi-parametric Analysis. *2013 Euromicro Conference on Digital System Design*, pages 807–810, September 2013. No citations.

[RDK13] Suparat Rujihan, Badin Damrongsak, and Pattareeya Kittidachachan. Poly(dimethylsiloxane) microlens array integrated with microfluidic channel for fluorescence spectroscopy detection. In Prathan Buranasiri and Sarun Sumriddetchkajorn, editors, *Proceedings of SPIE*, volume 8883, page 88831M, June 2013. No citations.

[RHL+07] a. Renken, V. Hessel, P. Löb, R. Miszczuk, M. Uerdingen, and L. Kiwi-Minsker. Ionic liquid synthesis in a microstructured reactor for process intensification. *Chemical Engineering and Processing: Process Intensification*, 46(9):840–845, September 2007. No citations.

[RPJW97] John A Rogers, Kateri E Paul, R J Jackman, and George M Whitesides. Using an elastomeric phase mask for sub-100 nm photolithography in the optical near field. *Applied Physics Letters*, 70(20):2658–2660, 1997. No citations.

[RRAC09] Charles Richard, Alan Renaudin, Vincent Aimez, and Paul G Charette. An integrated hybrid interference and absorption filter for fluorescence detection in lab-on-a-chip devices. *Lab on a chip*, 9(10):1371–6, May 2009. No citations.

[SB09] Philipp Schulze and Detlev Belder. Label-free fluorescence detection in capillary and microchip electrophoresis. *Analytical and bioanalytical chemistry*, 393(2):515–25, January 2009. No citations.

[SBP+11] S.Z. Szilasi, J. Budai, Z. Pápa, R. Huszank, Z. Tóth, and I. Rajta. Refractive index depth profile and its relaxation in polydimethylsiloxane (PDMS) due to proton irradiation. *Materials Chemistry and Physics*, 131(1-2):370–374, December 2011. No citations.

[Sey12] Dana Seyringer. Design and Simulation of 128-channel 10 GHz AWG for Ultra-Dense Wavelength Division Multiplexing. *IEEE*, (Cvd):2–5, 2012. No citations.

[SGMS+13] Raphael St-Gelais, Gillian Mackey, John Saunders, Jingjing Zhou, Antoine Leblanc-Hotte, Alexandre Poulin, Jack a. Barnes, Hans-Peter Loock, R. Stephen Brown, and Yves-Alain Peter. Gas sensing using polymer-functionalized deformable Fabry–Perot interferometers. *Sensors and Actuators B: Chemical*, 182:45–52, June 2013. No citations.

[SI03] Helen Song and Rustem F Ismagilov. Millisecond kinetics on a microfluidic chip using nanoliters of reagents. *Journal of the American Chemical Society*, 125(47):14613–9, November 2003. No citations.

[SJA+11] N Suwanpayak, M a Jalil, M S Aziz, F D Ismail, J Ali, and P P Yupapin. Blood cleaner on-chip design for artificial human kidney manipulation. *International journal of nanomedicine*, 6:957–64, January 2011. No citations.

[SK04] Milan N Stojanovic and Dmitry M Kolpashchikov. Modular aptameric sensors. *Journal of the American Chemical Society*, 126(30):9266–70, August 2004. No citations.

[SKWvdB13] Rogier M Schoeman, Evelien W M Kemna, Floor Wolbers, and Albert van den Berg. High-throughput deterministic single-cell encapsulation and droplet pairing, fusion, and

shrinkage in a single microfluidic device. *Electrophoresis*, pages 385–392, July 2013. No citations.

[SLL09] Y. C. Seow, S. P. Lim, and H. P. Lee. Tunable optofluidic switch via hydrodynamic control of laminar flow rate. *Applied Physics Letters*, 95(11):114105, 2009. No citations.

[SNA+90] Yoshikazu Sano, Toru Nomura, Hiromitsu Aoki, Sumio Terakawa, Hirotatsu Kodama, Tadashi Aoki, and Yoshimitsu Hiroshima. SUBMICRON SPACED L E N S ARRAY PROCESS TECHNOLOGY. In *Electron Devices Meeting*, pages 283–286, 1990. No citations.

[SP10] Wuzhou Song and Demetri Psaltis. Pneumatically tunable optofluidic dye laser. *Applied Physics Letters*, 96(8):081101, 2010. No citations.

[SP11] Wuzhou Song and Demetri Psaltis. Pneumatically tunable optofluidic 2 x 2 switch for reconfigurable optical circuit. *Lab on a chip*, 11(14):2397–402, July 2011. No citations.

[SRG+05] Kashan a Shaikh, Kee Suk Ryu, Edgar D Goluch, Jwa-Min Nam, Juewen Liu, C Shad Thaxton, Thomas N Chiesl, Annelise E Barron, Yi Lu, Chad a Mirkin, and Chang Liu. A modular microfluidic architecture for integrated biochemical analysis. *Proceedings of the National Academy of Sciences of the United States of America*, 102(28):9745–50, July 2005. No citations.

[SRKB+11] Ali Salehi-Reyhani, Joseph Kaplinsky, Edward Burgin, Miroslava Novakova, Andrew J DeMello, Richard H Templer, Peter Parker, Mark a a Neil, Oscar Ces, Paul French, Keith R Willison, and David Klug. A first step towards practical single cell proteomics: a microfluidic antibody capture chip with TIRF detection. *Lab on a chip*, 11(7):1256–61, April 2011. No citations.

[SWT+06] Seiji Sowa, Wataru Watanabe, Takayuki Tamaki, Junji Nishii, and Kazuyoshi Itoh. Symmetric waveguides in poly(methyl methacrylate) fabricated by femtosecond laser

pulses. *Optics express*, 14(1):291–7, January 2006. No citations.

[SYHM88] P. M. Sarro, H. Yashiro, A. W v Herwaarden, and S. Middelhoek. An integrated thermal infrared sensing array. *Sensors and Actuators*, 14(2):191–201, 1988. No citations.

[Tab05] Patrick Tabeling. *Introduction to microfluidics*. Oxford university Press, 2005. No citations.

[TB12] Genni Testa and Romeo Bernini. Integrated tunable liquid optical fiber. *Lab on a chip*, (207890), 2012. No citations.

[TCS+10] Ashleigh B Theberge, Fabienne Courtois, Yolanda Schaerli, Martin Fischlechner, Chris Abell, Florian Hollfelder, and Wilhelm T S Huck. Microdroplets in microfluidics: an evolving platform for discoveries in chemistry and biology. *Angewandte Chemie (International ed. in English)*, 49(34):5846–68, August 2010. No citations.

[TDK+10] Varun Trivedi, Ankur Doshi, G K Kurup, E Ereifej, P J Vandevord, and Amar S Basu. A modular approach for the generation, storage, mixing, and detection of droplet libraries for high throughput screening. *Lab on a chip*, 10(18):2433–42, September 2010. No citations.

[THRF10] D J Thomson, Y Hu, G T Reed, and Jean-marc Fedeli. Low Loss MMI Couplers for High Performance MZI Modulators. *October*, 22(20):1485–1487, 2010. No citations.

[THS+10] Genni Testa, Yujian Huang, Pasqualina M Sarro, Luigi Zeni, and Romeo Bernini. High-visibility optofluidic Mach-Zehnder interferometer. *Optics letters*, 35(10):1584–6, May 2010. No citations.

[THZ+12] Genni Testa, Yujian Huang, Luigi Zeni, Pasqualina M Sarro, and Romeo Bernini. Hybrid Silicon-PDMS Optofluidic ARROW Waveguide. *IEEE Photonics Technology Letters*, 24(15):1307–1309, 2012. No citations.

[TJA+79] C Stephen Terry, John H Jerman, James B Angell, Y Goldstein, N B Grover, C Chang, A Jelli, J Andre, P Mark, and A Goodwin. A Gas Chromatographic Air Analyzer Fabricated. *IEEE transactions on electron devices*, 26(12):1880–1886, 1979. No citations.

[TKL+12] Michelle Tsai, Ashley Kita, Joseph Leach, Ross Rounsevell, James N Huang, Joel Moake, Russell E Ware, Daniel A Fletcher, and Wilbur A Lam. In vitro modeling of the microvascular occlusion and thrombosis that occur in hematologic diseases using microfluidic technology. *The Journal of Clinical Investigation*, 122(1):408–418, 2012. No citations.

[TMB+96] B. D. Terris, H. J. Mamin, M. E. Best, J. a. Logan, D. Rugar, and S A Rishton. Nanoscale replication for scanning probe data storage. *Applied Physics Letters*, 69(27):4262, 1996. No citations.

[TMK+13] M. Tsuwaki, J. Mizuno, T. Kasahara, T. Edura, S. Matsunami, J. Oshima, C. Adach, and S. Shoji. SIMPLE AND HIGH-THROUGHPUT FABRICATION OF LARGE-AREA AND MULTILAYER FLEXIBLE POLYMER FILM STRUCTURES FOR MICROFLUIDIC ORGANIC LIGHT EMITTING DIODE. In *MEMS*, pages 303–306, Taiwan, 2013. No citations.

[TMQ02] Todd Thorsen, Sebastian J Maerkl, and Stephen R Quake. Microfluidic large-scale integration. *Science (New York, N.Y.)*, 298(5593):580–4, October 2002. No citations.

[TRAQ01] Todd Thorsen, Richard W. Roberts, Frances H. Arnold, and Stephen R Quake. Dynamic Pattern Formation in a Vesicle-Generating Microfluidic Device. *Physical Review Letters*, 86(18):4163–4166, April 2001. No citations.

[UPW00] P. B. Umbanhowar, V. Prasad, and David Alain Weitz. Monodisperse Emulsion Generation via Drop Break Off in a Coflowing Stream. *Langmuir*, 16(2):347–351, January 2000. No citations.

[VBSN01] Y a Vlasov, X Z Bo, James C Sturm, and David J Norris. On-chip natural assembly of silicon photonic bandgap crystals. *Nature*, 414(6861):289–93, November 2001. No citations.

[VBvdE+09] Siva a Vanapalli, Arun G Banpurkar, Dirk van den Ende, Michel H G Duits, and Frieder Mugele. Hydrodynamic resistance of single confined moving drops in rectangular microchannels. *Lab on a chip*, 9(7):982–90, April 2009. No citations.

[VGdM08] F.A. Voltarelli, C.A. Gobatto, and M.A.R. de Mello. MINIMUM BLOOD LACTATE AND MUSCLE PROTEIN OF RATS DURING SWIMMING EXERCISE. *Biology of sport*, 25(005519):23 – 34, 2008. No citations.

[VMA+06] Paul Vulto, G Medoro, L Altomare, Gerald a Urban, M Tartagni, R Guerrieri, and N Manaresi. Selective sample recovery of DEP-separated cells and particles by phaseguide-controlled laminar flow. *Journal of Micromechanics and Microengineering*, 16(9):1847–1853, September 2006. No citations.

[VMWW05] Dmitri V Vezenov, Brian T Mayers, Daniel B Wolfe, and George M Whitesides. Integrated fluorescent light source for optofluidic applications. *Applied Physics Letters*, 86(4):041104, 2005. No citations.

[VPDBL12] Jordi Vila-Planas, Stefanie Demming, Stephanus Büttgenbach, and Andreu Llobera. PDMS based micro-optical beam splitters. *Optica Pura y Aplicada*, 1380(2006):209–213, 2012. No citations.

[VPM+11] Paul Vulto, Susann Podszun, Philipp Meyer, Carsten Hermann, Andreas Manz, and Gerald a Urban. Phaseguides: a paradigm shift in microfluidic priming and emptying. *Lab on a chip*, 11(9):1596–602, May 2011. No citations.

[vSKD+13] Volkert van Steijn, Piotr M Korczyk, Ladislav Derzsi, Adam R Abate, David A Weitz, and Piotr Garstecki.

Block-and-break generation of microdroplets with fixed volume. *Biomicrofluidics*, 7(2):24108, January 2013. No citations.

[Wal11] RafałWalczak. Fluorescence detection by miniaturized instrumentation based on non-cooled CCD minicamera and dedicated for lab-on-a-chip applications. *BioChip Journal*, 5(3):271–279, September 2011. No citations.

[WBD+93] V. White, S. Bajikar, D. Denton, F. Cerrina, B. Lai, W.B. Yun, D. Legnini, Y. Xiao, J. Chrzas, E. DiFabrizio, L. Grella, and M. Baciocchi. Microfabrication of phase shifting zone plates for hard x-rays. *Microelectronic Engineering*, 21(1-4):99–102, April 1993. No citations.

[WCD+13] Liang Wu, Pu Chen, Yingsong Dong, Xiaojun Feng, and Bi-Feng Liu. Encapsulation of single cells on a microfluidic device integrating droplet generation with fluorescence-activated droplet sorting. *Biomedical microdevices*, 15(3):553–60, June 2013. No citations.

[Wid83] H Michael Widmers. Trends in industrial analytical chemistry. *TrAC Trends in Analytical Chemistry*, 2(1):VIII–X, January 1983. No citations.

[WLX+06] Fawen Wu, Lei Li, Zhihong Xu, Shujuan Tan, and Zhibing Zhang. Transport study of pure and mixed gases through PDMS membrane. *Chemical Engineering Journal*, 117(1):51–59, March 2006. No citations.

[WNS09] Maureen a Walling, Jennifer a Novak, and Jason R E Shepard. Quantum dots for live cell and in vivo imaging. *International journal of molecular sciences*, 10(2):441–91, February 2009. No citations.

[WPW+02] Ian M. White, Richard Penty, Matthew Webster, Yew Jun Chai, and Adrian Wonfor. Wavelength Switching Components for Future Photonic Networks. *IEEE communications Magazine*, (September):74–81, 2002. No citations.

[WSK+14] Andreas Weltin, Kinga Slotwinski, Jochen Kieninger, Isabella Moser, Gerhard Jobst, Marcus Wego, Ralf Ehret, and Gerald a Urban. Cell culture monitoring for drug screening and cancer research: a transparent, microfluidic, multi-sensor microsystem. *Lab on a chip*, 14(1):138–46, January 2014. No citations.

[WYZ14] G. R. Wang, Fang Yang, and Wei Zhao. There can be turbulence in microfluidics at low Reynolds number. *Lab on a Chip*, 2014. No citations.

[XKZ+96] Younan Xia, Enoch Kim, Xiao-mei Zhao, John A Rogers, Mara G. Prentiss, and George M Whitesides. Complex Optical Surfaces Formed by Replica Molding Against Elastomeric Masters. *Science*, 273:347–349, 1996. No citations.

[XLTL08] J. H. Xu, S. W. Li, J. Tan, and G. S. Luo. Correlations of droplet formation in T-junction microfluidic devices: from squeezing to dripping. *Microfluidics and Nanofluidics*, 5(6):711–717, May 2008. No citations.

[XW98] Younan Xia and George M Whitesides. Soft Lithography. *Angewandte Chemie International Edition*, 37(5):550–575, 1998. No citations.

[YAL13] Ali Kemal Yetisen, Muhammad Safwan Akram, and Christopher R Lowe. Paper-based microfluidic point-of-care diagnostic devices. *Lab on a chip*, 13(12):2210–51, June 2013. No citations.

[YB60] Rosalyn S Yalow and Solomon A Berson. Immunoassay of endogenous Plasma Insulin in Man. *Journal of clinical investigation*, 39(7):1157–1175, 1960. No citations.

[YCCF10] Leslie Y Yeo, Hsueh-chia Chang, Peggy P. Y. Chan, and James R. Friend. Microfluidic Devices for Bioapplications. *Small*, (1):n/a–n/a, November 2010. No citations.

[YGL91] E Yablonovitch, TJ Gmitter, and KM Leung. Photonic Band Structure: The Face-Centered-Cubic Case Employing Nonspherical Atoms. *Physical Review Letters*, 67(17):2295–2299, 1991. No citations.

[YKDD12] M Yamazaki, S Krishnadasan, Andrew J DeMello, and John C Demello. Non-emissive plastic colour filters for fluorescence detection. *Lab on a chip*, 12(21):4313–20, November 2012. No citations.

[Yue08] Po Ki Yuen. SmartBuild-a truly plug-n-play modular microfluidic system. *Lab on a chip*, 8(8):1374–8, August 2008. No citations.

[YWH+00] Piedong Yang, Gernot Wirnsberger, Howard C Huang, Steven R Cordero, Michael D McGehee, Brian Scott, Tao Deng, George M Whitesides, Bradley F Chmelka, Steven K Buratto, and Galen D Stucky. Mirrorless Lasing from Mesostructured Waveguides Patterned by Soft Lithography. *Science*, 287(5452):465–467, January 2000. No citations.

[ZHF14] He Zhang, Xinjiang Hu, and Xin Fu. Aptamer-based microfluidic beads array sensor for simultaneous detection of multiple analytes employing multienzyme-linked nanoparticle amplification and quantum dots labels. *Biosensors & bioelectronics*, 57:22–9, July 2014. No citations.

[ZJ13] Xuefeng Zeng and Hongrui Jiang. Liquid Tunable Microlenses based on MEMS techniques. *Journal of physics D: Applied physics*, 46(32):323001, August 2013. No citations.

[ZTI04] Bo Zheng, Joshua D Tice, and Rustem F Ismagilov. Formation of droplets of alternating composition in microfluidic channels and applications to indexing of concentrations in droplet-based assays. *Analytical chemistry*, 76(17):4977–82, September 2004. No citations.

[Zuy81] J. Zuylen. The microscopes of Antoni van Leeuwenhoek. *Journal of Microscopy*, 121(3):309–328, March 1981. No citations.

[ZX96] Xiao-mei Zhao and Younan Xia. Fabrication of Three-Dimensional Micro-Structures: Microtransfer Molding. *Advanced Materials*, 8(10):837–840, 1996. No citations.